SPECIFIC INTERACTIONS IN POLYMER + CO_2 + COSOLVENT SYSTEMS: EXPERIMENT AND MODELING

A Thesis
Presented to
The Academic Faculty

by

Yanhui Yuan

In Partial Fulfillment
of the Requirements for the Degree
Doctor of Philosophy in the
School of Chemical and Biomolecular Engineering

Georgia Institute of Technology
December 2010

SPECIFIC INTERACTIONS IN POLYMER + CO_2 + COSOLVENT SYSTEMS: EXPERIMENT AND MODELING

Approved by:

Dr. Amyn S. Teja, Advisor
School of Chemical and Biomolecular Engineering
Georgia Institute of Technology

Dr. William J. Koros
School of Chemical and Biomolecular Engineering
Georgia Institute of Technology

Dr. Peter J. Ludovice
School of Chemical and Biomolecular Engineering
Georgia Institute of Technology

Dr. David G. Bucknall
School of Polymer, Textile, & Fiber Engineering
Georgia Institute of Technology

Dr. David M. Collard
School of Chemistry and Biochemistry
Georgia Institute of Technology

Date Approved: 09/14/2010

Dedicated to my family and friends

ACKNOWLEDGEMENTS

I would like to thank all of the people who have helped me throughout my studies here at Georgia Tech. First, I would like to acknowledge my advisor Dr. Amyn S. Teja for his support and guidance in my research, and for his helpful discussions and comments and his patience during my progress. I would also like to acknowledge my committee members, Dr. Koros, Dr. Ludovice, Dr. Bucknall, and Dr. Collard for their help and advice over the years.

I would like to thank past and present members of the Teja research group, Michael, James, Anu, Pei Yoong, Angel, Pramod, Nelson, Firman and Devika who have provided help and friendship. I am especially grateful to Michael, Pei Yoong, Pramod and Devika who spent time helping me through various stages of my work. I would like to thank Pei Yoong for his help with SEM imaging and Xunjin for his help with NMR analysis of ionic liquid samples. I would also like to thank Dr. Ludovice and Dr. Swann for providing Molecular Dynamics code (MD2006.SVL) and advice.

I would like to acknowledge my family and friends for all of the encouragement and support they have provided throughout my education. Most importantly, I would like to thank my wife, Yi Ding and my son, Bobby Yilun Yuan. Their love and support have allowed me to accomplish my goals. I would not be where I am today without them.

TABLE OF CONTENTS

LIST OF TABLES

LIST OF FIGURES

LIST OF SYMBOLS AND ABBREVIATIONS

a_i	Activity of component *i*
c	Velocity of light in vacuum
d_p	Penetrated distance
d^+	Average segment diameter
k	Force constant in Equation (2.12)
m_i	Mass
f_0	Volume fraction of free volume
$\hat{f}_i$	Fugacity of component *i* in mixture
f_i	Fugacity of pure component *i*
r	Intermolecular distance in Equation (2.1), (2.2), (4.2) and (4.3)
r_a	Association distance
C_i	Constant
$[C]$	Concentration
A	Absorbance
I	Intensity of the IR radiation
ω	Interchange energy
z	Coordination number
p	Polarizability in Equation (2.2)
Q	Quadrapole moment in Equation (2.2)
μ	Dipole moment in Equation (2.2)
μ	Binding ratio
μ_i	Chemical potential
Γ	Intermolecular potential energy
δ	Solubility parameter
$\hat{\delta}$	Solubility parameter of non-polar homomorph
E	Intermolecular energy of attraction

V	Molar volume
ΔE_V	Molar energy of vaporization
ΔU_{mix}	Molar internal energy change of mixing
$\tilde{T}$	Reduced temperature
$\tilde{P}$	Reduced pressure
$\tilde{\rho}$	Reduced density
r	Number of lattices sites occupied by a molecule
S_w	Swelling ratio
T^*	Characteristic temperature
P^*	Characteristic pressure
ρ^*	Characteristic density
v^*	closed packed molar volume
ε^*	interaction energy per mer
$\Delta\varepsilon_{ex}$	Exchange lattice energy
R	Gas constant
M	Molecular weight
ϕ_i	Volume fraction *of* a component *i*
η	Volume fraction in Equation (2.23), (2.24) and (2.25)
η_{ij}	Binary interaction parameter
k_{ij}	Binary interaction parameter
T_g	Glass transition temperature
G	Gibbs free energy
A	Helmholtz energy
k	Boltzmann constant
g_{ii}^{hs}	Radial pair distribution function for segments of component *i* in the hard sphere system
ε	Dielectric constant in Equation (3.2)
u_0	Nonspecific interaction energy between segments
χ	Flory Huggins parameters
γ_i	Activity coefficient of component *i*

V_i	Molar volume of component *i*
V_{wi}	Van der Waals volume of component *i*
ΔG^E	Excess Gibbs energy
ΔG_{mix}	Gibbs energy of mixing
Ω_i	Configuration of component i
χ^a	Association interaction constant
χ^u	Dispersion interaction constant
K	Equilibrium constant
K_0	Equilibrium constant for association at a reference temperature T_0
ΔH_a	Enthalpy of association
α	Association ratio
α_T	Isobaric coefficient of thermal expansion
β	Isothermal compressibility coefficient
ξ	Number of segments in a polymer molecules
w_i	Weight fraction
υ	Frequency
φ_i	Fugacity coefficient of pure component *i*
$\hat{\varphi}_i$	Fugacity coefficient of component *i* in mixtures
θ_c	Critical angle
ω	Acentric factor
Q	Lattice-fluid partition function
Ψ	Gibbs partition function
E	Lattice energy
Ω_c	Combinational term

Superscripts and Subscripts

LF	Lattice fluid
ARTL	Generalized associative reformulation of thermodynamic lattice
P	Polymer
T	Total

H	Hydrogen bonding
hs	Hard sphere
hc	Hard sphere chain
h	Hydrogen bonding
0	Hole
c	Critical point
a	Association
d	Dispersion
p	Polar
r	Reduced
ab	Acid-base
res	Residual
ref	Reference
mix	Mixing
m	Mixture
vdW	van der Waals
*	Characteristic
ˆ	Average
R	Residual
CO	Carbonyl group
OH	Hydroxyl group
C	Combinatorial
FV	Free volume

Polymer Abbreviations

PMMA	Poly (methyl methacrylate)
PMA	Poly (methyl acrylate)
PVAc	Poly (vinyl acetate)
EVA	Poly (ethylene-co-vinyl acetate)
PVMK	Poly (vinyl methyl ketone)
PVME	Poly (vinyl methyl ether)

PS	Poly (styrene)
PE	Poly (ethylene)
PLA	Poly (lactic acid)
PLGA	Poly (lactide-co-glycolide)
PCL	Poly (ε-caprolactone)
PVDF	Poly (vinylidene fluoride)
PBS	Poly (butylene succinate)
PSF	Poly (sulfone)
PMSSQ	Poly (methyl silsesquioxane)
PIPA	Poly (isopropyl acrylate)
PIDA	Poly (isodecyl acrylate)
PPL	Poly (pivalolactone)
PA	Poly (acetal)
PEG	Poly (ethylene glycol)
PDMS	Poly (dimethyl siloxane)
PFA	Poly (fluoroalkyl acrylate)

SUMMARY

Systems in which there are strong specific interactions between the polymer and CO_2 are of interest in a number of applications including polymer foaming, coating and impregnation. Unfortunately, experimental data on the phase behavior of such systems are relatively scarce, as are models that explicitly consider specific interactions in such systems. The overall goal of this work was therefore to develop a method for the measurement of specific interactions in polymer + CO_2 systems and to apply such measurements to the development of a thermodynamic model for polymer solutions.

This work demonstrates that *in situ* ATR-FTIR spectroscopy may be used to quantify specific interactions in CO_2 + polymer- systems that incorporate carbonyl, ether, siloxane and sulfone groups. However, carbonyl stretching frequencies cannot be used to quantify such interactions between CO_2 and carbonyl polymers, contrary to what has been suggested in the literature. This is because blue shifts in the carbonyl stretching frequencies were observed in the ATR-FTIR spectra of CO_2 + PVAc, CO_2 + PMMA, CO_2 + PLA, and CO_2 + PLGA85 systems. These CO_2 induced blue shifts can be attributed to dielectric effects, and therefore cannot be used to quantify specific interactions in these systems. We propose the use of the temperature dependence of the CO_2 bending mode to quantify specific interactions in CO_2 + carbonyl polymers. With this method, the enthalpies of association for C=O…CO_2 specific interactions were found to be between -7 and -10 kJ/mol in the order: CO_2 + PVAc > CO_2 + PCL ≈ CO_2 + PLA > CO_2 + PLGA85 > CO_2 + PMMA. The method was also extended to other CO_2 philic

polymers, leading to enthalpies of association in the order CO_2 + PEG > CO_2 + PVAc > CO_2 + PSF > CO_2 + PMSSQ >> CO_2 + PVDF & PS.

Specific interactions in polymer + CO_2systems were also investigated via NVT molecular dynamics simulations Such interactions were found to decrease in the order: CO_2...C-O-C > CO_2... O-C=O > CO_2...Si-O-Si . In addition, the association distance was identified to be 3.2 Å. Finally, CO_2 accessibility was found to decrease in the order PVAc > PVMK > PLA > PMA. It was also confirmed that 96 % of associated CO_2 molecules interact with one carbonyl group in these systems.

A ternary extension of the Compressible Lattice Model (CLM) was developed and the enthalpy of specific interactions obtained from ATR-FTIR spectra was incorporated into the model to correlate and predict phase behavior in polymer + CO_2 + cosolvent systems. This work shows that model parameters obtained from binary data can be used to predict ternary system behavior with average absolute deviations between calculated and experimental values (AAD) less than 10 %.

The Sanchez-Lacombe lattice-fluid partition function was extended to associated systems by incorporating an association factor obtained from the Compressible Lattice Model. The resulting Associated Lattice Fluid (ALF) EOS has the same form as the SL EOS, but includes the effects of specific interaction in the calculation of lattice energies, and chemical potentials. We demonstrate that ALF model parameters obtained from correlation of sorption equilibria can be used to predict swelling of polymers with AAD less than 10 %.

.

In summary, specific interactions between CO_2 and C=O and other CO_2-philic groups have been quantified using *in situ* ATR-FTIR spectroscopy. The results have been directly incorporated into a lattice model that is able to correlate cloud points, and sorption equilibria, using a single parameter. The model is therefore likely to be beneficial in many applications involving polymer + CO_2 or polymer + CO_2 + cosolvent systems including polymer impregnation, coating, foaming, and polymer membranes for CO_2 capture. An EOS formulation for the model has been derived for the calculation of swelling in these systems.

CHAPTER 1

INTRODUCTION

CO_2 is attracting considerable attention as a promising alternative to noxious organic solvents and chlorofluorocarbons in the processing of polymers. Due to its relatively low critical parameters (T_c = 31.1 ºC and P_c = 73.8 bar) and because it is non-toxic, non-flammable, chemically inert, and inexpensive, supercritical CO_2 has also shown considerable promise as a reaction medium for processing and modifying polymers [1-3]. The ability of CO_2 to swell biocompatible polymers and lower their glass transition temperatures, thereby facilitating the diffusion of small drug molecules into such polymers, has also led to much interest in the use of CO_2 in drug delivery applications [4-5]. In addition, the precipitation of polymer particles from supercritical CO_2, and the coating of surfaces with fluoropolymer films deposited from supercritical CO_2 solutions, have also proved to be of considerable practical interest [6-8]. An area of emerging interest is the use of polymeric membranes for CO_2 separation from natural gas or flue gases [9]. In these applications, the process path through single and two-phase regions of the polymer + CO_2 phase diagram often determines the morphological and physical-chemical characteristics of the product [10]. Ternary polymer + CO_2 +cosolvent mixtures are of interest in processes in which an organic solvent is used to tune the solvating power of carbon dioxide. For example, Byun et al [11] reported that the cloud point pressure of polyε-caprolactone in CO_2 could be lowered by about 1000 bar by adding the about the 15 wt% dimethylether (DME) as a cosolvent. Teranry polymer + CO_2 + modifier mixtures are also of interest in determining polymer plasticization by

CO_2, which leads to low selectivity and short life span of polymer membranes. One strategy to overcome membrane plasticization is by the addition of modifiers or antiplasiticizers. Therefore, a systemic study of phase equilibrium and solubility in polymer + CO_2 and polymer + CO_2 + modifier (cosolvent or antiplasiticizer) is required for designing and understanding these polymer processes.

The development of a model requires phase equilibrium data on the system of interest. Although some experimental data are available for polymer-CO_2 systems [12], more data are needed for polymer processing applications. Compared with the cost of experiments, the development of thermodynamic models can be an inexpensive way to describe and predict phase equilibrium and solubility. Thermodynamic models include equations of state, such as the Sanchez-Lacombe (SL) and Statistical Association Fluid Theory (SAFT) equation, as well as activity coefficient models, such as the Flory-Huggins equation. Obviously, model parameters should be related to solvent and polymer molecular structure and inter/intra-molecular interactions. A desirable model will contain a minimum number of fitted parameters obtained from direct information on molecular interactions in these systems.

Recent studies have shown that specific interactions between CO_2 or CO_2 + cosolvent and the polymer lead to electron donor-acceptor (EDA) complexes in systems containing Lewis acid groups (e.g. CO_2) and Lewis base groups (e.g. carbonyl, C=O). These interactions have a dramatic effect on the phase behavior of mixtures [13]. Although CO2 + carbonyl polymers have been studied extensively, less is known about specific interactions between CO_2 and polymers with other functional groups (e.g. ether

and fluorine), and between CO_2 and cosolvents. In addition, we need a general method to quantify these interactions, and to relate them to parameters of a model.

A thermodynamic model for associating polymer solutions based on lattice theory was recently proposed by Ozkan and Teja [13], and modified by Kasturirangan and Teja [14]. Their model accounts for specific solute-solvent complex formation in polymer-CO_2 solutions as well as the compressibility of the lattice. The model was used to calculate cloud point curves in polyacrylate + CO_2 systems using two adjustable parameters. Agreement with experiment was within 2 % average absolute deviation [13] which is comparable to the performance of the SAFT EOS commonly used to represent such phase behavior. Kasturirangan and Teja [14] showed that the modified model is able to correlate experimental data both at high pressure range (cloud point) and low pressure range (sorption) well in CO_2 + biopolymer systems. An additional advantage of their methodology is that one of their model parameters can be obtained from infrared spectroscopic (IR) measurements and quantifies the strength of specific interactions found in such systems. Therefore, only one fitting parameter is used in their model. However, the applicability of the above model to polymer + CO_2 + cosolvent systems has not been established.

The overall goal of this work therefore is to develop a thermodynamics model with physical meaningful parameters that are quantitatively related to molecular interactions. In the present study, specific interactions between polymer and CO_2 were studied experimentally (Chapter 3) and via molecular modeling (Chapter 4). A compressible lattice model for ternary system was developed, and used to correlate and predict cloud points curves for polymer + CO_2 + cosolvent systems (Chapter 5).

Furthermore, the compressible lattice model was extended to an equation of state form, and used to correlate and predict of sorption and swelling (Chapter 6).

CHAPTER 2

LITERATURE REVIEW

2.1 Introduction

2.1.1 Polymer processing with supercritical fluids

Supercritical fluids (SCFs) have shown promise for a variety of processes and technologies [2, 15], because they exhibit properties of both gas and liquid phases. In particular, supercritical CO_2 ($scCO_2$) is being considered for polymer processes, such as surface cleaning, foaming, polymer impregnation, particle formation and polymerization, (see Figure 2.1) [16-17]. Tomasko et al [2], Lora and Kikic [18], Nalawade et al [19] give an overview on the use of SCFs in polymer processing. As pointed out by Tomasko et al [2], thermodynamic phase equilibrium in polymer and SCF systems is one of key fundamentals to help us design and optimize these processes. However, the development of polymer processes with SCFs currently is hindered by the limitation that the available thermodynamic models are still not good enough to describe the unique characteristics of polymer in SCF solutions [12]. The challenge remains for developing a thermodynamic model to describe the polymer + SCF phase behaviors over a large range of temperature and pressure.

2.1.2 Phase behavior of polymer + SCF systems

Polymers commonly show only limited solubility in SCF such as $scCO_2$. Also, the solubility is a function of temperature, pressure, concentration and molecular weight and polydispersity of the polymer. The solubility of polymer + SCF systems is commonly

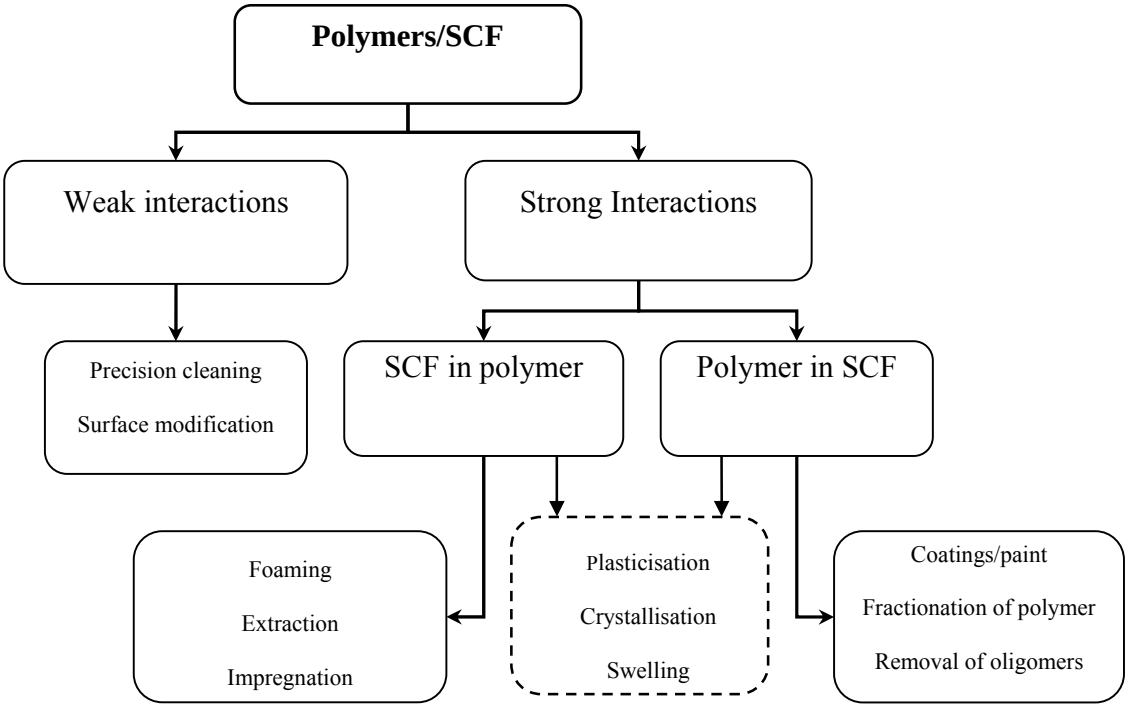

Figure 2.1 Interaction of SCFs with polymers

represented as a *p-T* phase diagram. Although there are five basic types of binary phase diagrams as summarized by McHugh and Krukonis [20], polymer + SCF phase behavior can be commonly described by either Type-III or Type-IV diagram (see Figure 2.2). Figure 2.2 shows a typical *p,T* projection of a polymer + solvent or SCF phase diagram, also called cloud point graph, where the solid lines denote the transitions from a homogeneous solution (L) to a demixed system (LL) and to a vapor-liquid system (VL), respectively [21]. Many literature studies present such phase diagram for a fixed polymer concentration of 5 wt%. As shown in Figure 2.2, the UCST (Upper Critical Solution Temperature) curve has a (mostly) negative slope and depends only slightly on pressure; the LCST (Lower Critical Solution Temperature) curve is much more pressure dependent. With increasing differences in chemical nature and size of polymer and solvent, the homogeneous region L becomes smaller and is shifted to higher pressures [20-21]. Finally, the UCST and LCST curves merge to give the so-called U-LCST behavior, which is typical for polymer + supercritical solvent mixtures.

Figure 2.3 summarizes the qualitative impacts of various polymer properties on the solubility in $scCO_2$. Whereas an increase in molecular weight always causes a decrease in solubility and thereby leads to a shrinking of the homogeneous region (L), increasing branching and polydispersity of the polymer have a converse effect. Increasing polarity of the polymer mostly leads to improved solubility in CO_2. Finally, in polymer + CO_2 system, the solubility can be significantly improved with the aid of a cosolvent [21]. For example, the solvating power of $scCO_2$ may be tuned by cosolvents such as dimethyl ether, Freons®, ethanol or alkanes. The basic strategy in the selection of a co-solvent to improve miscibility of a given polymer is the introduction of polarity with polar solvents

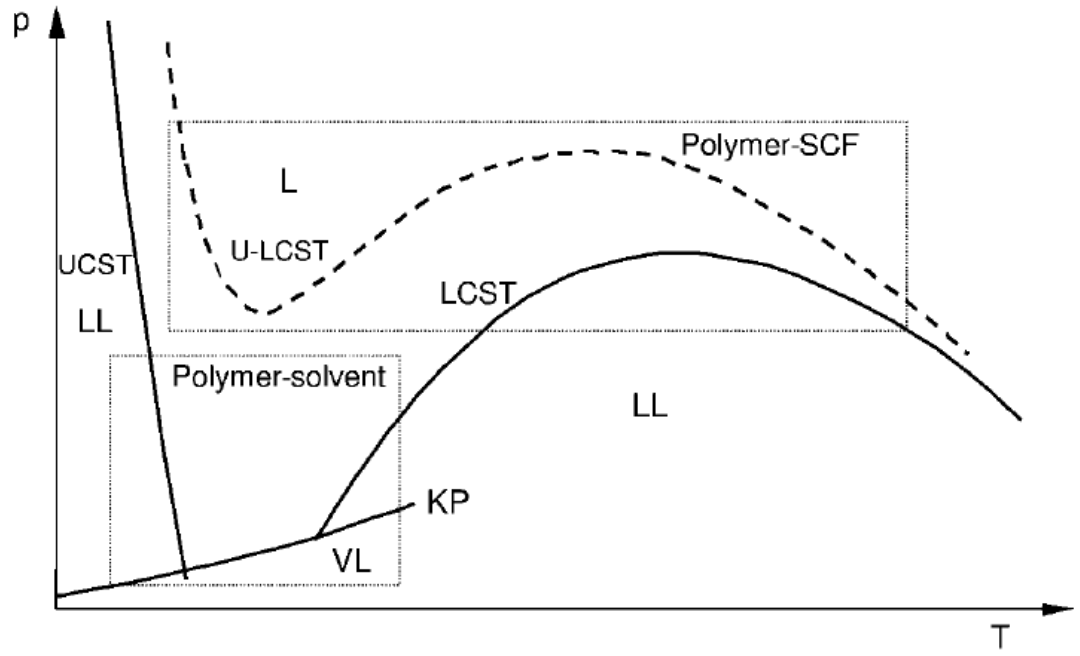

Figure 2.2 Phase behavior of polymer + SCFs systems as a function of temperature and pressure [21].

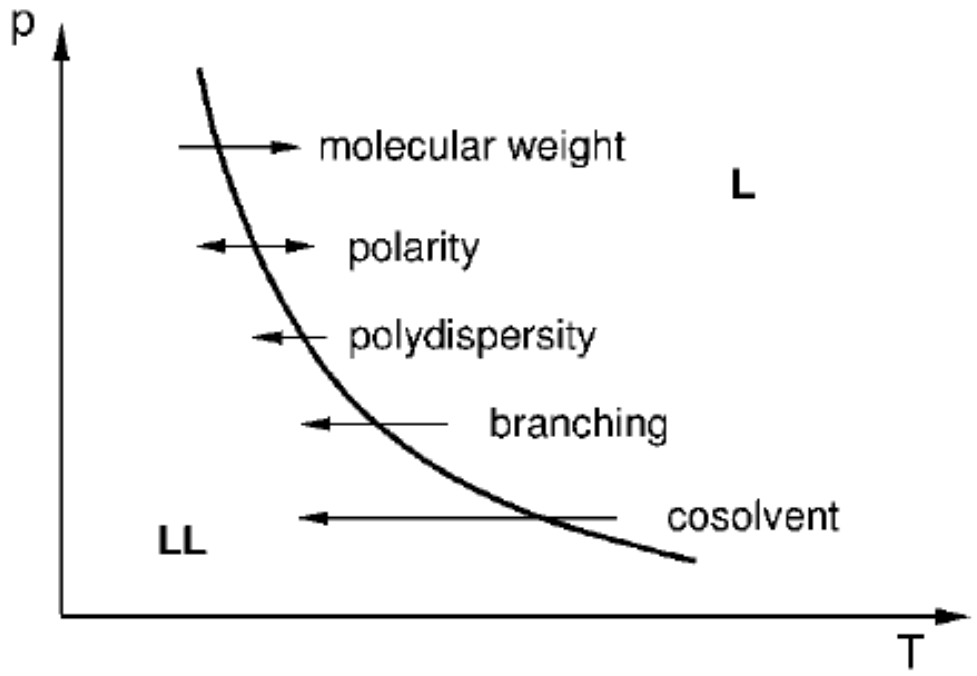

Figure 2.3 Qualitative impact of various system properties on polymer solubility in carbon dioxide [21].

like ethanol, methanol, acetone, or non-polar attributes with alkanes like propane, butane, pentane, and hexane. In the last decade, several research groups have measured the phase behavior of polymer + CO_2 + cosolvent systems [11, 22-24].

2.1.3 Impact of specific interactions on phase behavior in polymer + CO_2 systems

There are a number of previous studies that show CO_2 can be used as a solvent for some polymers and copolymers at high pressures and temperatures [20, 25]. However, we know little about the impact of specific interactions (e.g. electron donor acceptor, charge transfer complex, and Lewis acid-base interaction, etc [26]) on the phase behavior of polymer + CO_2 systems. A typical example is given in Figure 2.4 where the cloud point curves of poly (vinyl acetate) (PVAc) and poly (methacrylate) (PMA) in CO_2 have been plotted [27].

PMA and PVAc are isomers with very similar chemical structures, except for n the position of the carbonyl group. However, as shown in Figure 2.4, the cloud points curves are quite different. At 30 °C the PMA cloud-point curve is more than 1500 bar higher than the PVAc curve even though the molecular weight of PVAc is 4 times higher than that of PMA. As suggested by Kazarian et al [28], CO_2 can more easily access the carbonyl group in PVAc than in PMA, and forms electron donor-acceptor complexes with PVAc. Similarly, other functional groups may lower the cloud pressure dramatically, such as siloxane and fluorine group [29] (See Figure 2.5). We may therefore conclude that specific interactions between CO_2 and polymer have a significant effect on phase behavior and properties. However, quantitative measurements of such specific interactions are lacking. Also, the addition of a small amount of cosolvent may have an

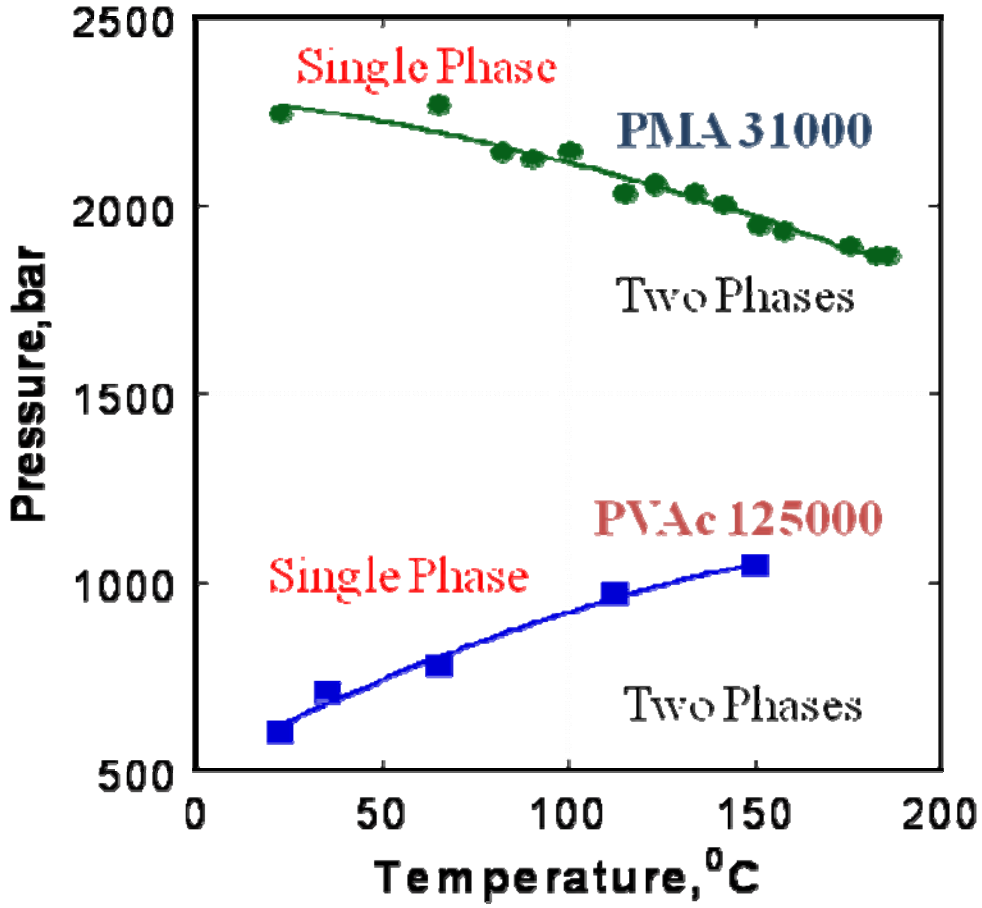

Figure 2.4 Cloud point curves of poly (vinyl acetate) (PVAc) and poly (methacrylate) (PMA) in CO_2 [30].

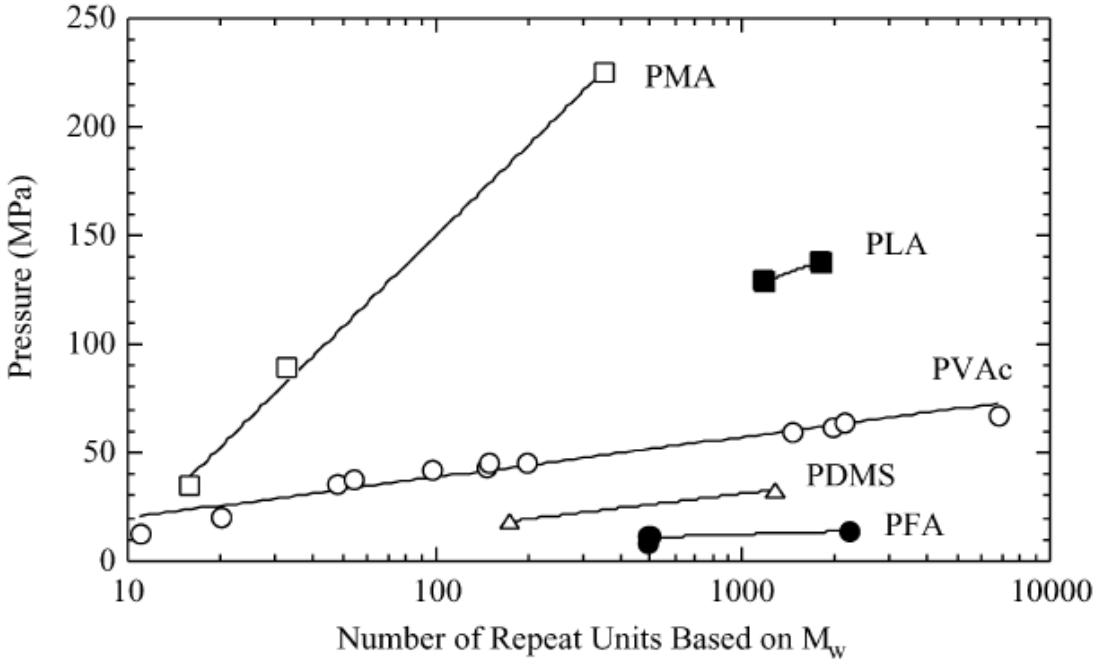

Figure 2.5 Cloud-point pressures at 298 K for binary mixtures of CO_2 with poly(methyl acrylate) (PMA), poly(lactide) (PLA), poly(vinyl acetate) (PVAc), poly(dimethyl siloxane) (PDMS), and poly(fluoroalkyl acrylate) (PFA) as a function of number of repeat units based on Mw [29].

effect on specific interactions. Therefore, a method to quantify these interactions and incorporate them into a thermodynamic model is of theoretical as well as practical interest.

In the following, we will briefly review molecular interactions in polymer solutions, the methods to quantify specific interactions, and some basic background of infra red spectroscopy. Finally, thermodynamic models for polymer solutions will be discussed.

2.2 Molecular Interactions in Polymer Solutions

Thermodynamic properties and phase behaviorof polymer solutions are determined by intermolecular interactions between solvent molecules (solvent-solvent), between polymer segments (segment-segment), and between solvent molecules and polymer segments (solvent-segment). These intermolecular interactions can be approximately expressed in term of the interchange energy (ω), given by

$$\omega = z\left[\Gamma_{ij}(r,T) - \frac{1}{2}\left(\Gamma_{ii}(r,T) + \Gamma_{jj}(r,T)\right)\right] \tag{2.1}$$

where $\Gamma_{ij}(r,T)$ is the intermolecular pair-potential energy.

An approximate form of the attractive part of the intermolecular potential energy $\Gamma_{ij}(r,T)$ for small molecule mixtures is

$$\Gamma_{ij}(r,T) \approx -\left[C_1\frac{p_i p_j}{r^6} + C_2\frac{\mu_i^2\mu_j^2}{r^6 kT} + C_3\frac{\mu_i^2 Q_j^2}{r^8 kT} + C_4\frac{\mu_j^2 Q_i^2}{r^8 kT} + C_5\frac{Q_i^2 Q_j^2}{r^{10} kT} + Specific\ Interaction\right] \tag{2.2}$$

where p is the polarizability, μ is the dipole moment, Q is the quadrupole moment, and C_1-C_5 are constants.

The leading terms in the expansion for the potential energy are dipole and quadrupole interactions which are inversely proportional to temperature. At elevated temperatures, thermal energy disrupts the configurational alignment of the polar moments of the molecules so that they behave as if they were non polar. Specific interactions such as complex formation or hydrogen bonding can also contribute to the intermolecular pair potential energy. The strength of these "directional" interactions, which are also very temperature sensitive [12], can be of the same order of magnitude as the other interaction in Equation (2.2). Therefore specific interactions if present may have a significant impact on the phase equilibra in polymer + CO_2 + cosolvent systems.

2.2.1 Non-specific interactions in polymer + SCFs systems

The simplest method to quantify non-polar intermolecular interaction in a liquid is the solubility parameter approach of Hildebrand and Scott [31-32]. The solubility parameter is defined as the square root of the cohesive energy density,

$$\delta = \sqrt{\frac{\Delta E_V}{V}} \tag{2.3}$$

where E is the intermolecular energy of attraction, ΔE_V is the molar energy of vaporization, and V is the liquid molar volume.

According the Regular Solution Theory (RST), the molar energy change of mixing can be expressed as

$$\Delta U_{mix} = \left(x_1 V_1 + x_2 V_2\right)\phi_1\phi_2\left(\delta_1 - \delta_2\right)^2 \tag{2.4}$$

where V_i is the molar volume, ϕ_i is the volume fraction of component *i*, and x_i is the molar fraction of component *i*. Although RST was developed for small molecular systems, it can be also applied to polymer solutions to estimate the enthalpy change of mixing. It should be noted that the enthalpy change of mixing estimated by Equation (2.4) is always positive, which means that energy must be added into the system to obtain a positive interchange energy (ω).

In the original Hildebrand solubility parameter approach, the existence of polar interactions and of specific interactions such as hydrogen bonding, were neglected. Hansen proposed a 3-parameter model by separating the total cohesive energy into three parts, nonpolar (dispersion) interaction (E_d), polar (dipole-dipole and dipole-induced dipole) interactions (E_p), and hydrogen bonding or other specific association interactions (including Lewis acid-base interactions) (E_h) [33]. Thus:

$$E = E_d + E_p + E_h \tag{2.5}$$

so that,

$$\delta_T^2 = \delta_d^2 + \delta_p^2 + \delta_h^2 \tag{2.6}$$

The Hansen solubility parameters in Equation (2.6) are determined empirically based on multiple experimental solubility observations. Hansen's total solubility parameter, δ_T, should equal the Hildebrand solubility parameter. If we only consider non-specific interaction, only the first two terms in Equation (2.6) are needed. Equation (2.5) is more generally applicable than Equation (2.4) or (2.6) as suggested by Hildebrand et al [31].

In the supercritical state, the density of the fluid changes significantly with respect to temperature and pressure. The solubility parameter will therefore be a function of pressure and temperature. Giddings proposed a method based on a corresponding states approach to obtain [34].

$$\delta = 1.25 P_c^{0.5} \left(\frac{\rho_r}{\rho_{r(liquid)}} \right) \tag{2.7}$$

where δ is in $(cal/cm^3)^{0.5}$, P_c is the critical pressure (atm), ρ_r is reduced density of fluid, and $\rho_{r(liquid)}$ is the reduced density of the liquid phase at its normal boiling point.

Recently, Williams et al [35] calculated the solubility parameter of CO_2 as a function of temperature and pressure using an EOS. They used the following equations to estimate the solubility parameter.

$$\delta^2 = \left(\frac{\Delta E}{V} \right) \approx \left(\frac{\partial E}{\partial V} \right) = T \left(\frac{\partial P}{\partial T} \right)_V - P \tag{2.8}$$

According to their calculation (see Figure 2.6) the solubility parameter of supercritical CO_2 varies from 5 to 15 $MPa^{0.5}$. Therefore, in polymer + SCF systems, we may need to take account of the temperature and pressure (volume) effect on the solubility parameter (see Table 2.1).

2.2.2 Specific interactions in polymer + SCFs (CO_2) systems

The most familiar specific interaction is hydrogen bonding, which is the attractive force between the hydrogen attached to an electronegative atom (e.g. O, F, N) of one molecule and an electronegative atom of a different molecule. Hydrogen bonds can vary

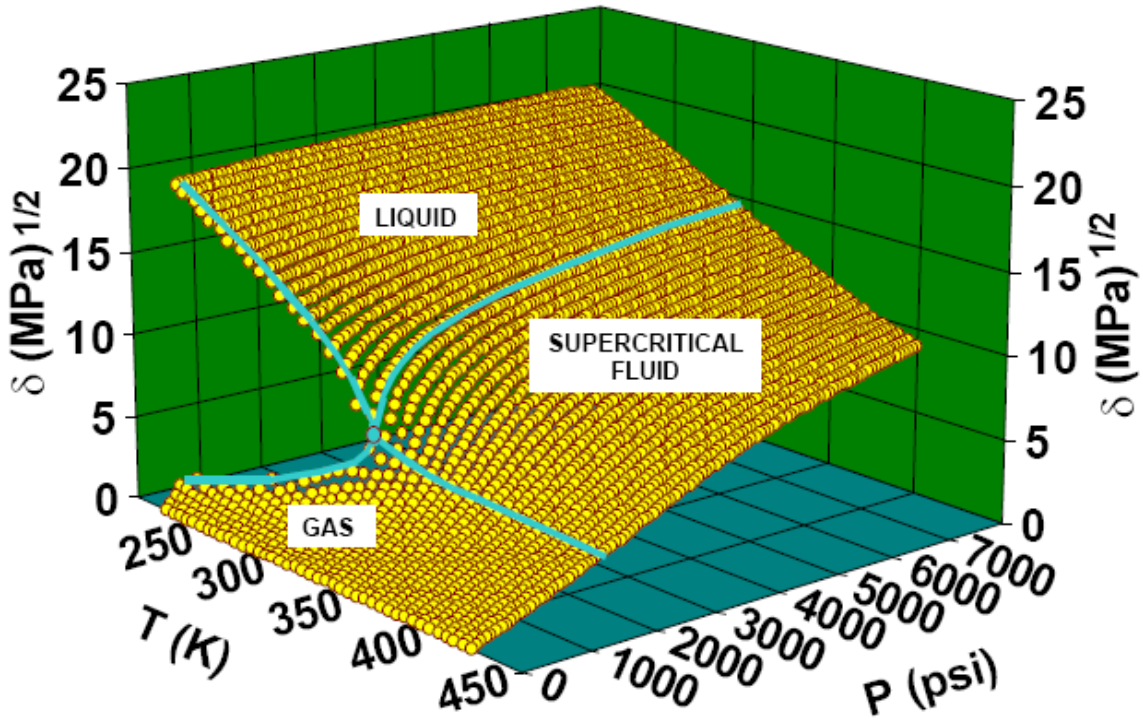

Figure 2.6 Solubility parameter of pure CO_2 [35]

Table 2.1 Temperature, pressure or volume dependence of Hansen solubility parameters [35].

	δ_d	δ_p	δ_h
Temperature	$\left(\frac{\partial \delta_d}{\partial T}\right)_P = -1.25\alpha_T \delta_d$	$\left(\frac{\partial \delta_p}{\partial T}\right)_P = -\left(\frac{\alpha_T}{2}\right)\delta_P$	$\left(\frac{\partial \delta_h}{\partial T}\right)_P = -\left(1.32\times10^{-3} + \frac{\alpha_T}{2}\right)\delta_h$
Pressure	$\left(\frac{\partial \delta_d}{\partial P}\right)_T = 1.25\beta\delta_d$	$\left(\frac{\partial \delta_p}{\partial P}\right)_T = \left(\frac{\beta}{2}\right)\delta_P$	$\left(\frac{\partial \delta_h}{\partial P}\right)_T = -\left(\frac{1.32\times10^{-3}}{\alpha_T} + \frac{1}{2}\right)\beta\delta_h$
Volume (Integrated)	$\frac{\delta_{d\_ref}}{\delta_d} = \left(\frac{V_{ref}}{V}\right)^{-1.25}$	$\frac{\delta_{p\_ref}}{\delta_p} = \left(\frac{V_{ref}}{V}\right)^{-0.5}$	$\frac{\delta_{h\_ref}}{\delta_h} = \exp\left[-1.32\times10^{-3}\left(T_{ref} - T\right) - \ln\left(\frac{V_{ref}}{V}\right)^{-0.5}\right]$

in strength from very weak (1-2 kJ/mol) to extremely strong (140 kJ/mol), which is somewhere between a covalent bond and an electrostatic intermolecular attraction.

It has been suggested that CO_2 might serve as an electron donor [36] or as an electron acceptor [28]. Thus, electron donor-acceptor (EDA) complexes can be formed in polymer + CO_2 systems, when there are chemical groups with basic or acidic properties in the polymer chain. This kind of Lewis acid-base interaction between CO_2 and the polymer can be regarded as a type of specific interaction, and IR spectroscopic evidence has been obtained by Kazarian [28]. Possible interactions of CO_2 with different chemical groups, such as carbonyl (C=O) and ether (C-O-C) are shown in Figure 2.7.

Because of such specific interactions, immiscible polymers can be made soluble in CO_2 by incorporating carbonyl groups in the polymer [37]. In addition, the solubility of CO_2 in polymers such as poly (methyl methacrylate) (PMMA) with carbonyl groups is greater than the solubility of CO_2 in polymers without carbonyl groups, such as polystyrene (PS) or poly (vinyl chloride) (PVC). These observations suggest that EDA complex formation between the carbon atom in CO_2 and carbonyl oxygen atoms can strongly affect the phase behavior [28]. Using FTIR spectra, Kazarian et al [28] have shown that CO_2…C=O interactions are of the order of 4 kJ/mol, and therefore only slightly stronger than dispersion forces. *Ab initio* calculations have also confirmed these observations [38-39].

However, a value of the enthalpy of specific interaction of -4 kJ/mol reported by Kazarian et al [28] is quite a bit lower the value of -15 kJ/mol from the quantum calculations [40]. Therefore, it is necessary to resolve the discrepancy in order to properly model polymer + CO_2 mixtures. There are two methods to achieve this: FTIR

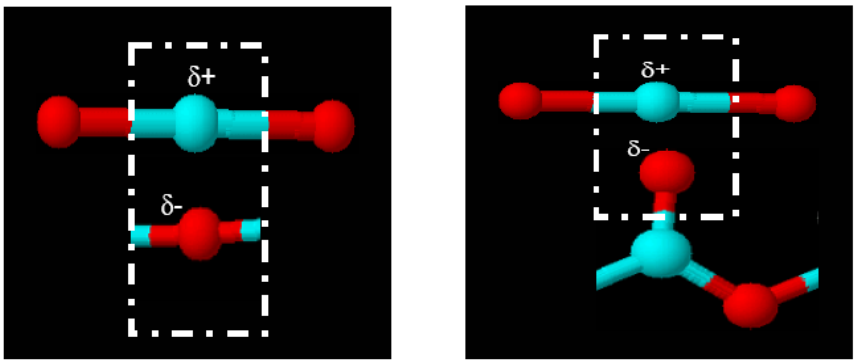

a) ether+ CO_2 b) carbonyl+CO_2

Figure 2.7 Specific interactions of CO_2 with different chemical groups (blue-carbon, red-oxygen)

measurements, and molecular dynamics simulations or quantum calculations. A brief review of these methods is presented below.

Frequency Shift Method

Vibration frequencies of certain bonds in a molecule will generally change if the molecule associates with another molecule. These vibration frequency changes or shifts in the peaks of vibration frequency bands can be detected by IR spectroscopy. As shown by Purcell and Drago [41-43], it is reasonable to assume that there is a linear relationship between the OH stretching frequency peak shift and hydrogen-bonding enthalpy. A frequency shift-enthalpy correlation was proposed by Drago [41] and Purcell [42-43] for hydrogen-bonding acids mixed with various bases. The correlation was obtained from data on a number of acids such as phenols, t-butanol, hexafluoroisopropanol, and has the general form

$$-\Delta H_{ab} = m_a \Delta \upsilon_{OH} + n_a \tag{2.9}$$

where ΔH_{ab} is the enthalpy of the acid-base interaction, $\Delta \upsilon_{OH}$ is the stretching frequency shift for OH absorption, and m_a and n_a are two correlation constants for the given acid. For a given base b mixed with various hydrogen-bonding acids

$$-\Delta H_{ab} = k_b^a \Delta \upsilon_{OH} \tag{2.10}$$

A similar correlation was obtained for ethyl acetate mixtures with various acids using the stretching frequency of the carbonyl group (C=O) [44], The correlation equation is given by

$$\Delta H_{ab} = 0.236 \frac{kcal}{mol\ cm^{-1}} \Delta \upsilon_{CO}^{ab} \tag{2.11}$$

Fowkes et al [44] also found that the frequency shift is dependent on the surface tension of the solvent, and they estimated the enthalpy of acid-base interaction between PMMA and several chlorinated hydrocarbons on the basis of Equation (2.11) (See Table 2.2).

Many studies of polymer systems have examined these frequency shifts [28]. For example, using small acid molecules as probes, Cangelosi et al [45] qualitatively ordered the strength of specific interaction between polymers and cyclohexanol as follows: PVME > PCL > PA > PB > PPL. Also, Kwei et al [46] reported a method to quantify the acidity or basicity of polymers using the same correlation constants obtained from small molecule analogs. Nevertheless, the frequency shift method has not been studied extensively for polymer + CO_2 systems.

Equilibrium Constant Method

In the equilibrium constant method, specific interactions between CO_2 and a polymer are treated in terms of a reversible reaction. Therefore, if the concentration of associated CO_2 and free CO_2 in the system are measured via FTIR or NMR, then the equilibrium constant can be obtained and the enthalpy of specific interaction calculated via the van't Hoff relation. Meredith et al [47] used the method to study specific interactions between CO_2 and tributyl phosphate. Recently, Dharmalingam has measured the equilibrium constant for alcohol and ethyl methacrylate by means of FTIR [48-49]. Utilizing Nash's method [50], the equilibrium constant (K) for the 1:1 EDA complex was determined by plotting a graph of $Y = [C]^{-1}$ and $X = (1-(A/A_0))^{-1}$, where A and A_0 are the absorbances of the carbonyl band of ethyl methacrylate in the presence and absence of

alcohol, respectively. However, the method has not been applied to polymer + CO_2 system as yet.

Molecular Simulation

In principle, molecular modeling can be used to compute specific interactions in polymer + CO_2 + cosolvent systems through statistical mechanical simulations. However, due to the large system sizes and weak interactions among molecules, only several segments of polymer and some small molecules can be simulated in a limited size periodic box. Moreover, intermolecular potential models are not accurate enough to allow high precision calculation of specific interactions, and only qualitative results can be obtained [14].

Another alternative is to bypass the use of potential models and directly use *ab initio* methods to calculate the interaction energy between polymer segments or some specific functional groups and CO_2 or a cosolvent. Diep et al [51] have investigated the interactions of CO_2 with small hydrocarbons and fluorocarbons (CH_4, C_2H_6, CF_4, and C_2F_6) using the Hartree-Fock and Møller-Plesset second-order perturbation theory (MP2). They reported binding energies of CO_2 + hydrocarbon clusters ranging from 0.79 to 1.17 kcal/mol. Recently, Kim and Kim [52] reported that the binding energy of CO_2 + methyl acrylate was approximately 3.1 kcal/mol at the MCCM-CO-CCSD(T) level, and the binding energies for CO_2 + acetaldehyde and CO_2 + dimethylether complexes including cooperative weak hydrogen bonding with α-protons were 2.5 and 3.8 kcal/mol respectively. Kilic et al [40] reported two binding geometries for the C=O…CO_2 complex identified from *ab initio* calculations (see Figure 2.8). These structures differ mainly in

Table 2.2 Relative acidities of chlorinated hydrocarbons determined from $\Delta\upsilon_{CO}^{ab}$ of PMMA [44].

Solvent	$\upsilon_{CO}(cm^{-1})$	$\gamma(dyn/cm)$	$\upsilon_{CO}^{d}(cm^{-1})$	$\Delta\upsilon_{CO}^{ab}(cm^{-1})$	$\Delta H^{ab}(kcal/mol)$
1,2-Dichloroethane	1718	31.9	1735	-17	-4.0
1,1,2-Trichloroethane	1726	22.0	1742	-16	-3.8
Chloroform	1728	26.6	1738	-10	-2.4
1,1,1-Trichloroethane	1732	25.1	1739	-7	-1.7
1,1,2,2-Tetrachloroethane	1725	35.6	1732	-7	-1.7
1,1,1,2-Tetrachloroethane	1728	35.6	1732	-4	-1.0

Note: υ_{CO}^{d} is the expected carbonyl frequency if these solvents were not acidic

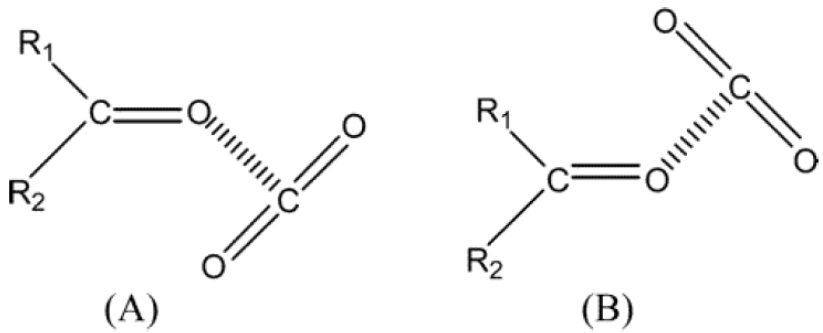

Figure 2.8 Binding geometries for C=O…CO_2 [40]

the orientation of CO_2 with respect to the different R groups of the C=O containing molecule, but can lead to quite different solubilities in the polymer. Kilic et al [40] also report the interaction energies between CO_2 and polymer monomers. They found that some ether group has similar interaction strength as the ester group (Table 2.3). It should be noted that these results are about three times greater than experimental values by Kazarian et al [28].

In summary, both non-specific and specific interactions can be quantified without phase equilibrium data using molecular simulations. Temperature and pressure effects can be taken into account for non-specific interactions by using the RST method. The strength of specific interactions between polymers with carbonyl groups (C=O) and CO_2 can be estimated by both experiment and *ab initio* calculation. However, large discrepancies exit between these two methods. Finally, the strength of specific interactions between CO_2 and other functional groups not been measured. Thus, it is necessary to develop a general method to quantify specific interactions between CO_2 and functional groups in order to properly model polymer + CO_2 systems.

2.3 Infrared Spectroscopy

Infrared radiation is defined as light with wavenumbers (reciprocal of wavelength) between 400 cm^{-1} and 4000 cm^{-1}. Infrared spectroscopy is based on the interaction of electromagnetic radiation with molecular bonds. The easiest way to consider molecular vibrations is to treat the atoms in a molecule as balls, and the chemical bonds connecting

Table 2.3 Interaction energies with CO_2 [40].

Molecules	Interaction energies (kJ/mol)		
	Ether oxygen/CO_2	Carbonyl oxygen/CO_2 (A)	Carbonyl oxygen/CO_2 (B)
IPA	-14.8	-14.2	-15.9
MIE	-18.0	N/A	N/A
EIE	-18.6	N/A	N/A
IBA	-15.1	-14.1	-14.3
MIK	N/A	-13.6	-16.0

Note: A, B are two conformations as shown in Figure 2.8;

IPA, isopropyl acetate; MIE, methyl isopropyl ether; EIE, ethyl isopropyl ether; IBA, isobutyl acetate; MIK, methyl isobutyl ketone

them as springs. The vibration frequency, υ (in wavenumber, cm^{-1}) of the harmonic in terms of classical mechanics is given by

$$\upsilon = \frac{1}{2\pi c}\sqrt{\frac{k}{m}} \tag{2.12}$$

where c is the velocity of light in a vacuum (2.997925×10^{10} cm/s), k is the force constant of the spring, and m is the harmonic average mass:

$$m = \frac{m_1 m_2}{m_1 + m_2} \tag{2.13}$$

In Equation (2.13), m_1 and m_2 are the masses of the two atoms involved in the bond. From Equation (2.12 and 2.13), molecular properties, the force constant of the chemical bond and the reduced mass of the atoms, determine the frequency (wavenumber in IR spectroscopy) at which a bond will absorb infrared radiation. As a result, the IR radiation absorption for a molecular bond is very selective. Each individual functional group absorbs IR radiation at a unique wavenumber. This consistent behavior of chemical bonds is what IR spectroscopy exploits in order to reveal the molecular structure of a chemical compound. It should also be noted that in order to be IR active, the vibrations or rotations within a molecule must cause a net change in the dipole moment of the molecule [53].

2.3.1 Attenuated total reflection infrared spectroscopy (ATR-IR)

Attenuated total reflection is the phenomenon that the incident light will be totally reflected back into the dense medium at the interface. Attenuated total reflection is also known as total internal reflection [53].

Two conditions must be satisfied in order to observe total internal reflection, (1) the angle of incidence of the infrared radiation must be larger than the critical angle, $\theta_c = \sin^{-1}\left(\frac{n_1}{n_2}\right)$, where n_1 and n_2 are the refractive indices of samples and internal reflection material (e.g ZnSe), respectively and (2) $n_2 > n_1$.

When internal reflection occurs, an evanescent wave penetrates into the sample at the interface (Figure 2.9). The formation of the wave is due to the electromagnetic field produced by the superposition of incident and reflective radiation in the internal reflection material. The extent of penetration of the radiation into the sampley depends on the wavelength (λ) and on the optical properties refractive indices and angle of incidence of IR beam in the system. The radiation penetrated short distance (d_p) can be calculated by Equation (1.30) [54]. For example, it will be about 1 μm at 1700 cm^{-1} for a liquid or polymer sample (n_1 = 1.5) in contact with ZnSe (n_2 = 2.4) at 45° angle of incidence.

$$d_p = \frac{\lambda}{2\pi n_2 \sqrt{(\sin\theta)^2 - (n_1/n_2)^2}} \tag{2.14}$$

ATR-IR spectroscopy has been used in various studies of polymers because of the shorter penetration distance than common transmission IR which is limited by the thickness of the polymer sample. This type of spectroscopy can be used for characterizing polymer chain orientation, functional group analysis, curing rate, oxidation studies, as well as characterization of unsaturation and crystallinity [54-56].

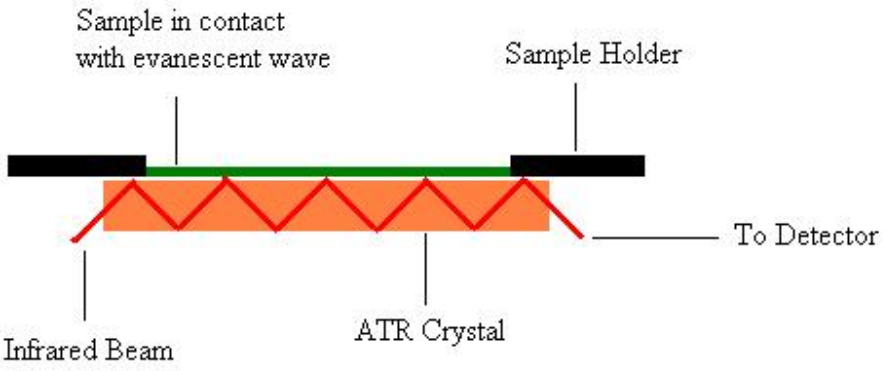

Figure 2.9 Schematic diagram of a multi-reflection ATR-IR system

2.3.2 Quantitative analysis

IR spectroscopy can provide quantitative information, such as the concentration (or relative concentration) of molecules and the relationship between absorbance and concentration (via the Beer-Lambert law):

$$A = \varepsilon L[C] \tag{2.15}$$

where ε is the molar absorptivity, L is the path length, $[C]$ is the concentration, and A is the absorbance, measured directly, and defined as

$$A = -\log(I / I_0) \tag{2.16}$$

where I is the intensity of the radiation absorbed by a particular molecular groups and I_0 is for the background. In practice, when large absorption values are measured, dilution is required to achieve accurate results. Measurements of absorption in the range of A = 0 to 1 are less affected by the *Shadow Effect* [53].

2.4 Thermodynamic Models

Many thermodynamic models have been developed for polymer + solvent systems. These can be broadly divided into: equation of state (EOS) models and activity coefficient models. Representative examples are described in the following sections and their advantages and disadvantages are outlined.

2.4.1 Equations of state

An advantage of the equation of state method is its applicability over wide ranges of temperature and pressure to mixtures of diverse components, from the light gases, heavy liquids, to supercritical phases. The most familiar EOS is van der waals type EOS such as vdW, Peng-Robinson, Patel-Teja, and Soave-Redlich-Kwong and so on [26, 57].

However, However, other EOS have been developed for polymer solutions based on cell models (Prigogine, Flory-Orwoll-Vrij), lattice-fluid models (Sanchez-Lacombe, Costas and Sanctuary, Panayiotuou-Vera), hole models (Simha-Somcynsky), and hard sphere chain models (Pertubed-Hard-Sphere-Chain, and Statistical Associated-Fluid Theory (SAFT)) [58]. In associated systems, representative models include Associated Perturbed Anisotropic Chain Theory (APACT) [59], Lattice Fluid Hydrogen Bonding (LFHB) [60-62], Cubic Plus Association (CPA) EOS [63-64], and SAFT variations [61, 65].

The main disadvantage of the EOS approach is that characteristic parameters for polymers must be obtained by fitting experimental data and the physical meaning of these parameters may be lost to some extent. Furthermore, mixing rules are required that introduce more adjustable parameters. Therefore, only a few EOS models are used for polymer solutions. These will be discussed in the following section.

Sanchez-Lacombe (SL) EOS

The Sanchez-Lacombe equation of state is based on a lattice-fluid model that accounts for the compressibility of the lattice, or the "free volume", by introducing holes into the lattice [66-69]. In reduced form, it has the form:

$$\tilde{\rho}^2 + \tilde{P} + \tilde{T}\left[\ln(1-\tilde{\rho}) + \left(1-\frac{1}{r}\right)\tilde{\rho}\right] = 0 \tag{2.16}$$

where $\tilde{T}$, $\tilde{P}$ and $\tilde{\rho}$ are the reduced temperature, pressure and density, respectively. The reduced parameters are given by

$$\tilde{P} = \frac{P}{P^*} \qquad P^* = \frac{\varepsilon^*}{v^*}$$
$$\tilde{\rho} = \frac{\rho}{\rho^*} \qquad \rho^* = \frac{M}{rv^*} \tag{2.17}$$
$$\tilde{T} = \frac{T}{T^*} \qquad T^* = \frac{\varepsilon^*}{R}$$

where T^*, P^*, ρ^* and υ^* are the characteristic temperature, pressure, density, and closed packed molar volume, respectively, ε^* is the interaction energy per mer, R is the gas constant and M is the molecular weight.

For mixtures, mixing rules are defined as follows:

$$T^*_{mix} = \frac{\varepsilon^*_{mix}}{R} \tag{2.18}$$

$$\varepsilon^*_{mix} = \frac{\sum\sum \phi_i \phi_j \varepsilon^*_{ij} v^*_{ij}}{v^*_{mix}} \tag{2.19}$$

$$v^*_{mix} = \sum\sum \phi_i \phi_j v^*_{ij} \tag{2.20}$$

where ϕ_i is the volume fraction of component i, and the cross terms can be expressed as

$$\varepsilon^*_{ij} = \left(\varepsilon^*_{ii}\varepsilon^*_{jj}\right)^{0.5}\left(1-k_{ij}\right)$$
$$v^*_{ij} = 0.5\left(v^*_{ii} + v^*_{jj}\right)\left(1-\eta_{ij}\right) \tag{2.21}$$

the binary interaction parameters, k_{ij} and η_{ij}, are obtained by fitting experiment data.

The SL EOS has been used to model polymer + SCF solvent and polymer + SCF solvent + cosolvent phase behavior with varying degrees of success [20]. Usually it is necessary to allow both binary interactions parameters to be functions of temperature to obtain a good representation of the phase behavior even if the polymer and SCF solvent are both non polar [67]. In an alternative approach, Kiran and co-workers [70-71] advocate allowing k_{ij} to vary with the molecular weight of the polymer. Of course, if k_{ij} is

allowed to vary, additional fitted parameters are introduced. However, it is not apparent how to extrapolate the values of these parameters from one system to another, since there is no fundamental basis for choosing a particular functional form for the temperature or molecular weight dependence. Another difficulty with predicting phase behavior is that the calculated cloud-point curves are very sensitive to the value used for k_{ij} which is usually determined after fitting at least a small amount of binary data [14]..

However, there are no generalizations regarding the relationship between the parameter and system variables such as temperature and pressure. Thus the parameters are quite different across polymer molecular weight and pressure (fits to low pressure sorption isotherms and high pressure cloud point data yield very different parameter values). And, there is no theoretical basis for obtaining these binary interaction parameters, the SL EOS cannot be used for predictive purposes [14].

Statistical Associating Fluid Theory (SAFT)

The Statistical Associating Fluid Theory (SAFT) EOS [72-75] is based on Wertheim's cluster expansion theory [76-77], which gives a relation between the residual Helmholtz energy due to association and the monomer density. Hard sphere, chain and association effects are incorporated using a reference fluid. Additional intermolecular forces are included through a mean field perturbation term (dispersion term).

With this approach, the residual Helmholtz free energy relative to an ideal gas reference state is

$$A^{res} = A^{hs} + A^{chain} + A^{assoc} + A^{disp} \tag{2.22}$$

where A^{hs} for segment-segment, hard-sphere repulsion, A^{chain} for connectivity of the segments, A^{assoc} for site-site specific interaction such as hydrogen bonding based on Wertheim's associating fluid theory [77], and A^{disp} for the mean-field dispersion are given in detail in the literature [72].

A large number of SAFT pure-component parameters for small molecules have been reported in the literature [78]. Regression of polymer PVT data, however, yields parameters that lead to poor phase equilibrium predictions [79-80]. As pointed by Lambert et al [58], SAFT EOS usually has poor performance at low pressure and high temperatures, or at high pressures and low temperature. Moreover, like in SL EOS, a nonzero value of k_{ij} is introduced to reasonably correlate the phase behavior of polymer solutions.

As can be seen from Figure 2.10, SL EOS fails to represent the PBMA-CO_2 cloud point data even when two temperature dependent binary interaction parameters are used. SAFT representation is in good agreement with experimental data. However, SAFT calculations are very sensitive to parameter values and polymer molecular weight [13].

Perturbed-Chain SAFT

While most SAFT versions use the hard sphere reference fluid, the PC-SAFT EOS uses a more realistic term to account for dispersive interactions between chains. It does this by applying perturbation theory using a hard chain fluid as the reference system, instead of a hard sphere reference considered in the earlier SAFT models [81-82]. The chain and association terms are both given by Wertheim's theories [77] as in the original

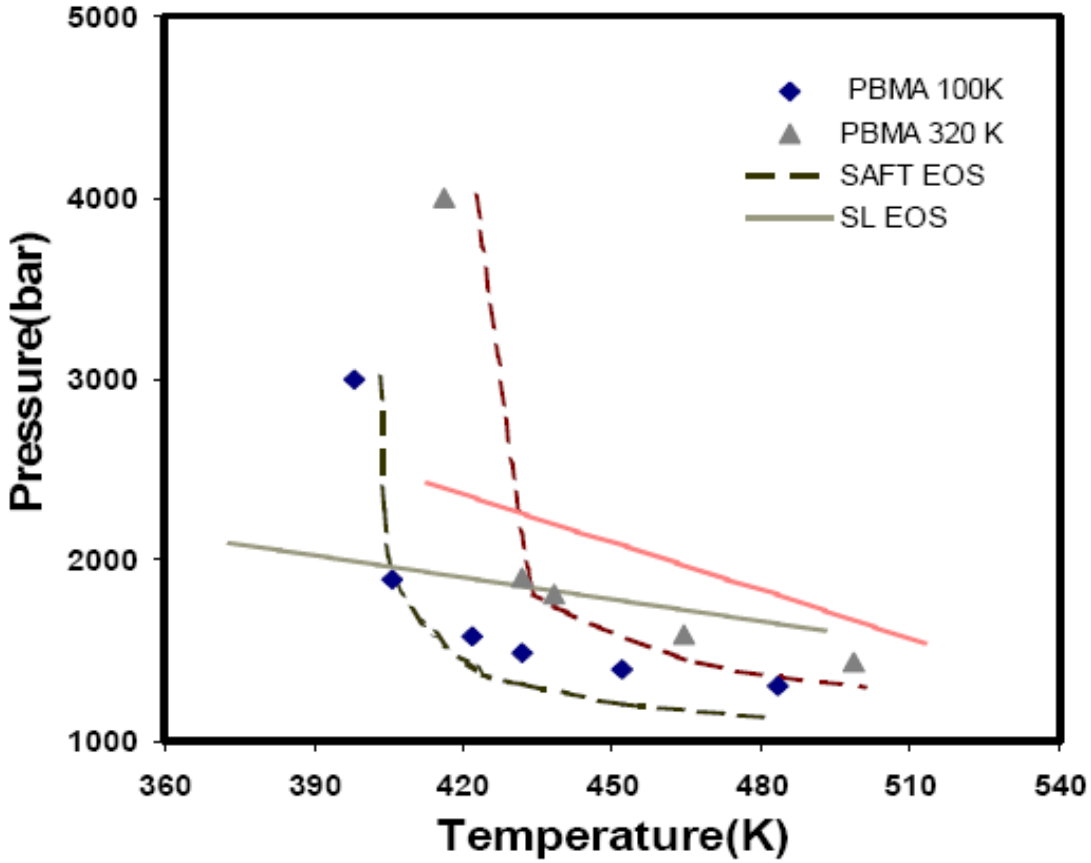

Figure 2.10 Experimental and calculated cloud point curves in PBMA + CO_2 for molecular weights of 100,000 and 320,000. Experimental data is from Ref. [30]. The polymer solubility is approximately 5 wt%. The solid lines represent SL EOS calculations and dashed lines are SAFT calculations [13].

SAFT version. The radial distribution function and hard-sphere Helmholtz energy function of simplified PC-SAFT are as follows [82]:

$$g^{hs}(d^{+}) = \frac{1-\eta/2}{(1-\eta)^3} \tag{2.23}$$

$$\frac{A^{hs}}{NkT} = \frac{4\eta - 3\eta^2}{(1-\eta)^2} \tag{2.24}$$

$$\eta = \zeta_3 = \frac{\pi}{6}\left(\frac{\sum_i x_i m_i d_i^3}{\sum_i x_i m_i}\right) \tag{2.25}$$

In comparison with the original SAFT version, calculations with the Perturbed-Chain SAFT model are more accurate using a temperature-independent binary parameter as seen in Figure 2.11 for CO_2 solubility in HDPE [83]. In general, the simplified PC-SAFT EOS is successful in modeling LLE, successfully predicting the correct behavior in many systems exhibiting upper, lower and both critical solution temperatures. Where predictions are not accurate, a small value of the binary interaction parameter is required to correlate experimental data. A limitation of PC-SAFT is the lack of a systematic method for estimating polymer parameters without the use of mixture data, particularly for associating polymer solutions. If possible such a general method should be based on data which are readily available for polymers e.g. solubility parameters.

2.4.2 Activity coefficient models

Activity coefficient models or excess Gibbs energy models provide the activity coefficient or activity from the following thermodynamic relationships,

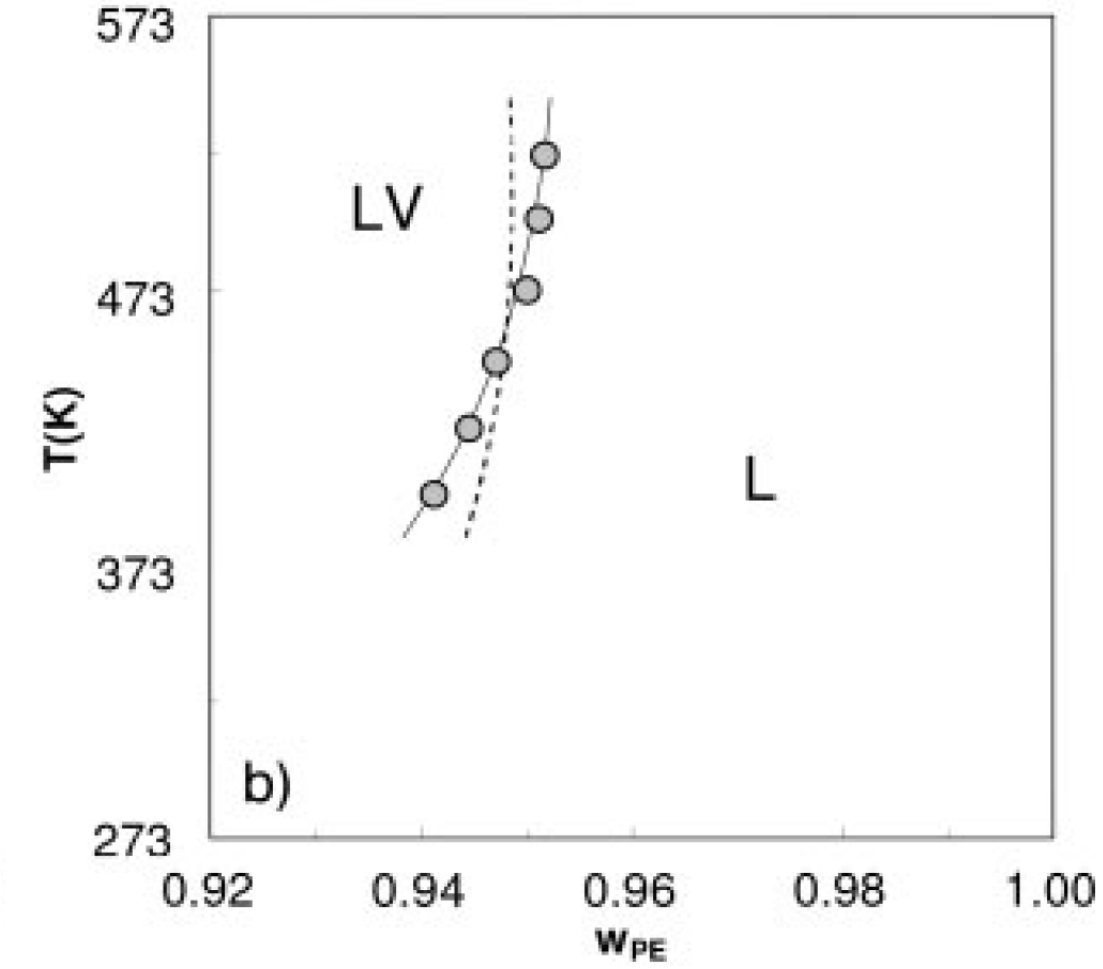

Figure 2.11 Solubility of CO_2 in HDPE at P = 90 bar (M_n = 87 kg/mol), soild line is for Perturbed-Chain SAFT (k_{ij}=0.181) and dashed line is for SAFT (k_{ij}=0.242) results [83].

$$RT\ln\gamma_i = \left(\frac{\partial nG^E}{\partial N_i}\right)_{T,P,N_{j\neq i}} \quad \text{or} \quad RT\ln a_i = \left(\frac{\partial n\Delta G_{mix}}{\partial N_i}\right)_{T,P,N_{j\neq i}} \tag{2.26}$$

Although the activity coefficient may also be calculated with an EOS model via Equation (2.27), the mixing rules used by an EOS are commonly not good enough to describe non-ideal behavior in solutions [84]. Therefore, in vapor-liquid equilibrium calculations we have to use the so called "gamma–phi" approach, where the vapor phase is described via an EOS (e.g. SRK, PR or PT) and the liquid phase is described via an activity coefficient model (e.g. RST) specifically suitable for liquid solutions.

$$\ln\gamma_i = \ln\left(\frac{\hat{\varphi}_i}{\varphi_i}\right) \tag{2.27}$$

where φ_i and $\hat{\varphi}_i$ are fugacity coefficient of pure component i and fugacity coefficient of i in mixture, respectively.

We may divide activity coefficient models in to two categories: (1) random-mixing model (e.g. Margules or van Laar equations); and (2) local composition models (e.g. Wilson, NRTL, or UNIFAC). For polymer solutions, the Flory-Huggins model, and UNIFAC model are widely used. We will discuss them and their variations in the following section.

Flory-Huggins Model

The most widely-used theory for calculating the Gibbs energy of mixing of polymer solutions is the Flory-Huggins (FH) theory [85-86] in which the polymer is assumed to consist of connected segments, each of which occupies one site of a lattice. Each solvent molecule also occupies a lattice site. Assuming that the segments are

randomly distributed, the free energy of mixing per mole of lattice sites for a mixture is given by

$$\frac{\Delta G_{mix}}{NRT} = \phi_A \ln \phi_A + \frac{\phi_B}{r} \ln \phi_B + \chi_{FH} \phi_A \phi_B \qquad (2.28$$

where R is the gas constant, N is the total number of lattice sites, r is the segment number of polymer molecule, ϕ is the volume fraction and χ is the Flory-Huggins interaction parameter. The first two terms on the right hand side of the above equation represent the combinatorial contribution to the entropy of mixing, which is derived by calculating all the different ways that chains can randomly pack on a lattice. Once the Flory Huggins χ parameter (which, in classical FH theory, includes only the enthalpy contribution to the free energy of mixing) is known, the entire phase behavior of the system can be calculated. With the adjustable χ parameter, FH model has been used for explaining the phase behavior, such as UCST, and osmotic pressure in dilute polymer solutions [87].

In the original theory, the entropy of mixing was assumed to be purely combinatorial, but it has been known for many years that non-combinatorial contributions are also important in polymer systems [88]. These are variously known as free volume effects, equation of state effects, and packing effects.

Limitations of FH theory include:

1. Segments are arranged on the lattice via a random walk. Thus, configurations where two polymer segments can occupy the same lattice cell are not excluded in a proper fashion.

2. Strong polar interactions or specific interactions like hydrogen bonding, which affect the enthalpy of mixing but can also significantly influence the entropy of

mixing, are not accounted for in the theory. These interactions can bias the orientation of certain types of molecules and lead to a decrease in the entropy of mixing.

3. Polymer molecules are constructed from freely jointed chains, and thus conformational characteristics are not affected by solution concentration.

4. The volume change upon mixing is assumed to be zero, which is a poor assumption when there are large differences in free volume between the polymer and the solvent [86].

Coleman Model

Coleman and Painter [89-90] combined an association model with the Flory-Huggins theory to develop a theory describing miscibility behavior of polymer blends with hydrogen bonding. Such a methodology can also be followed in describing solvent + polymer systems with specific interactions and hence is discussed here. The theory is based on the assumption that the Gibbs energy of mixing ΔG_{mix} consists of "weak" or "physical" interactions and "strong" or "chemical" interactions. Thus,

$$\frac{\Delta G_{mix}}{RT} = \frac{\phi_A}{M_A}\ln\phi_A + \frac{\phi_B}{M_B}\ln\phi_B + \chi\phi_A\phi_B + \frac{\Delta G_H}{RT} \tag{2.29}$$

The first two terms represent the combinational entropy of mixing. Since these entropy terms are usually small in polymer blends (in polymer-small molecule systems, the combinational entropy will also be affected by association), ΔG_{mix} is dominated by the balance between the third and fourth terms. The third term represent physical forces that are unfavorable for mixing and is controlled by the Flory parameter χ, which may be

estimated from solubility parameters for a set of carefully chosen groups which are free from association. The fourth term represents the favorable specific interaction for mixing due to hydrogen bonding. Its magnitude depends on two major factors. One is the relative strength of self-association to inter-association. If the strength of inter-association between two dissimilar polymers is greater than that of self-association of either of them, miscibility is favored. The other is the density of specific interacting sites in the blend. It is expected that otherwise immiscible blends will be made miscible if this density is increased by incorporating interacting groups. Hydrogen bonds are continually breaking and reforming by thermal agitation and, according to the association model, there exist instantaneous distributions of "free" monomers (B_1), dimers (B_2) and multimers (B_m), according to the association reaction scheme:

$$B_1 + B_1 \xleftrightarrow{K_2} B_2$$
$$B_m + B_1 \xleftrightarrow{K_B} B_{m+1} \quad (m > 1)$$

In the methodology of Coleman et al [89], K_2 and K_B for polymers containing hydroxyl groups are assumed to have the same values as those calculated from FTIR data on appropriate model compounds (e.g. 2-propanol or hexafluoro-2-phenyl-2-propanol). In general, K_A can be derived directly from IR studies of the single-phase blends.

$$B_m + A \xleftrightarrow{K_A} B_m A$$

With the values of K_2, K_B and K_A known in this way, ΔG_H can in principle be calculated and then the phase behavior of the blend becomes predictable. The book by Coleman et al. [89, 91] illustrates a wide range of hydrogen-bond-containing blends whose calculated phase diagrams agree with observed results. However, comparison of the calculated phase diagrams of a number of poly (4-vinylphenol), (PVPh) blends with

various polyacrylates, polyacetates, and polylactones (polymers of interest in this study) yield results that are poor when compared with experiments [89]. The inconsistency in prediction results may be attributed to discrepancies in spectroscopic measurements of equilibrium constants. Moreover, the Coleman model does not account for the compressibility of the lattice and free volume effects, therefore it cannot be used for Polymer-SCF systems without modification in the calculations of segment number, such as the free volume ratio can be used to calculate the segment number which is the idea in the modified g-ARTL [92].

UNIFAC-FV (Universal Functional Activity Coefficient-Free Volume) Model

The UNIFAC model is based on a two-liquid theory of liquid mixtures and does not explicitly take into account changes in free volume caused by mixing. To apply UNIFAC to polymer solvent mixtures Oishi and Prausnitz [93] modified the approach by replacing the volume fraction by the free volume fraction as follows

$$\ln \gamma_i = \ln \gamma_i^{FV} + \ln \gamma_i^{RES} \tag{2.30}$$

$$\ln \gamma_i^{FV} = \ln \frac{\phi_i^{FV}}{x_i} + 1 - \frac{\phi_i^{FV}}{x_i} \tag{2.31}$$

$$\phi_i^{FV} = \frac{x_i V_i^{FV}}{\sum_i x_i V_i^{FV}} \tag{2.32}$$

The residual contribution $\ln \gamma_i^{RES}$ is the contribution from interaction energies between each functional group, and calculated by the same method as the original UNIFAC [93-94]. The major limitation of UNIFAC-FV is that the method is commonly

useful only for low pressure systems over a narrow temperature range [84]. Therefore, the method may not be suitable for polymer + SCF systems.

g-ARTL (generalized Associative Reformulation of Thermodynamic Lattice) Model

The g-ARTL model was proposed by Sukhadia [95] and Variankaval [96] as a simple reformulation of the Flory–Huggins model to account for specific interactions between polymer segments and solvent molecules. In CO_2 + polymer systems with specific interactions, Electron-Donor-Acceptor (EDA) complexes can be formed between a polymer segment *P* and μ molecules of solvent S according to the following reaction:

$$\mathbf{P}+\mu\mathbf{S} \rightleftarrows \mathbf{PS}_{\mu}$$

The polymer + solvent mixture is thus assumed to consist of polymer-solvent complexes, unassociated solvent molecules and unassociated polymer molecules. The formation of complexes restricts a certain number of solvent molecules to specific positions on the lattice, with the remaining solvent molecules being distributed randomly. The expression for the Gibbs energy of mixing ΔG_{mix} is given by [13-14]

$$\begin{aligned}\frac{\Delta G_{mix}}{NRT} = {} & \chi_a \alpha \phi_2 + \chi_u (z-\alpha-2)\phi_2(\phi_1-\alpha\phi_2) + \frac{\phi_2}{\xi}\ln\phi_2 \\ & + \left(\frac{\phi_1-\alpha\phi_2}{1+\alpha}\right)\ln(\phi_1-\alpha\phi_2) - \phi_1 \ln\left(\frac{\phi_1}{\phi_1-\alpha\phi_2}\right) + \alpha\phi_2 \ln\left(\frac{\alpha\phi_2}{\phi_1-\alpha\phi_2}\right) \\ & + \phi_2(1-\alpha)\ln(1-\alpha) + \phi_2\alpha\ln\alpha\end{aligned} \tag{2.33}$$

where *z* is the lattice coordination number (generally assumed to be 10 in liquids), *N* is the total number of lattice sites, *R* is the gas constant, *T* is the temperature, ϕ_1 and ϕ_2 are the volume fractions of solvent (CO_2) and solute (polymer). The above expression includes an enthalpy of mixing term based on two types of contacts due to association

and dispersion, respectively. There are five characteristic quantities in this expression: the solvent–solute binding ratio μ; the association ratio α; the number of segments ξ; the interaction parameter for association χ_a; and the interaction parameter for dispersion χ_u. Several of these parameters take on constant values in specific systems, as discussed below. The specific interaction parameter for association α is related to the enthalpy of association ΔH_a via:

$$\chi_a = \frac{\Delta H_a}{RT} \tag{2.34}$$

Using the van't Hoff relationship, we may express the equilibrium constant K for the association reaction as follows:

$$\ln K - \ln K_0 = \frac{-\Delta H_a}{R}\left(\frac{1}{T} - \frac{1}{T_0}\right) \tag{2.35}$$

where K_0 is the equilibrium constant for association at a reference temperature T_0 (say, 298 K). In the above expression, ΔH_a has been assumed to be independent of T over the range of temperatures of interest. The equilibrium constant K is related to the association ratio α, the fraction of associated segments per polymer molecule, as follows:

$$\alpha = \frac{(1+K) - \sqrt{(1+K)^2 - 4\phi_1\phi_2 K(1+K)}}{2\phi_2(1+K)} \tag{2.36}$$

where ϕ_1 and ϕ_2 are volume fractions of the polymer and solvent, respectively. χ_a is therefore effectively replaced by ΔH_a and K_0 in the model.

The dispersion parameter χ_u is estimated from the solubility parameters δ_1 and δ_2 of CO_2 and the non-polar analog (homomorph) of the polymer as follows:

$$\chi_u = \frac{V_1\left(\delta_1 - \hat{\delta}_2\right)^2}{RT(z - \mu\alpha - 2)} \tag{2.37}$$

where the functional group in the polymer molecule which interacts with CO_2 is substituted with a non-polar group to obtain the homomorph. In Equation (2.37), V_1 is the molar volume of CO_2 [95].

Modified g-ARTL

The segment number (ξ) obtained by Sukhadia [95] from the ratio of the molar volumes of the solvent and the solute was obtained at ambient conditions (T= 298 K, P=1 bar). This works well for liquids, since liquid volumes are not significantly affected by pressure. However, it is quite inadequate at supercritical CO_2 conditions, because the molar volume of CO_2 changes dramatically with pressure above its critical point. Ozkan et al. [13] demonstrated the effect of pressure on segment number and suggested making the specific volume a function of pressure and temperature. The modified g-ARTL model (henceforth termed the Compressible Lattice Model) of Ozkan and Teja [97] uses the ratio of the molar volume of polymer and $scCO_2$ to calculate the segment number (ξ). Their model also needs two parameters to correlate phase equilibria in such systems, but the parameters do not depend on temperature or molecular weight. In addition, Ozkan and Teja have shown that it is possible to obtain one of the parameters from independent measurements (such as FTIR spectra) [13].

In more recent work, Kasturirangan and Teja [92] have shown that a better definition of ξ uses free volume difference as follows

$$\xi = \frac{v_p[T,P] - 1.2v_p^{vdW}}{v_{CO2}[T,P] - v_{CO2}^{vdW}} \tag{2.38}$$

where v_p is the specific volume of the polymer, v_{CO2} is the volume of CO_2, and v_{vdW} are van der Waals volumes.

The Compressible Lattice Model (CLM) model has been recently extended to predict both high pressure (cloud points) and low pressure (CO_2 sorption) equilibria within experimental error (lower than 5 %) using a single set of parameters [14]. In addition, Kasturirangan and Teja have combined the compressilbe lattice model with the Gibbs-DiMarzio criterion [98] to predict the depression in glass transition temperature in CO_2 + polymer systems.

2.5 Summary

In summary, the Sanchez-Lacombe and the SAFT or PC SAFT equation of state require two temperature and/or molecular weight dependent parameters to correlate experiment data over a range of temperatures, pressures, and molecular weights of the polymer [27, 79, 99]. The CLM model, which accounts for the compressibility appears to be a promising model for calculating phase equilibria and glass transition temperatures in polymer-SCFs systems. Both specific and non-specific interaction parameters in this model can be obtained by spectroscopy and simulation methods, so that a priori predictions of phase behavior can be accomplished. However, the model has not been evaluated for ternary systems such as polymer + CO_2 + cosolvent and polymer blends +CO_2. Also, a general method to obtain model parameters by experiment or simulation has not been established for this model.

CHAPTER 3

SPECIFIC INTERACTIONS IN POLYMER + CO_2 SYSTEMS FROM ATR-FTIR MEASUREMENTS

This chapter describes the measurement of specific interactions between carbonyl polymers and CO_2 by *in situ* ATR-FTIR spectroscopy and the extension of the methodology for other types of CO_2-philic functional groups.

3.1 Introduction

CO_2 is attracting much interest as a solvent for processing of polymers because it is non-toxic, non-flammable, chemically inert, and an inexpensive alternative to noxious organic solvents and chlorofluorocarbons [2, 36]. Kazarian et al [28] have shown that CO_2 and polymers such as poly(methyl methacrylate) (PMMA) exhibit evidence of Lewis acid-base interactions between the "electron poor" carbon atom of CO_2 and the "electron rich "oxygen atom of carbonyl group in the polymer. It has been suggested that such interactions give rise to many of the attractive properties of CO_2 – philic polymers such as PMMA [28]. Unfortunately, quantitative estimates of the strength of specific interactions have only been obtained in a small number of cases [19, 100-101]. In addition, *ab initio* estimates of these strengths [38, 40, 52] often differ significantly from the values obtained experimentally [102-104]. For example, quantum calculations indicate the existence of specific interactions between the fluorine atom and CO_2, although no such interactions have been detected between fluoromethanes and CO_2 in NMR studies [104]. It is therefore important to resolve these discrepancies in order to

develop or design CO_2 – philic polymers, and to exploit the properties of CO_2 - soluble surfactants [105-106] and physisorbents [107-108]. This work therefore attempts to establish a general experimental method to quantify specific interactions between CO_2 and CO_2 – philic functional groups in polymers.

Lewis acid-base interactions can often be estimated from the Drago correlation [109]

$$-\Delta H_a = C_A C_B + E_A E_B \qquad (3.1)$$

where C_A and E_A are measures of the acidity, and C_B and E_B are measures of the basicity. However, acid strength constants (C_A and E_A) are not available for carbon dioxide and therefore the Drago correlation cannot be used to estimate CO_2 + polymer interactions. An alternative is to measure the shift in the carbonyl (C=O) stretching frequency that occurs when a molecule containing the carbonyl group is exposed to a Lewis acid. This stretching frequency shift is often correlated to the Lewis acid-base interaction energy - ΔH_a [41-42]. Fowkes and Tischler [44] have shown that the carbonyl stretching frequency shifts to lower values in the presence of Lewis acid-base interactions. They derived a linear relationship between this frequency shift and ΔH_a. Kazarian et al [28] used this relationship to estimate the strength of specific interactions between CO_2 and C=O groups in PMMA. However, the Fowkes and Tischler relationship was obtained for interactions in the liquid phase containing small molecules, and its validity for CO_2 + polymer systems has yet to be confirmed. Furthermore, there is a large difference between the ΔH_a of -4 kJ mol^{-1} for CO_2 …C=O interactions reported by Kazarian et al [28] using the C=O stretching frequency shift and the value of -15 kJ mol^{-1} reported by Kilic et al [37, 102] using quantum calculations.

Quantitative estimates of interactions between CO_2 and small molecule Lewis bases have been provided by Meredith et al [47] via a van't Hoff plot of the equilibrium constant for the association reaction. This method is unambiguous and is extended to CO_2 + polymer systems in the present work. We have used ATR-FTIR (Attenuated Total Reflection Fourier Transform Infrared Spectroscopy) measurements to study peak shifts in the carbonyl stretching band and the CO_2 bending mode in carbonyl polymer + CO_2 systems, and related these frequency shifts to the equilibrium constant for the association reaction. We have then used the van't Hoff relation to obtain a quantitative estimate of the strength of the association interaction.

3.2 Experiment

3.2.1 Materials

Poly(vinyl acetate) (PVAc), poly(lactide) (PLA), poly(lactide-co-glycolide 85:15) (PLGA85), Poly(ε-caprolactone) (PCL) and Poly(ethylene gylcol) (PEG) were purchased from Aldrich Chemical Co. (St. Louis, MO); poly(methyl methacrylate) (PMMA) was purchased from Polysciences, Inc (Warrington, PA); Poly(vinylidene floride) (PVDF) was supplied by Du Pont (Wilmington, DE); Poly(methylsilsesquioxane) (PMSSQ) was purchased from Gelest, Inc (Morrisville, PA); Poly(sulfone) (PSF) was supplied by Solvay Advanced Polymers, L.L.C. (Alpharetta, GA); Polystyrene (PS) was purchased from 3M (Minneapolis, MN) and all other reagents were purchased from Aldrich (St. Louis, MO). High purity CO_2 gas (99.99 %) was purchased from Airgas Inc. (Radnor, PA) and used as received.

3.2.2 Experimental setup and procedure

ATR-FTIR spectra were measured at a resolution of 1 cm^{-1} using a Nicolet 550 Fourier transform spectrometer with a DTGS detector. Spectra were recorded using 64 scans in the 4000–500 cm^{-1} wavenumber range. The 2 mL cylindrical high pressure ATR Cell used to hold a sample was made by Axiom Analytical, Inc (Irvine, CA, USA) and incorporated a ZnSe crystal held by a Teflon O-ring. The incident angle of the IR beam was 45^{o}, giving 10 specimen-sensing reflections at the top face of the crystal. The cell was heated to a temperature of 353 K by circulating water, which also allowed the temperature in the cell to be controlled within ± 0.2 K using an Omega CN9000A controller. A CO_2 syringe pump connected to a pressure gauge (Heise, Model 710A) was used to keep the pressure in the cell constant within ± 0.1 bar.

ATR-FTIR spectra of polymer films coated on the ZnSe crystal were obtained as follows. A known volume (2.0 mL) of a solution containing 1-5 wt % polymer in toluene was injected into the cell and, after 1 h at room temperature, the solvent was evaporated by introducing a flow of nitrogen into the cell. A coating of polymer film on the ZnSe crystal surface was obtained upon volatilization of most of the solvent. The remaining solvent was removed by heating the film under vacuum until the temperature reached 353 K. The cell was kept at this temperature for 12 h to eliminate any residual solvent.

ATR-FTIR spectra of the polymer film under vacuum were collected at a set value of the temperature. Thereafter, CO_2 was slowly introduced into the cell until the pressure reached a predetermined value. The polymer was kept at this temperature and pressure for 2-24 h to ensure the attainment of equilibrium conditions. Spectra were collected during this time until no changes could be observed in the absorbance bands of

CO_2 or the polymer. Spectral results were displayed in terms of absorbance, defined as $-\log (I/I_0)$, where I and I_0 represent IR beam intensities in the sample and reference states, respectively. The reference spectrum was collected at vacuum conditions.

3.3 Results & Discussion

Figure 3.1 shows typical ATR-IR spectra of PMMA (under vacuum) and PMMA in the presence of CO_2 (at 40 bar) and 298 K. Note that IR bands of PMMA are clearly distinguishable from those of CO_2. Also, characteristic absorption bands of CO_2 of interest in this work can be found at 660 and 2338 cm^{-1}, corresponding to CO_2 bending and asymmetric stretching, respectively. The carbonyl stretching band of PMMA can be found at 1728 cm^{-1}. Although other characteristic bands were also measured during the scans, this work focuses on the carbonyl stretching and CO_2 bending modes only.

3.3.1 Carbonyl stretching

Figure 3.2 and Table 3.1 present FTIR measurements of carbonyl stretching vibrations in polymers exposed to different CO_2 pressures. To more clearly compare various spectra, the absorbance was normalized by the maximum absorbance in Figure 3.2. In the absence of CO_2, the peak of the PLGA85 carbonyl group stretching appears at a wavenumber of 1752 cm^{-1}. This peak shifts to higher wavenumbers in the presence of CO_2. At 40 bar CO_2, the peak can be found at 1754.6 cm^{-1}, corresponding to a higher frequency (blue-shift) of about 2.6 cm^{-1}. Similar results were obtained for other carbonyl polymers (see Table 3.1) in agreement with the experimental results of Nalawade et al [110].

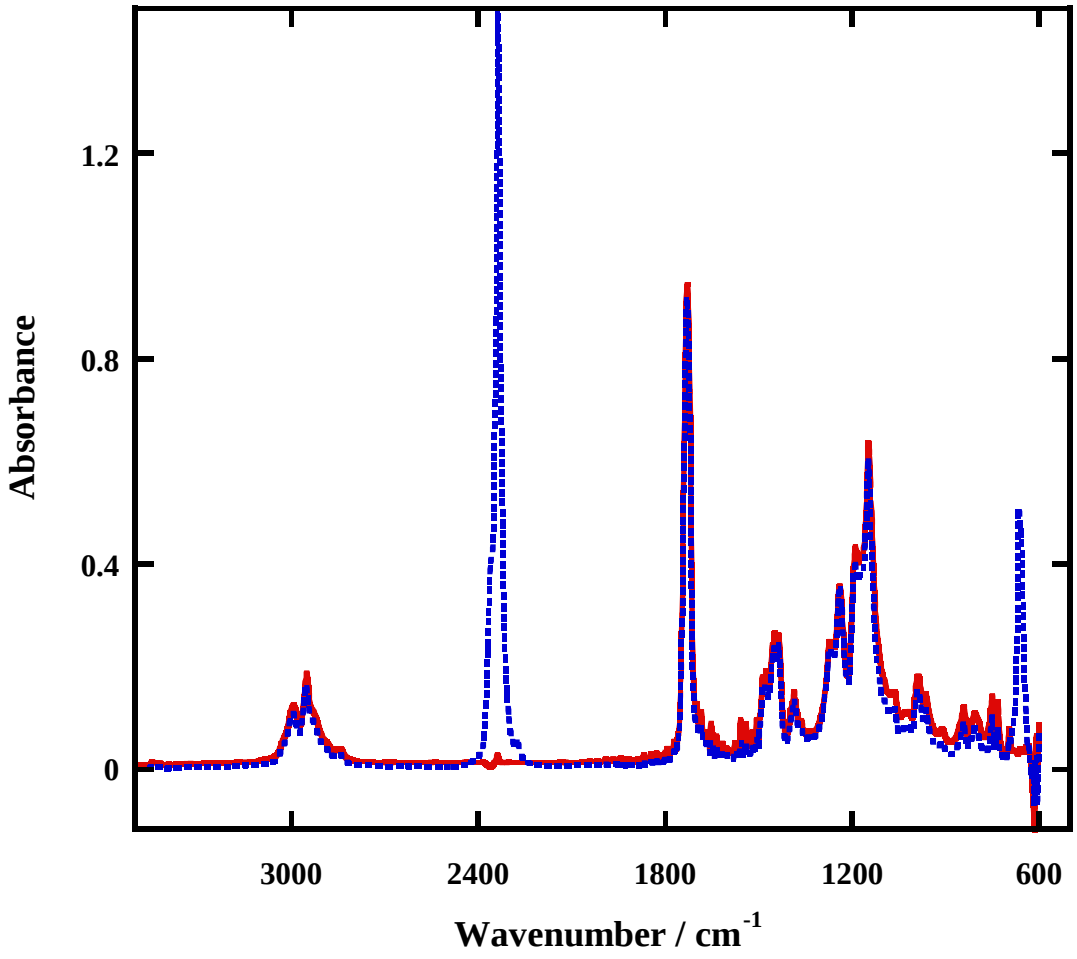

Figure 3.1 ATR-IR spectra of PMMA at 298 K before (red solid line) and after (blue dashed line) exposure to CO_2 at 40 bar.

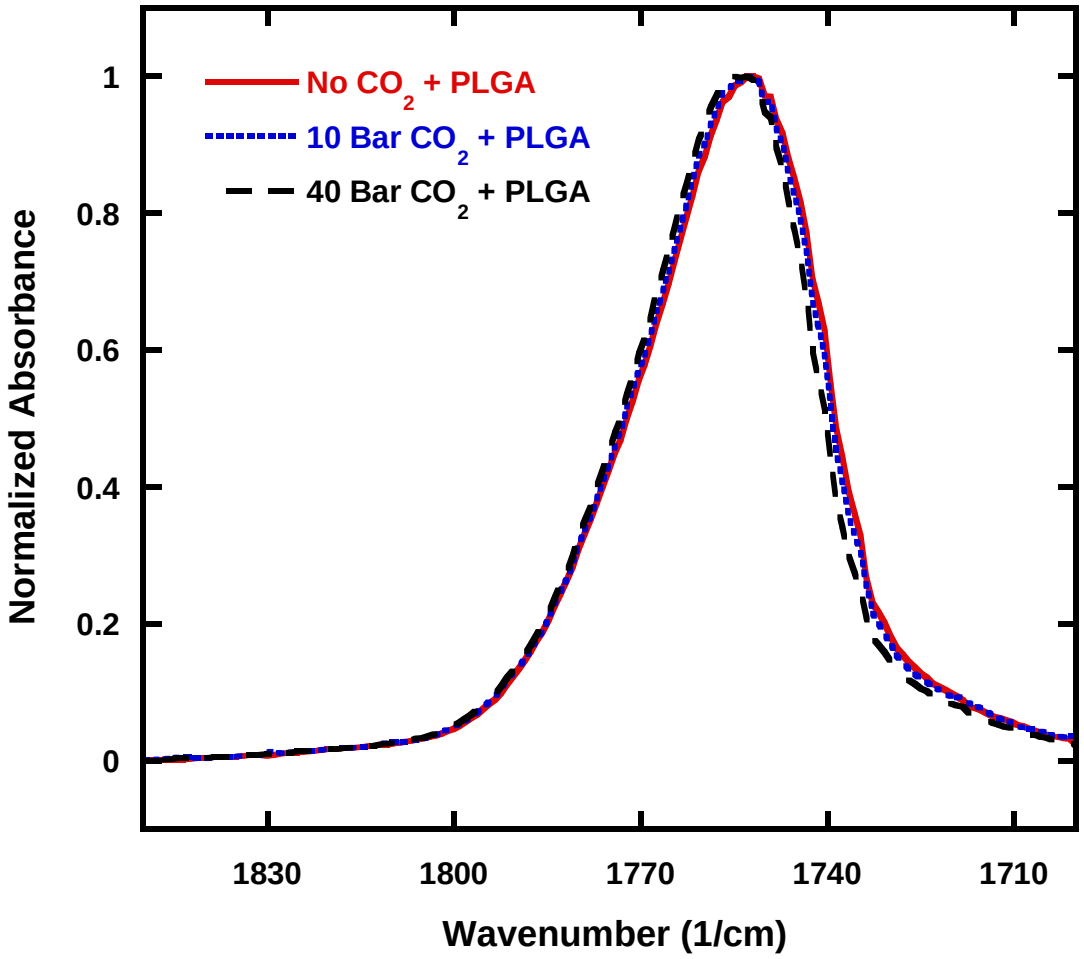

Figure 3.2 Normalized carbonyl stretching band in PLGA before and after exposure to CO_2.

Table 3.1 Wavenumbers of C=O stretching peaks in polymers.

C=O Stretching	Polymer in toluene	Solid polymer	Polymer + 10 bar CO_2	Polymer + 40 bar CO_2
PLGA85	1762.6	1752.3	1752.6	1754.6
PLA	1762.4	1754.9	-	1755.1
PVAc	-	1734.5	1735.0	1735.5
PMMA	1734.5	1728.2	1728.3	1729.6

Note: The C=O stretching peak of PMMA in 40 bar Ethane is at 1728.75 cm^{-1}

In contrast to the results reported above, both experiments [44] and quantum calculations [38] involving systems of small molecules show that the carbonyl stretching band shifts to lower frequency (red-shift) when there are Lewis acid-base interactions in solution. In order to explain the blue-shift obtained in our work, therefore, we explore solvent-induced stretching vibration frequency shifts [111-113] using the Kirkwood–Bauer–Magat (KBM) equation. This equation relates the stretching frequency shift $\nu_0 - \nu_S$ to the dielectric constant (ε) of the solvent as follows

$$\frac{\nu_0 - \nu_S}{\nu_0} = \frac{C(\varepsilon - 1)}{2\varepsilon + 1} \tag{3.2}$$

where ν_0 is the vibration frequency of the solute in the gas phase, ν_s is the frequency of the solute in the solvent, and C is a constant that depends on the properties of the solute. The dielectric constant of CO_2 in the liquid state is 1.5 [114], and is lower than that of carbonyl polymers such as PLA (= 3.6) [115]. According to Equation (3.2), therefore, CO_2 sorption in a carbonyl polymer should lead to a blue shift if dielectric effects are dominant. In order to account for solute-solvent interactions such as hydrogen bonding and association, a term that is proportional to the Gutmann acceptor number AN of the solvent is generally added to the KBM equation as follows [111-113]:

$$\frac{\nu_0 - \nu_S}{\nu_0} = \frac{C(\varepsilon - 1)}{2\varepsilon + 1} + k\,AN \tag{3.3}$$

where k is a constant. If the second term is greater than the dielectric term in Equation (3.3), then stretching frequencies would shift to lower values and a red-shift would be observed in experiments.

We did not detect any red-shifts in the carbonyl stretching frequency in our experiments (see Figure 3.2, and Table 3.1), which suggests that specific interactions were not large enough to overcome dielectric effects. To validate this hypothesis, we measured the ATR-FTIR spectrum of PMMA under 40 bar ethane pressure and found the carbonyl stretching peak at 1728.75 cm^{-1}. Therefore, we conclude that carbonyl stretching peak shifts are due mainly to dielectric effects and cannot be used to quantify specific interactions between CO_2 and the carbonyl group in polymers. It should be noted that Kazarian et al. [28] used the carbonyl stretching band of PMMA in toluene as a reference to estimate specific interactions via the carbonyl stretching frequency shift. FTIR spectra of CO_2 + PMMA in toluene were therefore measured at 298 K and different CO_2 pressures. The dielectric constant of toluene (= 2.4) is close to that of liquid CO_2, so that dielectric effects in the mixed solvent (CO_2 + toluene) would be about the same as in pure CO_2. We would expect to see a slight red shift in the carbonyl stretching band in these experiments if Lewis acid-base interactions between CO_2 and carbonyl group were significant. As shown in Figure 3.3, the maximum absorbance of carbonyl stretching of PMMA is at 1734 cm^{-1} in the absence of CO_2, with two smaller peaks are at 1739 and 1730 cm^{-1}. Increasing CO_2 pressure has an insignificant effect on the positions of these peaks. This means that shifts in the carbonyl stretching frequencies cannot be used to quantify specific interactions between CO_2 and carbonyl polymers contrary to what has been suggested in the literature [28].

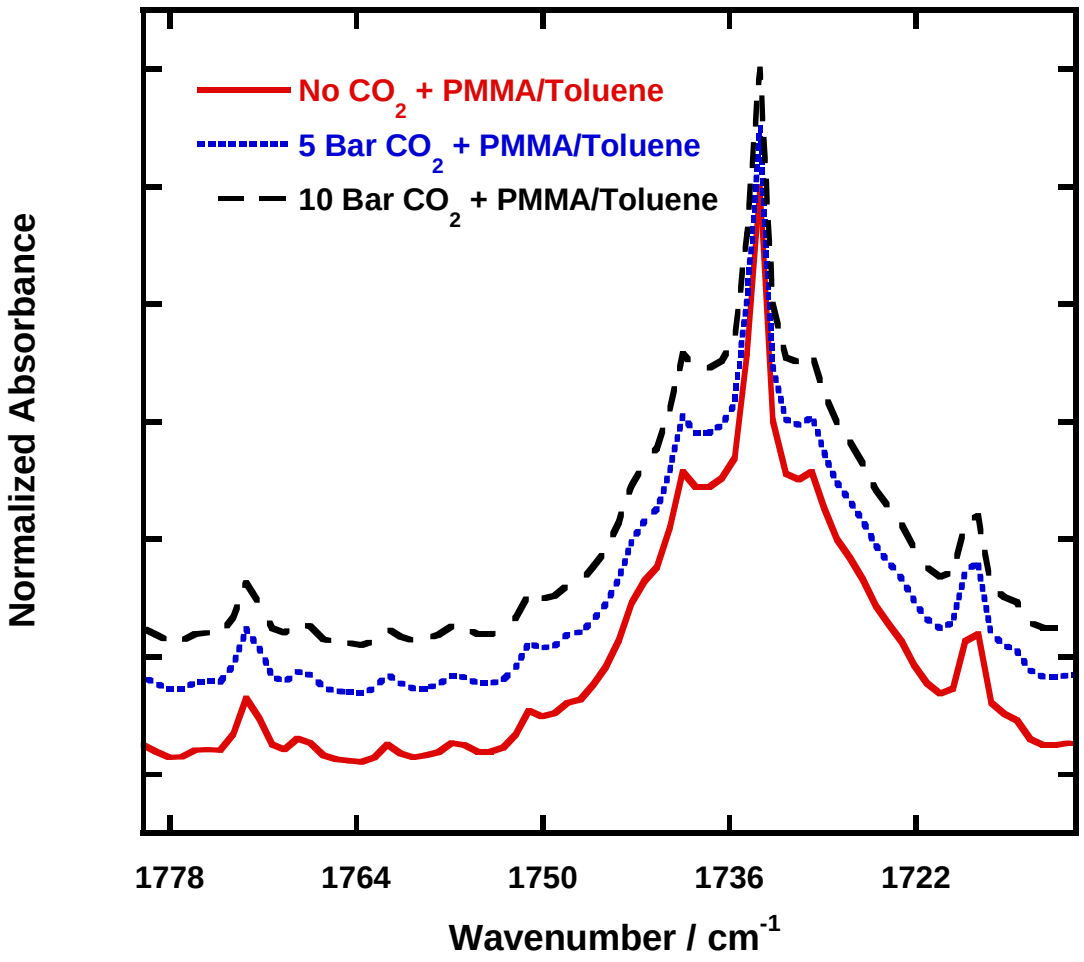

Figure 3.3 Normalized carbonyl stretching band in PMMA + toluene before and after exposure to CO_2. For clarity, the curves have been shifted upwards by 0.1 unit.

3.3.2 CO_2 bending

Changes in the CO_2 bending mode (v_2) when CO_2 is contacted with some liquids or polymers have been reported by Dobrowolski and Jamroz [116] and Kazarian et al [28]. As CO_2 is a weak Lewis acid, it can interact with Lewis bases such as the carbonyl group with its lone electron pair oxygen, forming an electron donor-acceptor (EDA) complex. Kazarian et al [28] pointed out that the v_2 bending mode of CO_2 can act as a sensitive probe of complex formation between CO_2 and polymers. However, they did not report any quantitative relationship between the strength of such interactions and the v_2 mode.

Figure 3.4 shows the IR spectrum for CO_2 + PMMA in the region of the CO_2 bending mode. Three peaks can be found in this region corresponding to the v_2 vibration of gas phase CO_2 at 667 cm^{-1}, the v_2 vibration of CO_2 absorbed in the polymer at 654 cm^{-1}, and another peak at 662 cm^{-1} that corresponds to free CO_2 trapped in the polymer matrix [116]. Dobrowolski and Jamroz [116] suggest that the peak with the lowest wavenumber corresponds to the EDA complex.

We assume that the EDA (CO_2…C=O) complex is formed according to the following reversible chemical reaction

$$\mathrm{P} + \mathrm{CO_2} \Leftrightarrow \mathrm{P...CO_2} \tag{3.4}$$

The equilibrium constant for this reaction is given by

$$K_C = \frac{[\mathrm{P...CO_2}]}{[\mathrm{P}][\mathrm{CO_2}]} \tag{3.5}$$

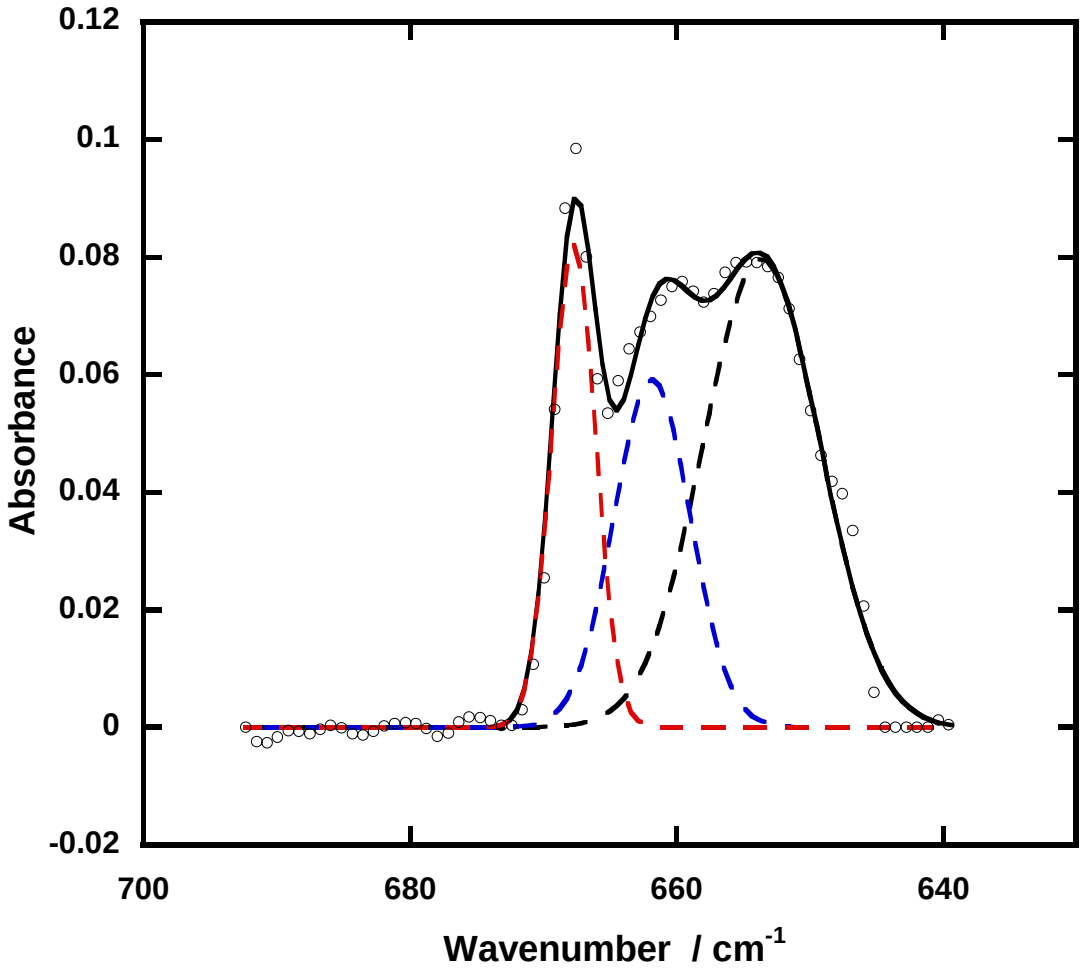

Figure 3.4 Bending mode of CO_2 in the IR spectrum of CO_2 + PMMA. Circles correspond to experimental data, the solid line represents the curve fit spectrum, and the dashed lines represent deconvoluted peaks. CO_2 gas phase peak at 667 cm^{-1}, absorbed CO_2 peaks at 662 cm^{-1} and 654 cm^{-1}.

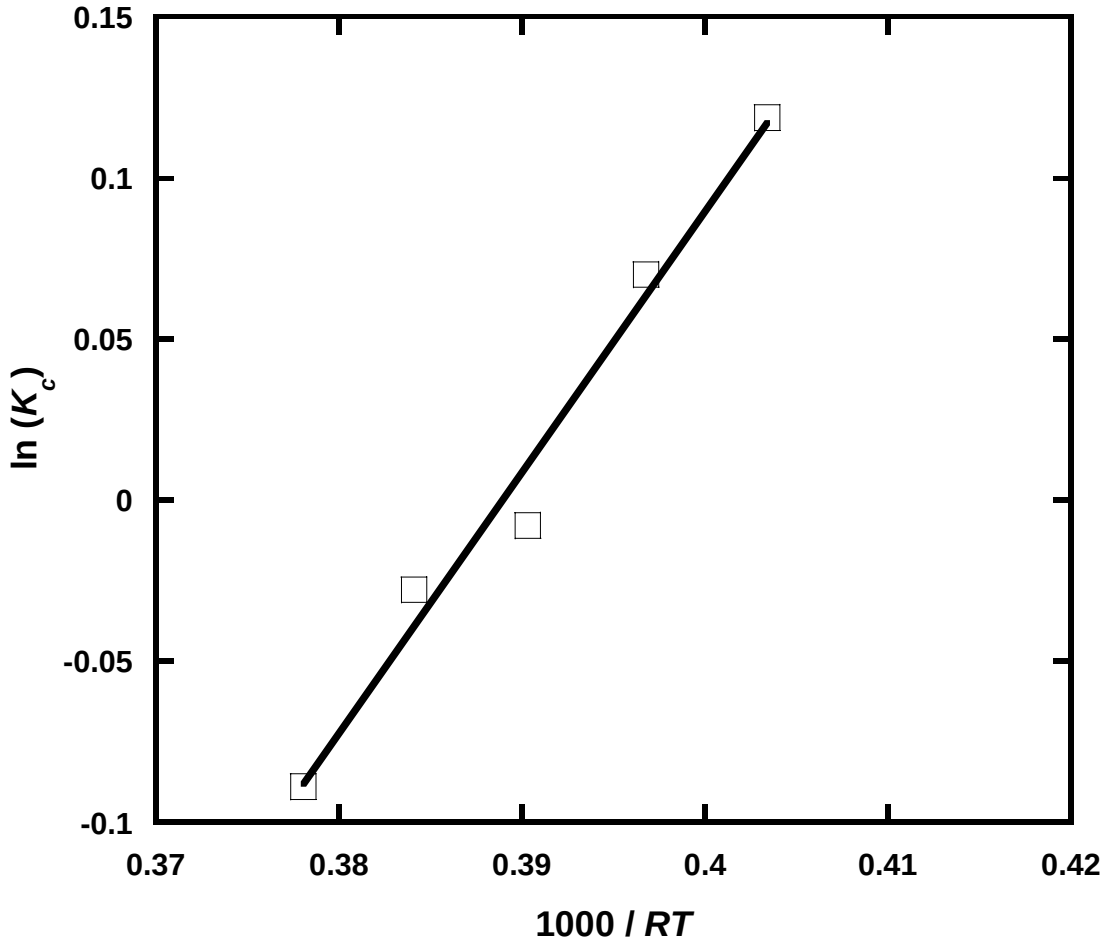

Figure 3.5 van't Hoff plot for the CO_2 - PMMA interaction at 10 bar CO_2 pressure and temperature range from 298 K to 318 K (R^2=0.9797).

where [P…CO_2] represents the concentration of the complex, and [CO_2] and [P] represent the concentrations of free CO_2 and polymer unit with C=O respectively. The enthalpy of complex formation ΔH_a can be obtained from the temperature dependence of $\ln(K_C)$ via to the van't Hoff relation.

We use the IR spectra to obtain the concentrations of free and associated CO_2 in order to calculate equilibrium constants in Equation (3.5). From the Beer-Lambert law, the concentration is given by $[C] = A/\varepsilon L$, where A and ε are the absorbance and extinction coefficients, and L is the path length. For the CO_2…P (carbonyl polymer) system, Equation (3.5) can be expressed as

$$K_C = \frac{[\mathrm{CO_2}]_\mathrm{A}}{[\mathrm{CO_2}]_\mathrm{F}\left(1-\frac{[\mathrm{CO_2}]_\mathrm{A}}{[\mathrm{P}]_0}\right)[\mathrm{P}]_0} = \frac{A_{[\mathrm{CO_2}]_\mathrm{A}}}{A_{[\mathrm{CO_2}]_\mathrm{F}}} \times \frac{(\varepsilon L)_{[\mathrm{CO_2}]_\mathrm{F}}}{(\varepsilon L)_{[\mathrm{CO_2}]_\mathrm{A}}} \times \frac{1}{\left(1-\frac{[\mathrm{CO_2}]_\mathrm{A}}{[\mathrm{P}]_0}\right)[\mathrm{P}]_0} \tag{3.6}$$

where $[\mathrm{CO_2}]_\mathrm{A}$ and $[\mathrm{CO_2}]_\mathrm{F}$ are the concentrations of associated CO_2 and free CO_2 respectively, $[\mathrm{P}]_0$ is the overall concentration of the polymer unit with C=O. Because the solubility of CO_2 in the polymer is low in our experiments (less than 5 wt %), the third term in Equation (3.6) can be approximated with a constant. Furthermore, we can assume that the second term in Equation (3.6) does not change with temperature or concentration of CO_2 in the polymer. In our calculation, the average absorbance of CO_2 bending mode at 662 ± 2 cm^{-1} was used for $A_{[\mathrm{CO_2}]_\mathrm{F}}$ and at 654 ± 2 cm^{-1} for $A_{[\mathrm{CO_2}]_\mathrm{A}}$ according to previous spectrum analysis (see Figure 3.4).

Figure 3.5 shows the van't Hoff plot for the specific interaction CO_2 and PMMA, where K_C values were calculated form Equation (3.6) using only the first term. The slope

of the van't Hoff plot yields an enthalpy of the association interaction $-\Delta H_a$ with an uncertainty of ± 3%. The strength of specific interactions and the half-width of CO_2 bending band for other carbonyl polymer + CO_2 systems are reported in Table 3.2. We infer from our results that the strongest interaction between CO_2 and the C=O group is exhibited in poly (vinyl acetate) because the half-width of the CO_2 bending band is largest in this polymer. This is in agreement with observations of Kazarian et al [28].

3.3.3 Comparison with quantum calculations

Several researchers [37-38, 102] have employed quantum calculations to quantify interactions between CO_2 and carbonyl polymers (using a single repeat unit in the ground state T = 0 K) and their results are listed in Table 3.3. Thus, Nelson and Borkman have reported CO_2 and methyl acetate binding energies are -16.6 kJ mol^{-1} and -17.3 kJ mol^{-1} for CO_2 attacking the carbonyl oxygen from the ester side and methyl side configurations, respectively [38]. Similarly, Kilic et al. have reported CO_2 and isopropyl acetate interaction energies of -15.9 and -14.2 kJ mol^{-1} for CO_2 attacking the carbonyl oxygen from the ester side and methyl side configurations, respectively [37, 40]. Based on these values, we may estimate the average interaction energy between CO_2 and the carbonyl group to be about -13 kJ mol^{-1} at room temperature (assuming a thermal energy kT of ~ 2.5 kJ mol^{-1} at 300 K). This is reasonably close to our measured value of -8.5 kJ mol^{-1}.

3.3.4 Specific interactions in polymers with other functional groups

We also studied other polymers with different functional groups. The typical CO_2 bending mode of CO_2 in the IR spectra of CO_2 + PEG, CO_2 + PMSSQ and CO_2 + PSF are shown in Figure 3.6. We can clearly see the associated CO_2 peak at 649 and 652 cm^{-1}

Table 3.2 Quantified specific interactions and half-width of the bending band of CO_2 in carbonyl polymers.

Polymer	ΔH_a kJ mol^{-1}	$\Delta \nu_{1/2}$ cm^{-1}
PLGA85	-8.5	15
PLA	-8.8	15
PCL	-8.8	14
PVAc	-9.3	16
PMMA	-8.0	15

Table 3.3 Binding energies between CO_2 and carbonyl group from quantum calculations.

	ΔH_a kJ mol^{-1} A	ΔH_a kJ mol^{-1} B	Reference
Methyl acetate	-16.6	-17.3	[38]
Isopropyl acetate	-15.9	-14.2	[40]
Isobutyl acetate	-14.3	-14.1	[40]

Note: (A) CO_2 attacking carbonyl oxygen from ester side

(B) CO_2 attacking carbonyl oxygen from methyl side

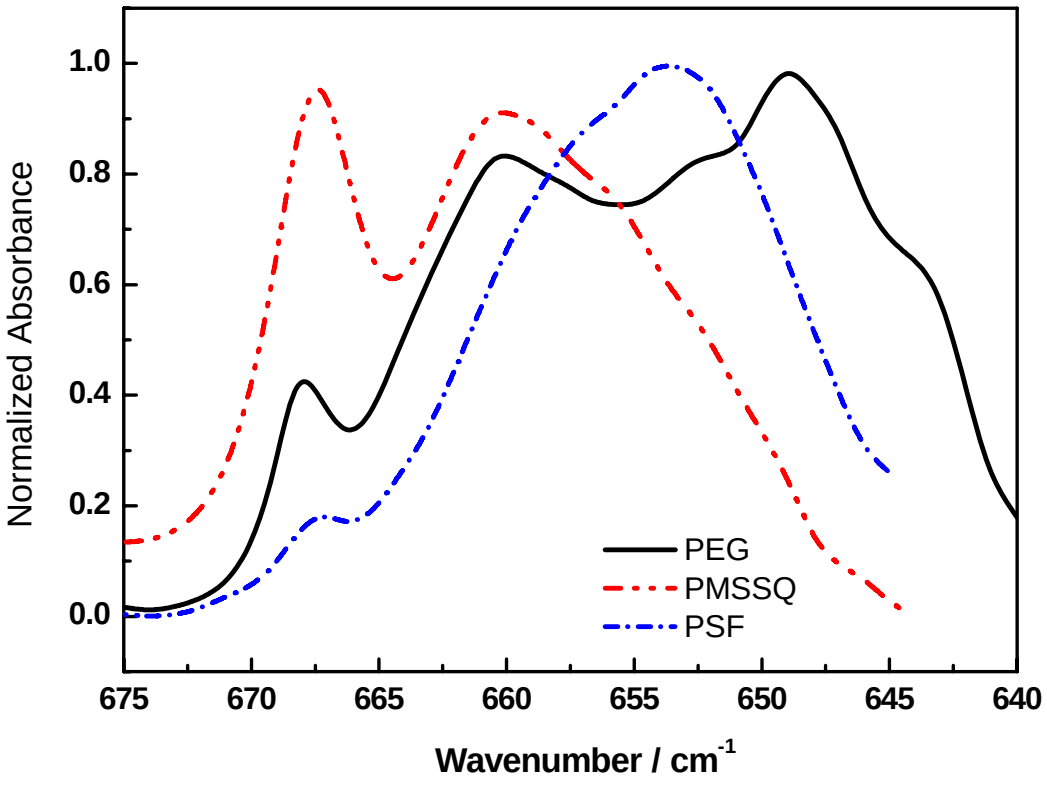

Figure 3.6 Bending mode of CO_2 in the IR spectrum of 10 bar CO_2 + PEG, 20 bar CO_2 + PMSSQ, and 20 bar CO_2 + PSF at 298K.

Table 3.4 Quantified specific interactions and half-width of the bending band of CO_2 in other polymers with different functional groups.

Polymer	Functional group	ΔH_a kJ mol^{-1}	$\Delta v_{1/2}$ cm^{-1}
PEG	C-O-C	-11.5	22
PSF	O=S=O	-8.5	13.5
PMSSQ	Si-O-Si	-6.8	13
PVDF	-F	-	8
PS	Benzene ring	-	11

for PEG, and 652 cm^{-1} for PSF, respectively. The associated CO_2 peak for PMSSQ is not very obvious, but around 655 cm^{-1} which can be determined at a higher temperature condition. The free CO_2 peak at 662 cm^{-1} can be assigned. The quantified specific interactions and half-width of CO_2 bending band are shown in Table 3.4. In our experiments, we did not see strong associated peak for CO_2 + PVDF, and CO_2 + PS. Therefore, only half-width the bending band are listed for PVDF and PS. According to the Table 3.4, as the increase of the strength specific interactions ($-\Delta H_a$), the half-width is also increased. This is in agreement with observations of Kazarian et al [28]. On the basis of both quantified specific interaction and half-width, we may conclude the the specific interaction in CO_2 + PVDF and CO_2 + PS are much weaker than that in CO_2 + PEG, CO_2+PVAc, CO_2+ PSF, and CO_2 + PMSSQ.

3.4 Conclusions

We have measured FTIR spectra of carbonyl polymers under CO_2 pressure using a high pressure ATR cell. Blue shifts in the carbonyl stretching frequencies were observed in CO_2 + PVAc, PMMA, PLA, or PLGA85 systems. These CO_2 induced blue shifts can be attributed to dielectric effects, which are much greater than specific interactions between CO_2 and carbonyl groups. As a result, CO_2 induced carbonyl stretching frequency shifts cannot be used to quantify specific interactions in these systems. However, we also show that an equilibrium constant method based on the CO_2 bending mode can be used to quantify specific interactions between CO_2 and carbonyl polymers. This method shows that the strength of these interactions is in the order: CO_2 + PVAc > CO_2 + PCL ≈ CO_2 + PLA > CO_2 + PLGA85 > CO_2 + PMMA. This method can

also be extended to other CO_2 philic polymers, leading to CO_2 + PEG > CO_2 + PVAc > CO_2 + PSF > CO_2 + PMSSQ >> CO_2 + PVDF & PS.

Yuan, Yanhui and Teja, Amyn S., *Quantification of specific interactions between CO_2 and the carbonyl group in polymers via ATR-FTIR measurements*, Journal of Supercritical Fluids, to be submitted.

CHAPTER 4

SPECIFIC INTERACTIONS IN POLYMERS + CO_2 FROM MOLECULAR DYNAMICS CALCULATIONS

4.1 Introduction

As mentioned in Chapter 2, specific interactions between CO_2 and several polymer repeat units have been studied using quantum mechanical calculations [37, 40, 52, 103, 117-118]. One of the major limitations of the quantum approach is that only a few polymer oligomers can be investigated. Recently, molecular dynamics simulations have been used to investigate specific interactions between CO_2 and solutes ranging from ionic liquids [119] to polymers [120-122]. However, there appears to be room for additional studies of specific interactions in CO_2 and polymer systems using molecular dynamics simulation [123-125]. This Chapter therefore deals with molecular dynamics (MD) simulations to investigate: (1) CO_2 accessibility in isomers such as PVAc and PMA; (2) the value of the binding ratio; (3) specific interactions between CO_2 and various functional groups.

4.2 Simulation Method

4.2.1 Molecular dynamics

Molecular dynamics essentially samples conformations by integrating Newton's equations of motion over time. In this work, MD simulations were carried out using the commercial software package MOE (Molecular Operating Environment) [126]. The OPLS (Optimized Potentials for Liquid Simulations) force field was selected to describe

the force between atoms, and combined NVT ensemble was used for CO_2 and polymer systems with Nose-Hoover thermostats to keep temperature constant [127].

A model was constructed for polymer chains consisting of 50 - 100 repeat units, and the polymer chains were folded into a 30 Å box with periodic boundaries. Then, 50 - 100 molecules of CO_2 were added into the box (shown in Figure 4.1). In each simulation, a minimized energy conformation at $T = 0$ K was used as the initial conformation.

The NVT MD simulations were run from 273 to 373 K. The time step was 0.002 ps, and the simulation was sampled every 0.5 ps. The simulations were run for 10000 ps to reach equilibrium, the potential energy levels off (shown in Figure 4.2), and the final 1000 samples (500 ps) were used in the data analysis. The custom SVL MD code (MD2006.SVL provided by Dr. Ludovice) was used for these simulations [127], and a pair distribution function code (pdf.SVL, in Appendix C) was used to analyze the results.

4.2.2 Quantify the specific interaction energy

As proposed by Variankaval [96], the equilibrium constant for association (K) can be determined from estimates of the relative amounts of associated and unassociated species present in a solution at different temperatures. For a binary solution containing ξN_2 polymer segments and N_1 solvent molecules, of which $n_{ij}(r_c)$ are associated, the equilibrium constant is given by

$$K = \frac{\left[\dfrac{n_{ij}(r_c)}{N_1 + \xi N_2 - n_{ij}(r_c)}\right]}{\left[\dfrac{\xi N_2 - n_{ij}(r_c)}{N_1 + \xi N_2 - n_{ij}(r_c)}\right]\left[\dfrac{N_1 - n_{ij}(r_c)}{N_1 + \xi N_2 - n_{ij}(r_c)}\right]} \tag{4.1}$$

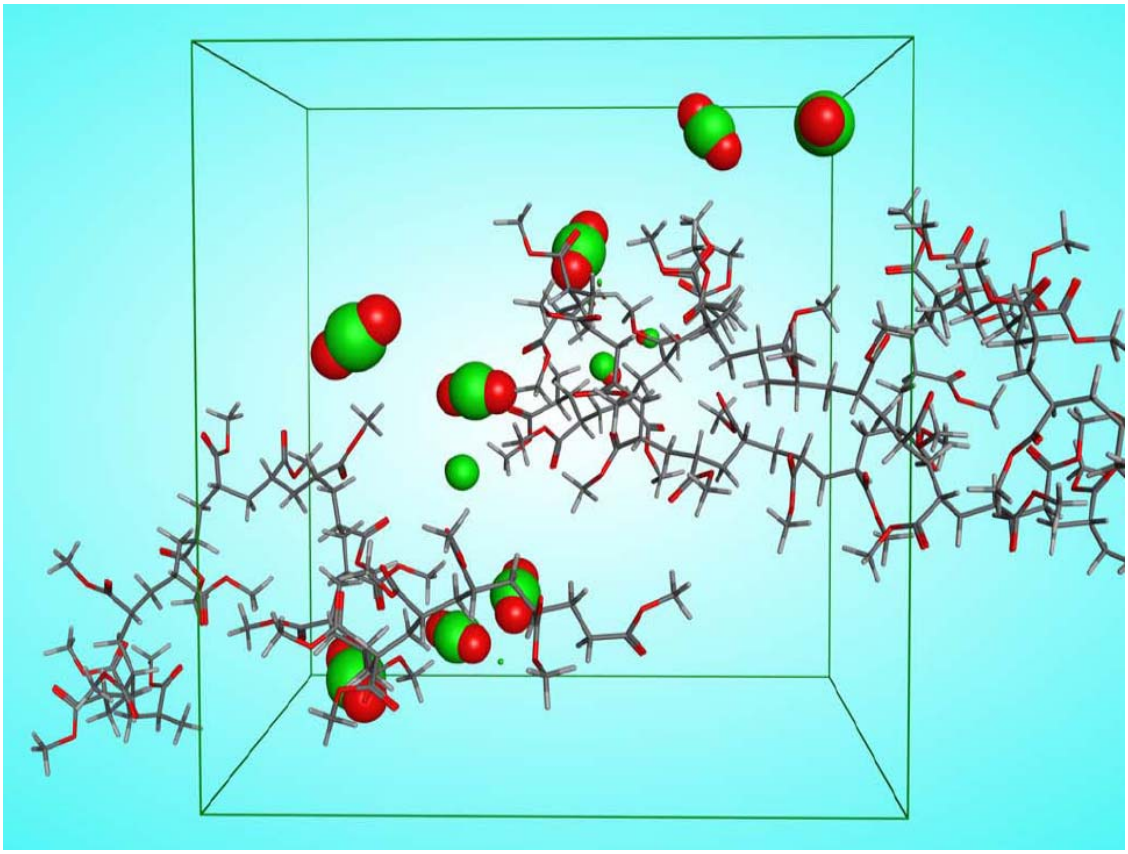

Figure 4.1 Representative structures for CO_2 + polymer system in a box with periodic boundaries.

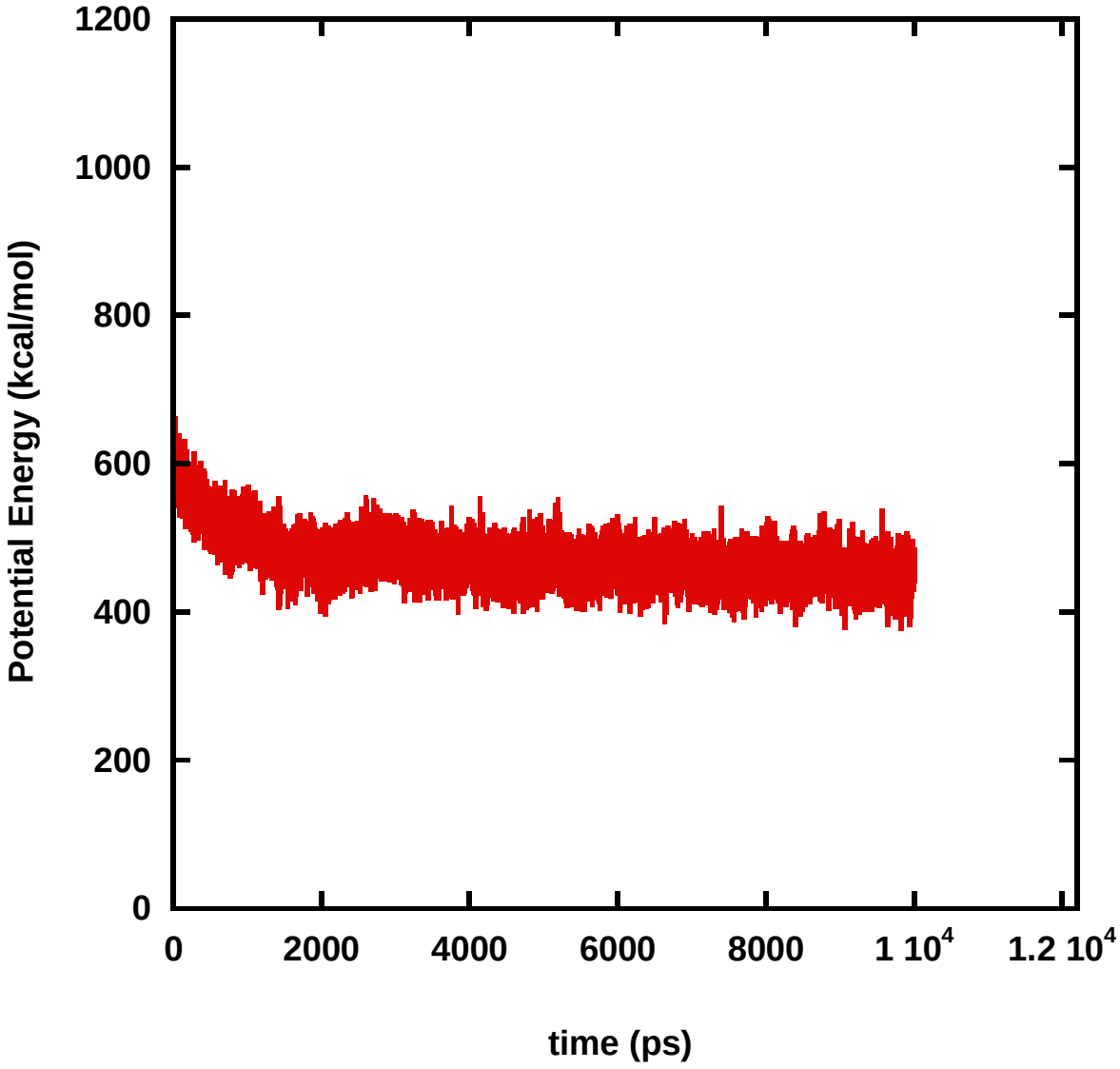

Figure 4.2 Potential energies in an equilibrated 10ns simulation of PVAc and CO_2 system.

In this equation, ξ is the number of repeat unit in a polymer chain, and $n_{ij}(r_c)$ indicates the number of associated pairs within a sphere of radius r_c. This distance (r_c) can be assumed to be the first minimum in the pair distribution function, which can then be integrated to obtain $n_{ij}(r_c)$. The pair correlation function and the number of associated pairs are expressed as

$$g_{ij}(r) = \frac{dn_{ij}(r)/dV}{N_{ij}/V} \tag{4.2}$$

and

$$n_{ij}(r_c) = \frac{N_{ij}}{V}\int_0^{r_c} g_{ij}(r)4\pi r^2 dr \tag{4.3}$$

NVT MD simulations were carried out at different temperatures to obtain the specific interaction energy ΔH_a from the slope of ln K versus 1/T plot.

4.3 Results and Discussion

4.3.1 Pair distribution function

Figure 4.3 shows the pair distribution functions (PDF) of carbonyl oxygen in PVAc and carbon in CO_2. In the MD simulations, the total number of PVAc repeat units (mer) is 60, and the number of CO_2 molecules is 60. The CO_2 density is 0.30 g/cm^3, comparable to the density of gas phase CO_2 at 300 K and 70 bar. As we can see from the graph, the position of first peak in the PDF is at 3.2 Å, which means that the most favored distance between O (C=O) and C (CO_2) is 3.2 Å. This value is reasonably close to the value (2.8~2.9 Å) of the minimized energy state from quantum calculation [40]. Because these MD simulations are run at 300 K, specific interactions between CO_2 and the

carbonyl group because of the effect of the kinetic energy. The first minimum of the PDF is at 4.5 Å. This can be treated as the maximum distance for specific interactions, or r_c in Equation (4.1) and the number of associated pairs $n_{ij}(r_c)$ obtained from Equation (4.3).

Figure 4.3 also shows the simulation results for a different number of repeat units. We can see that position of the first peak in PDF almost is still ~3.2 Å. Thus, the number of mers in a polymer chain will have little effect on the position of the peak for a polymer chain with more than 10 mers.

Figure 4.4 shows the simulation results for temperatures between 300 K and 380 K. We can see that the position of the first peak in the PDF is almost unchanged at ~ 3.2 Å. However, the intensity of the fist peak in PDF decreases as the temperature increases. This implies that the number of associated CO_2 molecules decreases but the most favored distance between O (C=O) and C (CO_2) remains the same in this temperature range.

Figure 4.5 shows the pair distribution functions (PDF) of carbonyl carbon in PVAc and oxygen in CO_2, ether oxygen in PVAc and carbon in CO_2. The first peak positions of these two PDFs are 4.6 Å and 5.5 Å respectively. These values are larger than the value 3.2 Å from the pair distribution functions (PDF) of carbonyl oxygen in PVAc and carbon in CO_2. Therefore, we may infer that the specific interaction between carbonyl oxygen in polyesters (such as PVAc, PMA) and carbon in CO_2 is dominated.

4.3.2 Accessibility

Accesibility of the carbonyl group to CO_2 will lead to differences in specific interactions between CO_2 and C=O in isomers (e.g. PVAc and PMA). Figure 4.6 shows the PDFs of PVAc and PMA at the same conditions. We can clearly see that the intensity

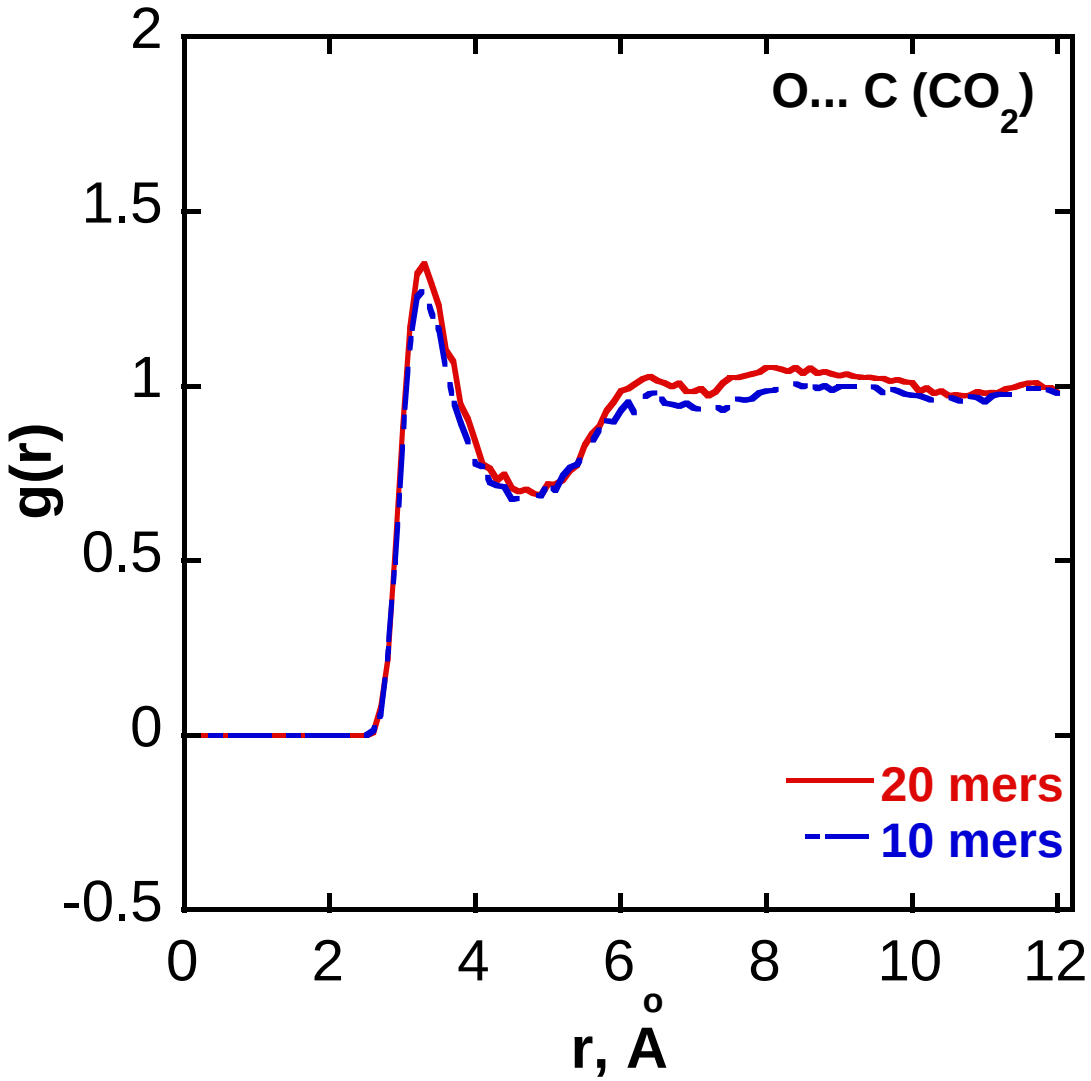

Figure 4.3 Pair distribution function of carbonyl oxygen O…C (CO_2) in PVAc + CO_2.

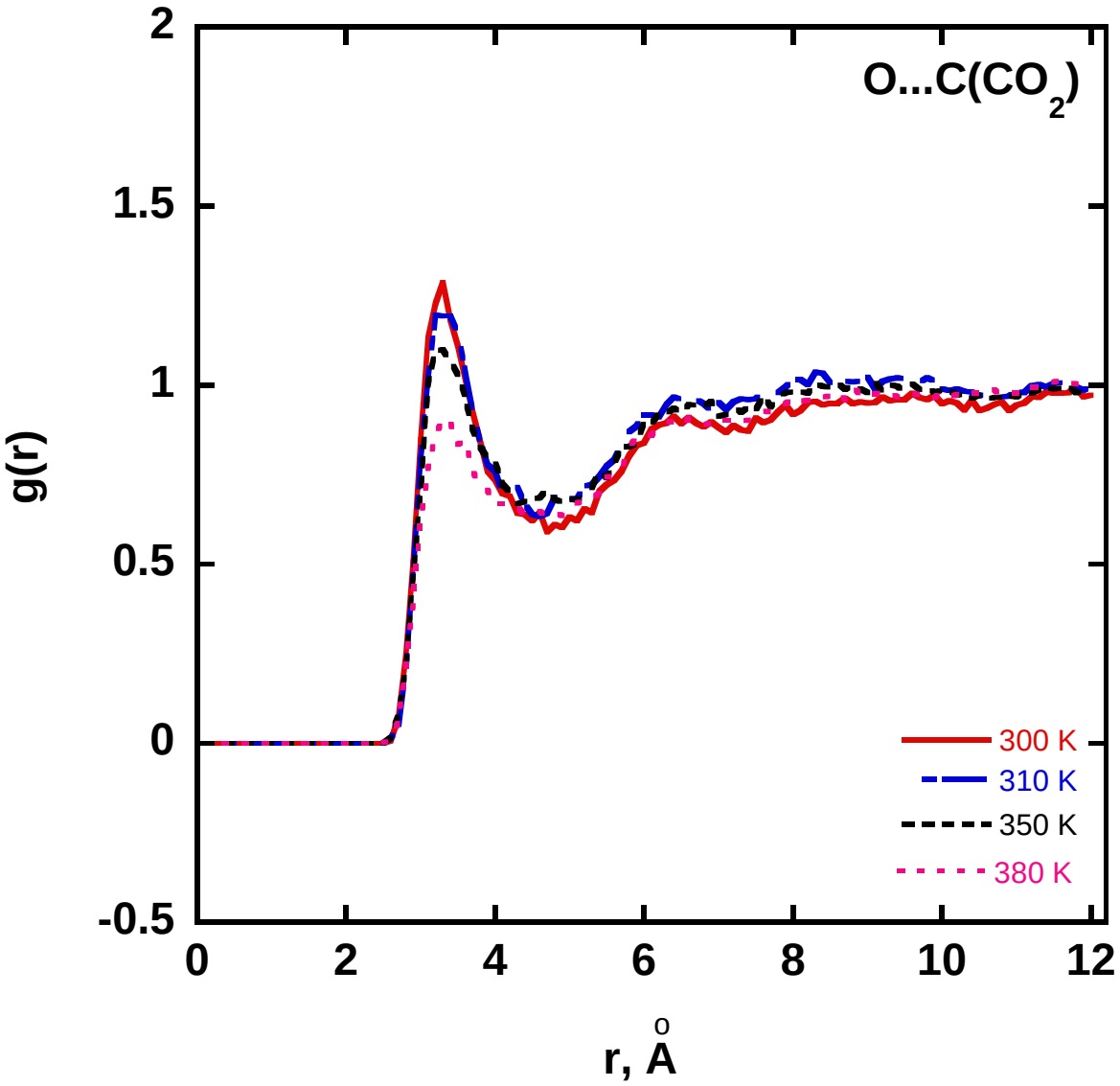

Figure 4.4 Pair distribution function of carbonyl oxygen O…C (CO_2) in PVAc + CO_2at different temperatures.

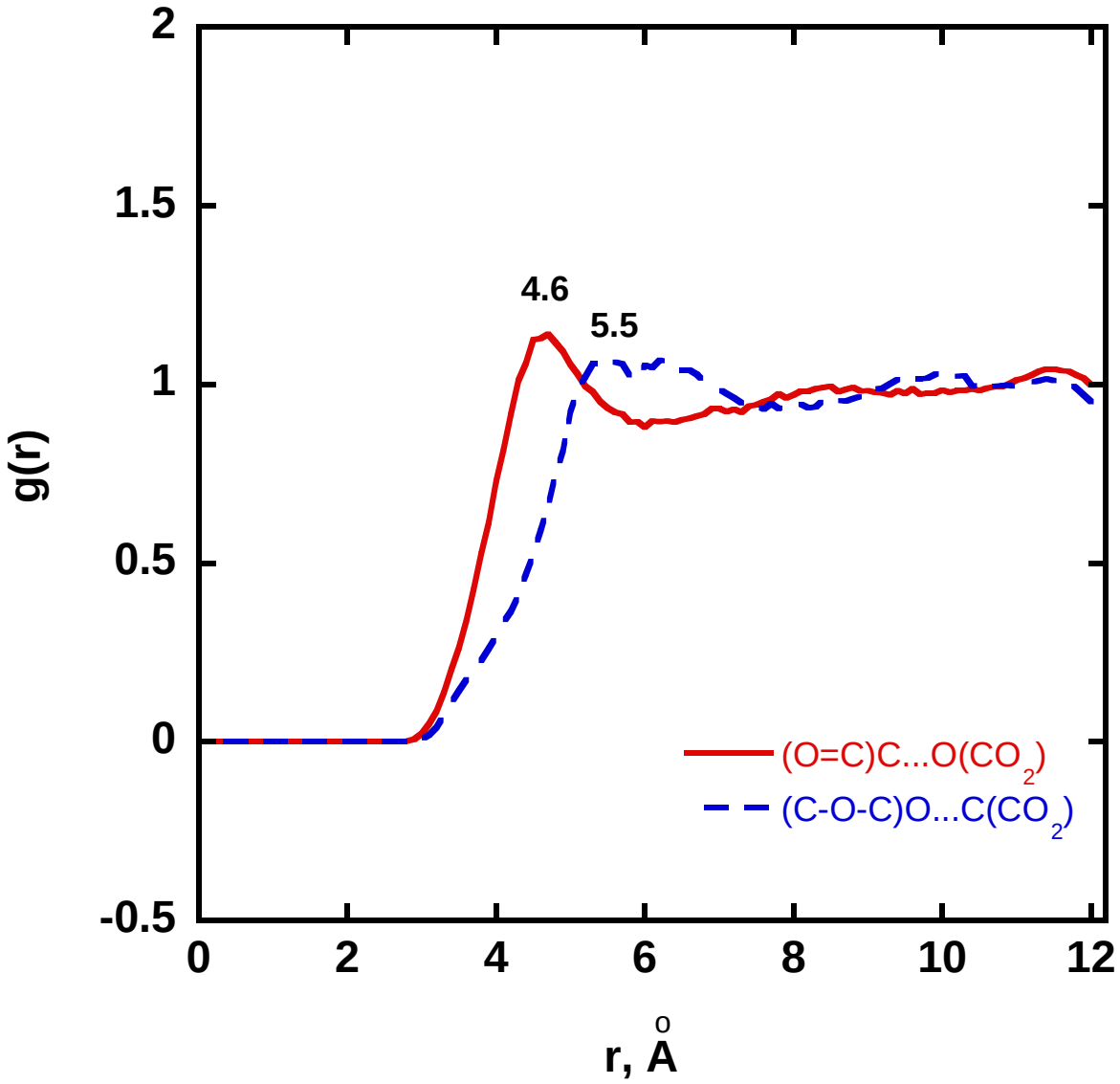

Figure 4.5 Pair distribution function of carbonyl carbon C…O (CO_2) and ether oxygen O…C (CO_2) in PVAc + CO_2 at 300 K.

of the first peak in CO_2 + PVAc is higher than that in CO_2 + PMA. This implies that the number of CO_2 molecules associated with PVAc is higher than the number associated with PMA, and that the carbonyl group in PVAc is quite accessible to CO_2. Similarly, the PDFs in Figure 4.7 for PVAc, PLA, and PVMK show that the carbonyl group accessibilities are in the order, PVAc > PVMK > PLA > PMA.

4.3.3 Binding ratio

In all previous studies of polymer + CO_2 systems, the binding ratio μ was assumed to be 1 [13-14]. It is necessary to validate this assumption using MD simulations. Figure 4.8 shows the single association (μ = 1) rate for 1000 conformations in the CO_2 + PVAc system. Each data point represents a conformation, and r_a is the association distance. As the association distance increases, the single binding rate should decrease as shown in Figure 4.9. We can see that the single association rates is 96 % with r_a =3.2 Å, and 85 % with r_a = 4.0 Å. We can see that the single association rates is 96 % with r_a =3.2 Å, and 85 % with r_a = 4.0 Å. This means that only about 10 % of the associated CO_2 molecules are associated with two or more carbonyl groups at the same time, or 10 % of the associated carbonyl groups are associated with two or more CO_2 at the same time. Thus, binding ratio equals 1 is a reasonable assumption for polymer + CO_2 systems.

4.3.4 Specific interaction energy

The specific interaction energy between CO_2 and a functional group can be calculated from Equation 4.1. Results from MD simulations for CO_2 + polymer systems are shown in Table 4.1. The strength of interaction increases in following order:

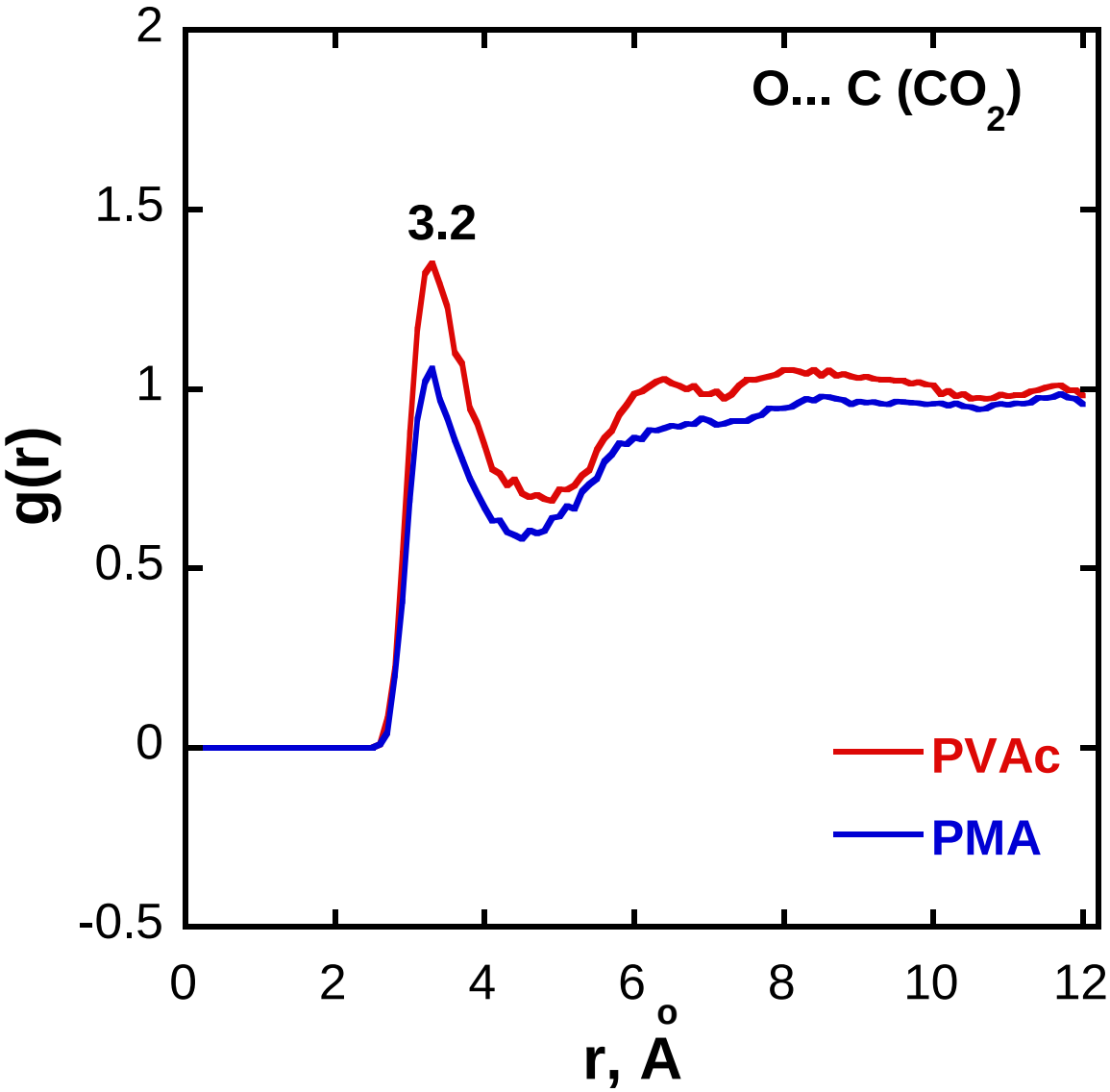

Figure 4.6 Carbonyl oxygen O…C (CO_2) pair distribution function of in PVAc and PMA.

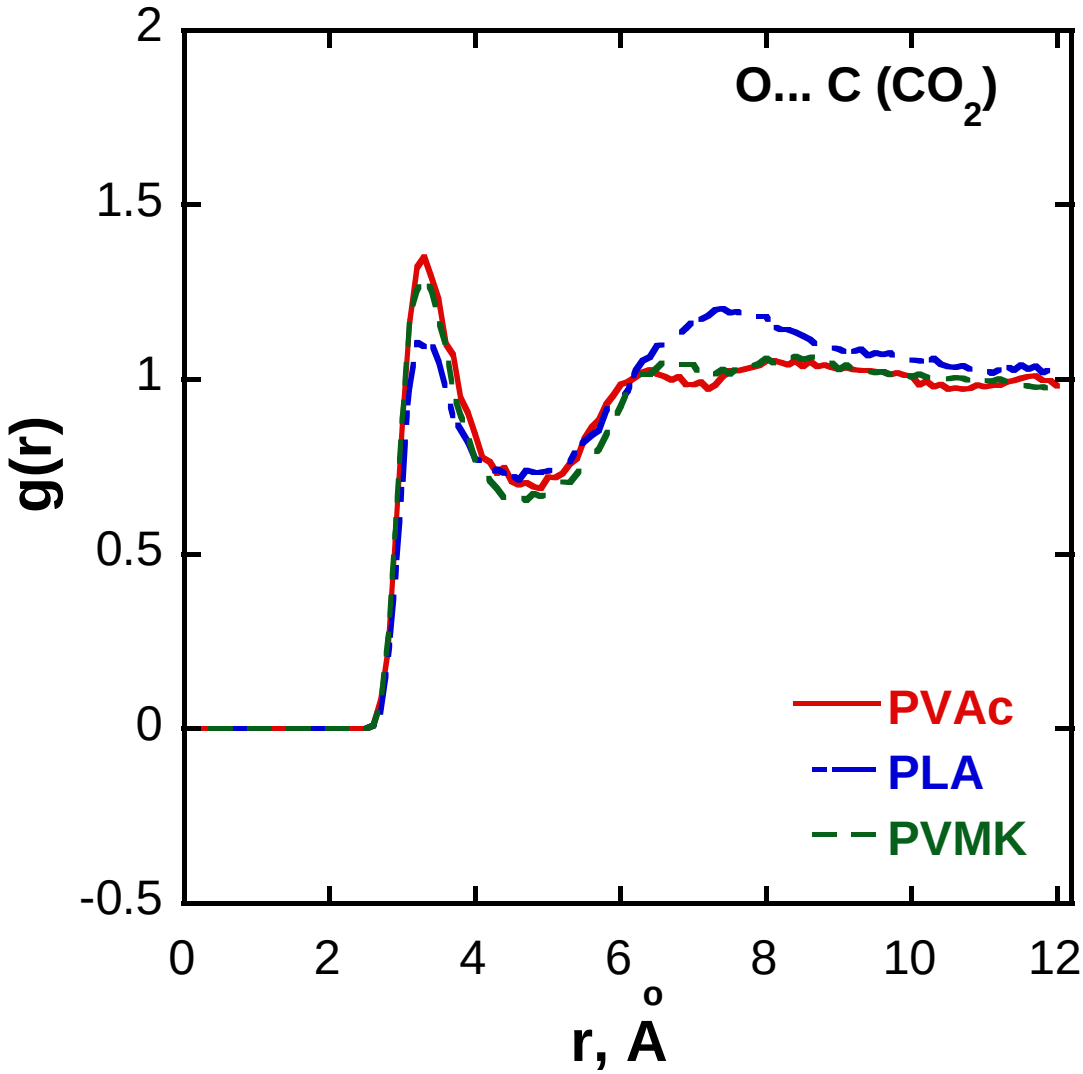

Figure 4.7 Pair distribution function of carbonyl oxygen O…C (CO_2) in PVAc + CO_2, PLA + CO_2, and PVMK + CO_2.

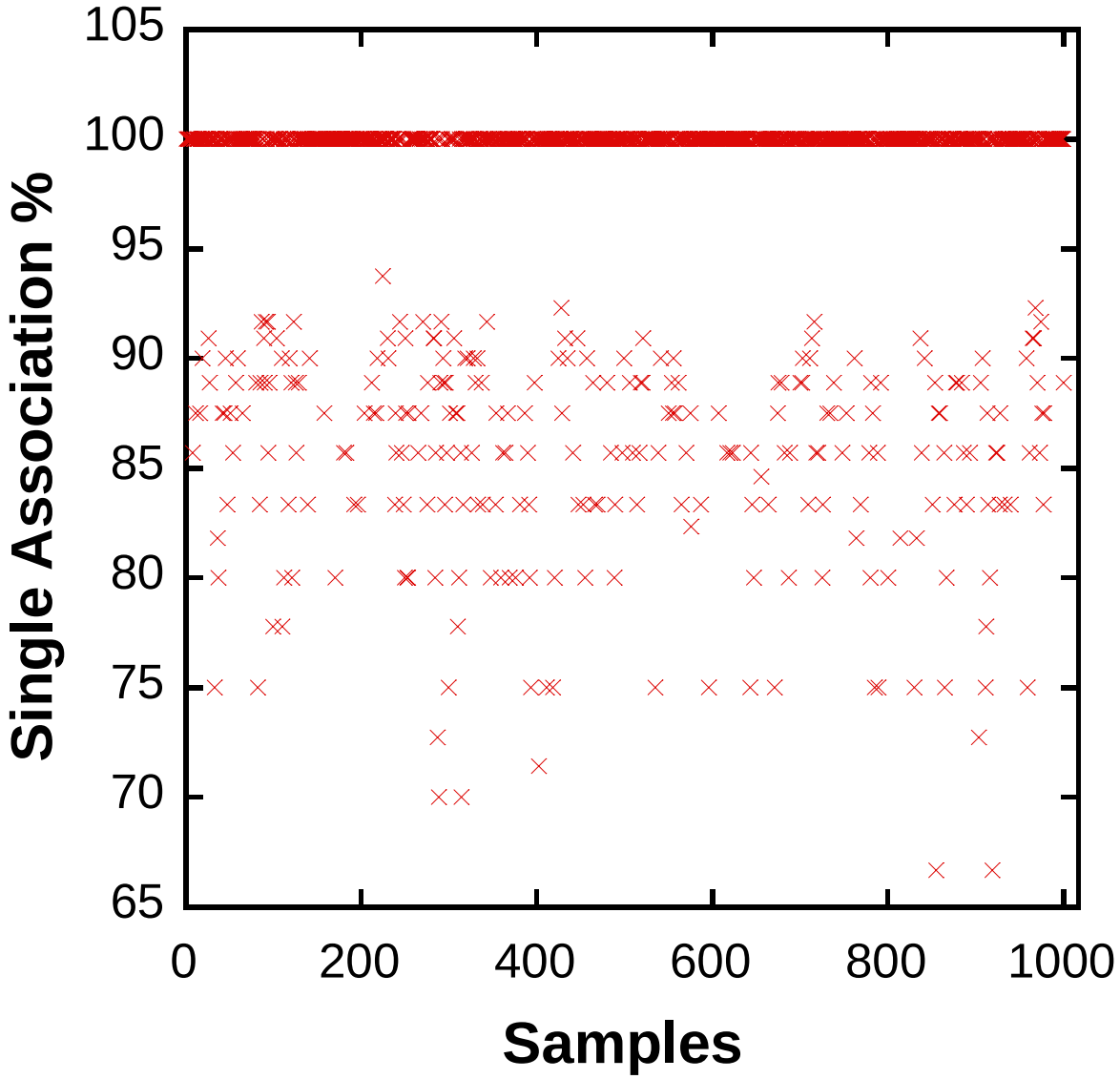

Figure 4.8 Single association rate in 1000 conformations for CO_2 and PVAc system, with the association distance, r_a = 3.2 Å.

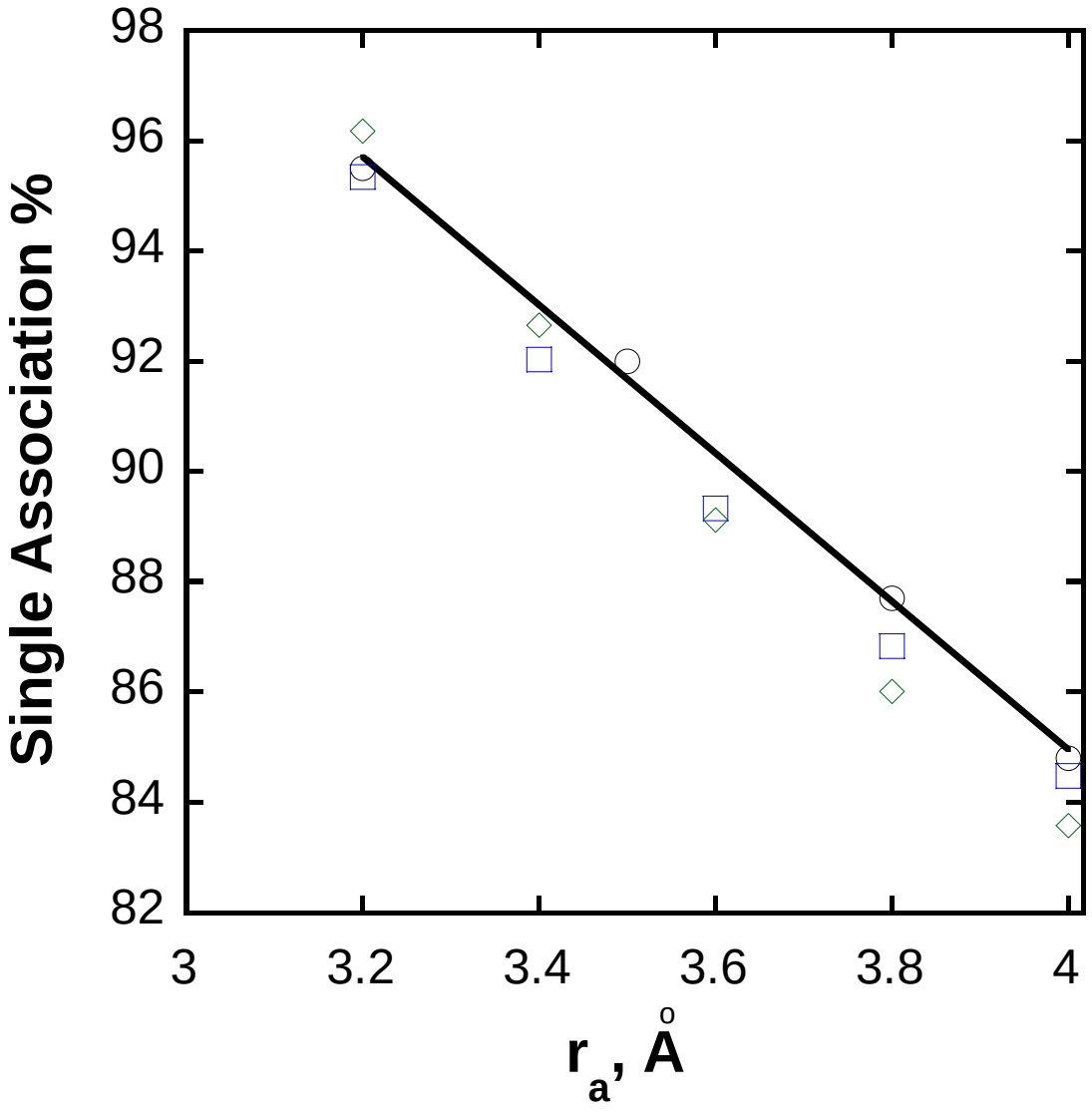

Figure 4.9 Average single association rate as a function of association distance, r_a, PVAc + CO_2 (○); PVMK + CO_2 (□), PLA + CO_2 (◊).

Table 4.1 Specific interaction energies from MD simulations.

Functional group	**Model Polymer**	**- ΔH_a, kJ/mol**
O-C=O	PVAc	10.64
Si-O-Si	PDMS	5.4
C-O-C	PEG	13.5

C-O-C > O-C=O > Si-O-Si . The estimates obtained are in agreement with experimental results. Note that MD simulations provide relative values of the interaction energy, since different values are obtained using different force fields. However, the trends do not depend on the force field chosen.

4.4 Conclusions

We have used NVT MD simulations to study specific interactions between carbonyl polymers and CO_2. Using pair distribution function analysis, we have identified the association distance to be 3.2 Å. CO_2 accessibility can be evaluated by the intensity of the first peak in the pair distribution function, and was found to decrease in the order PVAc > PVMK > PLA > PMA. The binding ratio was also calculated and it was concluded that 96 % of associated CO_2 molecules interact with only one carbonyl group. The strength of these interactions is in the order: C-O-C > O-C=O > Si-O-Si .

CHAPTER 5

EXTENSION OF THE COMPRESSILBE LATTICE MODEL TO POLYMER + CO_2 + COSOLVENT SYSTEMS

In Chapter 3 and 4, specific interactions between CO_2 and polymers were quantified using experiments and MD simulations. In this Chapter, the Compressible Lattice Model is extended to ternary systems and the quantified specific interactions are used to predict phase behavior in polymer + CO_2 + cosolvent systems..

5.1 Introduction

Supercritical CO_2 has been used as a green solvent in many polymer processes, including processes for precipitating polymer nanoparticles and for depositing polymer thin films [128-130]. The fluid-solid and liquid-liquid phase boundaries in these systems play an important role in determining the morphology of polymer particles that are obtained or films that are deposited. As a result, phase equilibrium calculations in CO_2 + polymer systems have received increasing attention in the literature [19, 21].

There is experimental evidence to suggest that CO_2 forms weak complexes with basic functional groups (such as the carbonyl group) in polymers [28]. Indeed, weak Lewis acid-base interactions between CO_2 and the carbonyl oxygen in the backbone of poly(vinyl acetate) (PVAc) and poly(methyl methacrylate) (PMMA) have been reported by Kazarian et al. [28] using Fourier transform infrared (FTIR) measurements. Such interactions play a significant role in the phase behavior of CO_2 + PMMA systems, as can be inferred from the measurements of Wissinger and Paulitis [131]. It is therefore

important to consider these interactions in thermodynamic models for CO_2 + polymer systems. Unfortunately, weak acid-base complexes are seldom accounted for explicitly in Flory-Huggins or Sanchez-Lacombe type models. Models for associated systems such as the Statistical Associating Fluid Theory (SAFT) [72], [81-82], as well as a recently proposed compressible lattice model [92, 97, 132] are able to account explicitly for these interactions. However, these models generally require two or more adjustable parameters in the calculations. For example, the SAFT equation uses two temperature-dependent parameters to correlate cloud point behavior in CO_2 + polymer systems [80, 99]. The compressible lattice model also uses two parameters for this purpose. However, we have shown that the parameters are not dependent on pressure, temperature or molecular weight [92, 97, 132]. Furthermore, one of the parameters can be obtained from independent measurements such as FTIR spectra [92, 132].

In the present study, we extend the compressible lattice model to CO_2 + cosolvent + polymer systems. Polar cosolvents are often added to CO_2 to increase the solubility of polymers such as poly(ε-caprolactone) (PCL), poly(isopropyl acrylate) (PIPA), and poly(isodecyl acrylate) (PIDA) [11, 133-134]. These polymers are not very soluble in CO_2 even though they contain carbonyl repeat groups that are capable of forming weak complexes with CO_2. There is interest in processing PCL with CO_2 because it is biodegradable and has shown promise in drug delivery applications. This interest also extends to polyacrylates such as PMMA, PIPA and PIDA which are widely used in photopolymer printing, adhesives and coatings [135-136]. The ability to identify cosolvents via the phase behavior of CO_2 + cosolvent + polymer systems is therefore of practical interest in processing these polymers with CO_2.

In this work, we use the ternary extension of the compressible lattice model to predict cloud points in CO_2 + dimethyl ether (DME) + PCL, CO_2 + DME + PIPA, and CO_2 + DME + PIDA systems. Physical properties of CO_2 and DME are listed in Table 5.1.

5.2 Compressible Lattice Model

In the compressible lattice model, the solution of polymer *P* and solvent *S* is assumed to consist of associated and unassociated polymer segments, as well as associated and unassociated CO_2 molecules. Each polymer segment occupies a lattice site, with adjacent segments occupying adjacent lattice sites. Specific interactions between a CO_2 molecule and a functional group in a polymer segment restrict a certain number of these molecules to specific lattice sites, whereas the remaining unassociated CO_2 molecules are distributed randomly on the lattice. The entropy of mixing can be calculated from the total number of configurations of these molecules and segments. This is combined with an enthalpy of mixing (based on contacts resulting from association and dispersion) to obtain the following expression for the Gibbs energy of mixing ΔG^{mix}

$$\frac{\Delta G_{PS}^{mix}}{NRT} = \alpha_{PS}\phi_P\chi_{PS}^{a} + \phi_P\left\{1-\phi_P\left(1+\alpha_{PS}\right)\right\}\left[z-2-\alpha_{PS}\right]\chi_{PS}^{u} + \frac{\phi_P}{\xi_{PS}}\ln\phi_P + \left(\frac{1-\phi_P(1+\alpha_{PS})}{(1+\alpha_{PS})}\right)\ln\left\{1-\phi_P(1+\alpha_{PS})\right\} - \phi_S\ln\frac{\phi_S}{\phi_S-\alpha_{PS}\phi_S} + \alpha_{PS}\phi_S\ln\frac{\alpha_{PS}\phi_S}{\phi_S-\alpha_{PS}\phi_S} + \phi_P\left(1-\alpha_{PS}\right)\ln\left(1-\alpha_{PS}\right) + \alpha_{PS}\phi_P\ln\alpha_{PS} \tag{5.1}$$

In Equation (5.1), *z* is the lattice coordination number (=10 in this work), *R* is the gas constant, *T* the temperature, ϕ_S and ϕ_P are the volume fractions of the solvent (CO_2)

Table 5.1 Physical properties of CO_2 and DME

Solvent	Chemical formula	Mw	T_c (K)	P_c (bar)	V^{vdW} (cm^3/mol)	ω	Dipole moment(D)
Carbon dioxide	CO_2	44.01	304.1	73.8	20.8	0.225	0.0
Dimethyl ether	CH_3OCH_3	46.06	400.0	52.4	36.5	0.192	1.3

and polymer, and N is the total number of lattice sites. Equation (5.1) contains four characteristic quantities for the binary system (P + S): the association ratio α_{PS}, the number of segments ξ_{PS}, the interaction parameter for association χ^{a}_{PS}, and the interaction parameter for dispersion χ^{u}_{PS}.

The association ratio α_{PS} is the fraction of associated segments per polymer molecule, and can be related to the equilibrium constant K_{PS} of the association reaction (**P** + **S** = **P**…**S** complex) as follows:

$$\alpha_{PS} = \frac{(1+K_{PS}) - \sqrt{(1+K_{PS})^2 - 4\phi_P\phi_S K_{PS}(1+K_{PS})}}{2\phi_P(1+K_{PS})} \tag{5.2}$$

Furthermore, the temperature dependence of K_{PS} can be expressed as:

$$\ln\frac{K_{PS}}{K'_{PS}} = -\frac{\Delta H^{a}_{PS}}{R}\left(\frac{1}{T} - \frac{1}{T'}\right) \tag{5.3}$$

where K'_{PS} is the equilibrium constant for association at a reference temperature T' (say, 300 K) and ΔH^{a}_{PS} is the enthalpy of association (assumed to be independent of T over the range of temperatures of interest). In turn, ΔH^{a}_{PS} can be expressed in terms of χ^{a}_{PS} as:

$$\chi^{a}_{PS} = \frac{\Delta H^{a}_{PS}}{RT} \tag{5.4}$$

The segment number ξ_{PS} can be calculated from the ratio of the free volume of the polymer to that of the solvent as suggested by Kasturiangan et al [92, 132]. It is given by:

$$\xi_{PS} = \frac{V_P[T,P] - 1.2V_P^{vdW}}{V_S[T,P] - V_S^{vdW}} \tag{5.5}$$

where V_P is the molar volume of the polymer, and V_S that of CO_2 at the temperature and pressure of the system. The superscript *vdW* denotes the van der Waals volume.

Finally, the interaction parameter for dispersion χ^u_{PS} is calculated from the solubility parameter δ_P of the polymer and δ_S of the solvent (CO_2) using regular solution theory. Thus

$$\chi^u_{PS} = \frac{V_S}{(z-2-\alpha_{PS})RT}\left(\hat{\delta}_P - \delta_S\right)^2 \tag{5.6}$$

Note that the interaction parameter for dispersion can be calculated from properties of the pure components at a given temperature. Also, K_{PS} and α_{PS} can be calculated at any temperature if ΔH^a_{PS} and K'_{PS} are known. In the absence of independent measurements of association, ΔH^a_{PS} and K'_{PS} can be treated as adjustable parameters.

It should be added here that we may also write Equation (5.1-5.4) for the cosolvent (*C*) + polymer (*P*) system with parameters ΔH^a_{PC} and K'_{PC} and for the solvent (*S*) + cosolvent system (*C)* with parameters ΔH^a_{SC} and K'_{SC}

To extend the lattice model to ternary systems, we may express the Gibbs energy of mixing as the sum of three binary terms to give [86, 137-138]:

$$\frac{\Delta G^{mix}_{PSC}}{NRT} = \frac{\Delta G^{mix}_{PS}}{NRT} + \frac{\Delta G^{mix}_{PC}}{NRT} + \frac{\Delta G^{mix}_{SC}}{NRT} \tag{5.7}$$

To simplify the resulting expression, we assume that there are no specific interactions between the solvent and cosolvent (ie. ΔH^a_{SC} and K'_{SC} are both zero) and that $\xi_{PS} = \xi_{PC.}$ In the systems we have studies (CO_2 + DME + polymer). There is no evidence to suggest that CO_2 and DME form complexes so that ΔH^a_{SC} and K'_{SC} are probably zero. Also, the number of segments "seen" by either CO_2 or DME molecules should be large and therefore any differences should not have a significant effect on the Gibbs energy of

the solution. This leads to the following expression for the Gibbs energy of mixing of the ternary system (detailed derivations were shown in Appendix B):

$$\begin{aligned}\frac{\Delta G^{mix}_{PSC}}{NRT} &= \alpha_{PS}\phi_P\chi^a_{PS} + \phi_P\left(\phi_S - \alpha_{PS}\phi_P\right)\left[z-2-\alpha_{PS}\right]\chi^u_{PS} \\ &+\alpha_{PC}\phi_P\chi^a_{PC} + \phi_P\left(\phi_C - \alpha_{PC}\phi_P\right)\left[z-2-\alpha_{PC}\right]\chi^u_{PC} \\ &+\left(\phi_S - \alpha_{PS}\phi_P\right)\left(\phi_C - \alpha_{PC}\phi_P\right)\left[z-2\right]\chi^u_{SC} \\ &+\frac{\phi_P}{\xi_{PSC}}\ln\phi_P + \left(\frac{2+\alpha_{PS}}{1+\alpha_{PS}}\right)\left(\phi_S - \alpha_{PS}\phi_P\right)\ln\left(\phi_S - \alpha_{PS}\phi_P\right) - \phi_S\ln\phi_S \\ &+\left(\frac{2+\alpha_{PC}}{1+\alpha_{PC}}\right)\left(\phi_C - \alpha_{PC}\phi_P\right)\ln\left(\phi_C - \alpha_{PC}\phi_P\right) - \phi_C\ln\phi_C \\ &+\left(\alpha_{PS}\phi_P\right)\ln\left(\alpha_{PS}\phi_P\right) + \phi_P\left(1-\alpha_{PS}\right)\ln\left(1-\alpha_{PS}\right) + \alpha_{PS}\phi_P\ln\alpha_{PS} \\ &+\left(\alpha_{PC}\phi_P\right)\ln\left(\alpha_{PC}\phi_P\right) + \phi_P\left(1-\alpha_{PC}\right)\ln\left(1-\alpha_{PC}\right) + \alpha_{PC}\phi_P\ln\alpha_{PC}\end{aligned} \tag{5.8}$$

This expression contains the binary quantities α_{PS}, ξ_{PS}, χ^a_{PS}, and χ^u_{PS} for the solvent + polymer system, as well as α_{PC}, ξ_{PC}, χ^a_{PC}, and χ^u_{PC} for the cosolvent + polymer system. As described above, these quantities can be calculated if ΔH^a_{PS} and K'_{PS} as well as ΔH^a_{PC} and K'_{PC} are known.

5.3 Cloud Point Calculations

At a cloud point, phase equilibrium between a polymer-rich phase (*h*) and a polymer-lean phase (*l*) can be described by

$$\gamma_i^l x_i^l = \gamma_i^h x_i^h \tag{5.9}$$

where component *i* can be the polymer, solvent, or cosolvent, and the activity coefficients γ_i depend on temperature, pressure, and composition. We have chosen the standard states of each component to be the same in the polymer-lean and polymer-rich phases.

Therefore, both phases are treated using the same model, in the spirit of van der Waals. There are four unknowns *T, P,* x_S^l and x_S^h in the two equations obtained when Equation (5.9) is applied to the two components (polymer and solvent) in a binary system. Similarly, there are six unknowns *T, P,* x_S^l, x_P^l, x_S^h and x_P^h in the three equations obtained when Equation (5.9) is applied to the three components (polymer, solvent, and cosolvent) in a ternary system. Therefore, if the composition of one of the phases is known, then the pressure and composition of the other phase can be calculated at a given temperature for both binary or ternary systems. Activity coefficients can be obtained by differentiation of Equation (5.8) in the case of ternary systems, or Equation (5.1) in the case of binary systems.

5.4 Results and Discussion

Cloud points of the six binary systems CO_2 + PCL, CO_2 + PIPA, CO_2 + PIDA, DME + PCL, DME + PIPA, and DME + PIDA, as well as three ternary systems CO_2 + DME + PCL, CO_2 + DME + PIPA, and CO_2 + DME + PIDA were calculated using the model. The volume of each polymer V_P was calculated using the Tait equation [139] or the group contribution modified cell model (GCMCM) of Sato et al [140]. Solvent (and cosolvent) volumes V_s were obtained using the Patel-Teja equation of state [141]. Solubility parameters of the non-polar analog (or homomorph) of each polymer required to obtain χ_{PS}^u using Equation (5.6) were estimated using the group additivity approach of van Krevelen [142] or Fedors [143].

5.4.1 Cloud point behavior of CO_2 + polymer binary systems

Cloud points in the CO_2 + PCL, CO_2 + PIPA and CO_2 + PIDA systems were correlated using one adjustable parameter K'_{PS} for each binary system. ΔH^a_{PS} values were obtained from FTIR measurements in the case of CO_2 + PCL, and assumed to be the same as that for CO_2 + PMMA in the case of CO_2 + PIPA and CO_2 + PIDA systems. This assumes that the strength of the association interaction was the same in the three polyacrylate systems. A detail of FTIR measurements was presented in Chapter 3. Figure 5.1 shows calculated cloud point curves for the three systems. The results are in good agreement with experiment with average deviations of less than 5 %. Effects of polydispersity were ignored in these calculations. The correlated K'_{PS} value (0.093) was slightly larger for CO_2 + PIPA than for CO_2 + PIDA (0.091) (see Table 5.2). This suggests that there are more CO_2 - PIPA complexes formed than CO_2- PIDA complexes. It is possible that the shorter side chain in PIPA offers less steric hindrance for CO_2 to access the carbonyl group. Also, the concentration of carbonyl group in PIPA is higher than that in PIDA leading to more complexes being formed.

5.4.2 Cloud point behavior of DME + polymer binary systems

Cloud points in the DME + PCL, DME + PIPA and DME + PIDA systems were correlated using one adjustable parameter K'_{PC} for each binary system (see Table 5.3). ΔH^a_{PC} values were assumed to be the same as for the corresponding CO_2 system. Calculated cloud point curves are plotted in Figure 5.2 and show good agreement with experiment (average deviations < 5 %). Effects of polydispersity were ignored in these

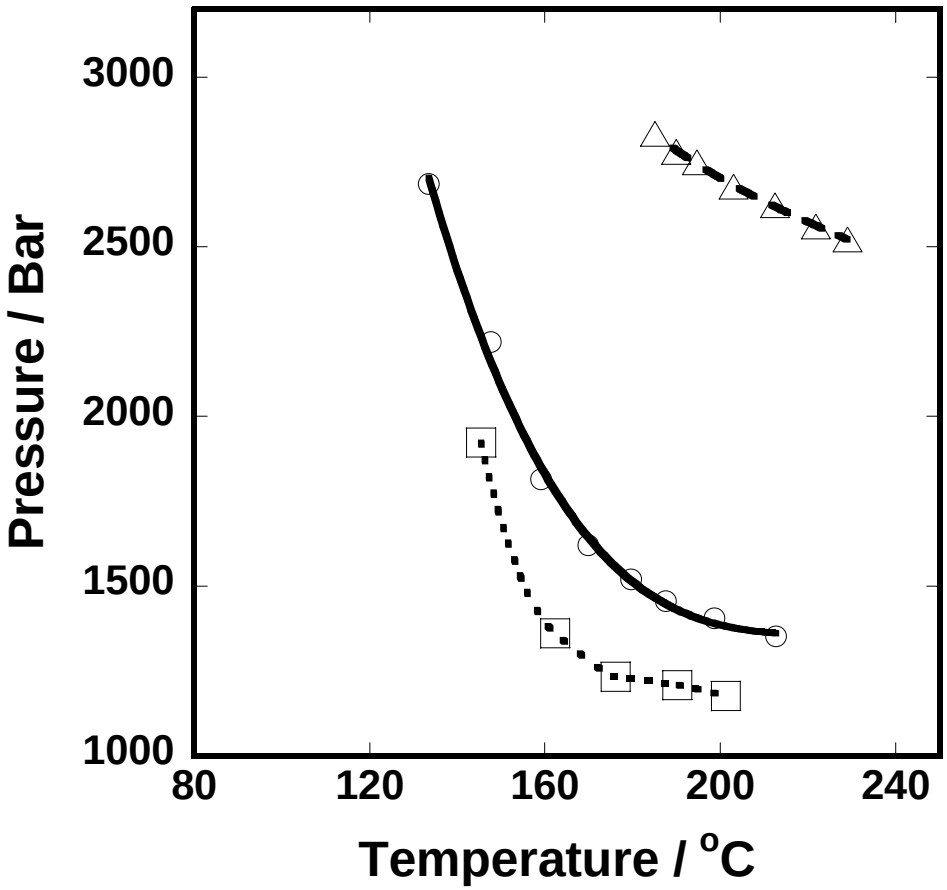

Figure 5.1 Cloud point curves in CO_2+ PCL, CO_2 + PIPA, and CO_2 + PIDA binary systems. Points represent experimental data for CO_2 + PCL (M_W = 170,000) (Δ); CO_2 + PIPA (M_W = 120,000) (O); and CO_2 + PIDA (M_W = 60,000) (□) from Reference [11, 133-134]. Lines represent calculated curves for polymer concentrations of ~5.0 wt %.

Table 5.2 Results of cloud point calculations for CO_2 + PCL, CO_2 + PIPA, CO_2 + PIDA

Polymer	Mw (×1000)	T_g (K)	Temperature range (K)	Pressure range (bar)	ΔH_{PS}^{a} (kJ/mol)	$K_{PS}^{'}$	AAD[a] %
PCL	170	213	458-502	2522-2832	-8.8[c]	0.135	4.2
PIPA	120	270	406-486	1352-2685	-8.0[b]	0.093	3.6
PIDA	60	213	418-475	1175-1922	-8.0[b]	0.091	2.7

[a] $AAD\ \% = \frac{1}{N}\sum_{i=1}^{N}\left|\frac{P_{i,\text{Model}} - P_{i,\text{Experiment}}}{P_{i,\text{Experiment}}}\right| \times 100\%$

[b] from FTIR spectra for PMMA + CO_2

[c] from FTIR spectra for PCL + CO_2

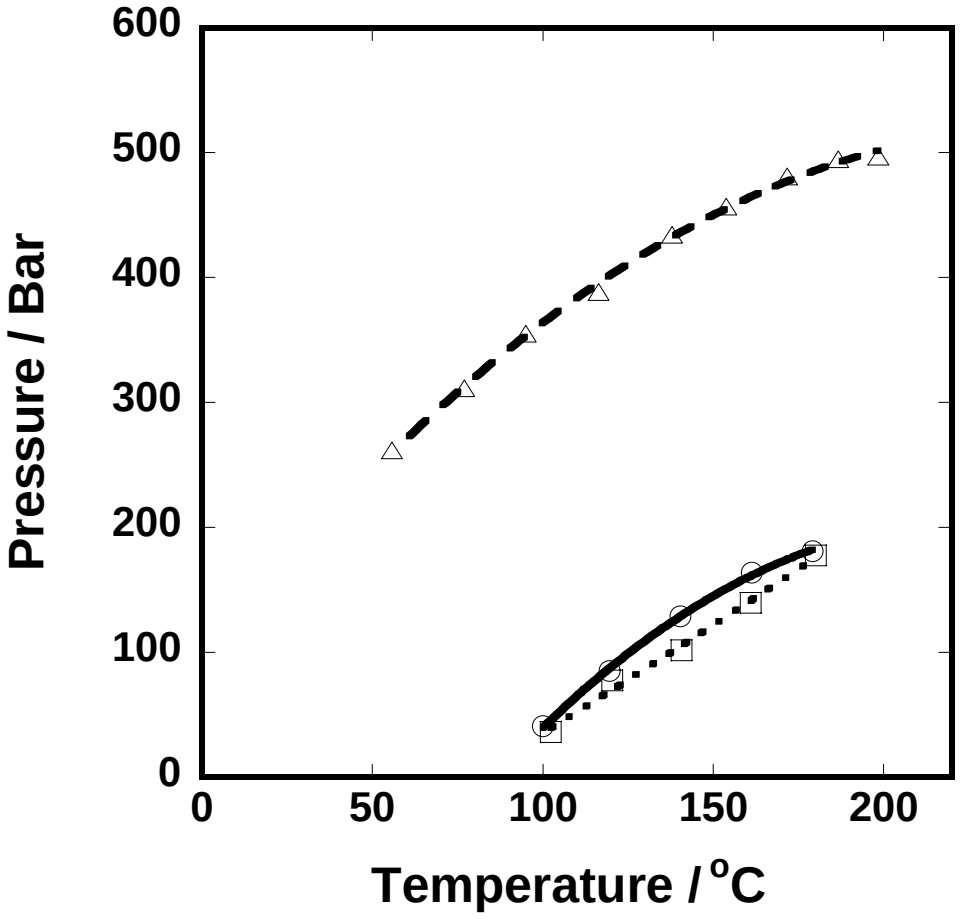

Figure 5.2 Cloud point curves in DME + PCL, DME + PIPA, and DME + PIDA binary systems. Points represent experimental data for DME + PCL (M_W = 170,000) (Δ); DME + PIPA (M_W = 120,000) (O); and DME + PIDA (M_W = 60,000) (□) Reference [11, 133-134]. Lines represent calculated curves for polymer concentrations of ~5.0 wt %.

Table 5.3 Results of cloud point calculations for DME + PCL, DME + PIPA, DME + PIDA

Polymer	Mw (×1000)	$\hat{\delta}_P$ $(MPa)^{0.5}$	Temperature range (K)	Pressure range (bar)	ΔH^a_{PC} (kJ/mol)	K'_{PC}	AAD %
PCL	170	17.9	329-472	261-497	-8.8	0.166	3.5
PIPA	120	17.0	373-453	41-181	-8.0	0.171	3.8
PIDA	60	17.3	375-454	36-178	-8.0	0.160	2.3

calculations. K'_{PC} values for DME systems were found to be larger than those for the corresponding CO_2 systems implying more complexes being formed between DME and the polymers than between CO_2 and the same polymer. The carbon atom can act as a Lewis acid in both CO_2 and DME and is able to interact with the oxygen atom in the carbonyl group which acts as a Lewis base. Our results suggest that Lewis acid - base interactions probably exist in DME + polymer and CO_2 + polymer systems. The results also confirm that DME is a good cosolvent for CO_2 + PCL, CO_2 + PIPA and CO_2 + PIDA.

5.4.3 Cloud point predictions in CO_2 + DME+ polymer ternary systems

Figure 5.3-5.5 present results of our calculations of cloud point curves in CO_2 + DME + PCL, CO_2 + DME + PIPA and CO_2 + DME + PIDA systems. No adjustable parameters were used in these calculations. It is obvious that cloud points in ternary systems can be predicted with AAD less than 10 % using our model. It should also be noted that both UCST behavior (negative slopes of cloud point curves) and LCST behavior (positive slopes) can be predicted equally well by our model. Finally, the assumption of no association between CO_2 and DME appears to be validated by our calculations.

5.4 Conclusions

We have extended the compressible lattice model to ternary systems and shown that model parameters obtained from binary data can be used to predict ternary system behavior with AAD less than 10 %. Both UCST and LCST behavior can be predicted by the model. Our results also suggest that DME - polymer complexes may also formed in

these systems, which is one reason why DME is a good solvent for processing acrylate polymers using CO_2.

Yuan, Yanhui and Teja, Amyn S., *Extension of a compressible lattice model to CO_2 + cosolvent + polymer systems*, Journal of Supercritical Fluids, accepted.

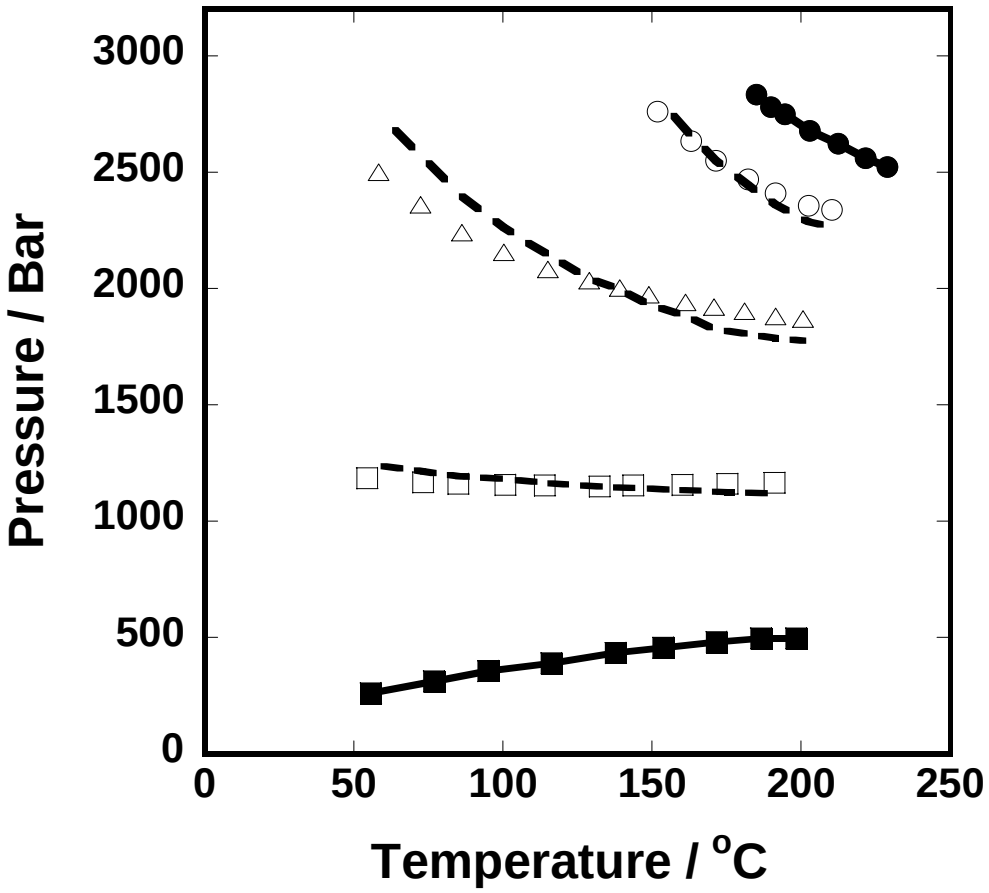

Figure 5.3 Cloud point behavior in CO_2 + DME + PCL ternary systems. Points represent experimental data for systems containing 0 wt % DME (●); 4.5 wt % DME (O); 14.5 wt % DME (Δ); 40 wt % DME (□); 100 wt % DME (■) from Reference [11, 133-134]. Lines represent calculated values for polymer concentrations of ~5.0 wt %.

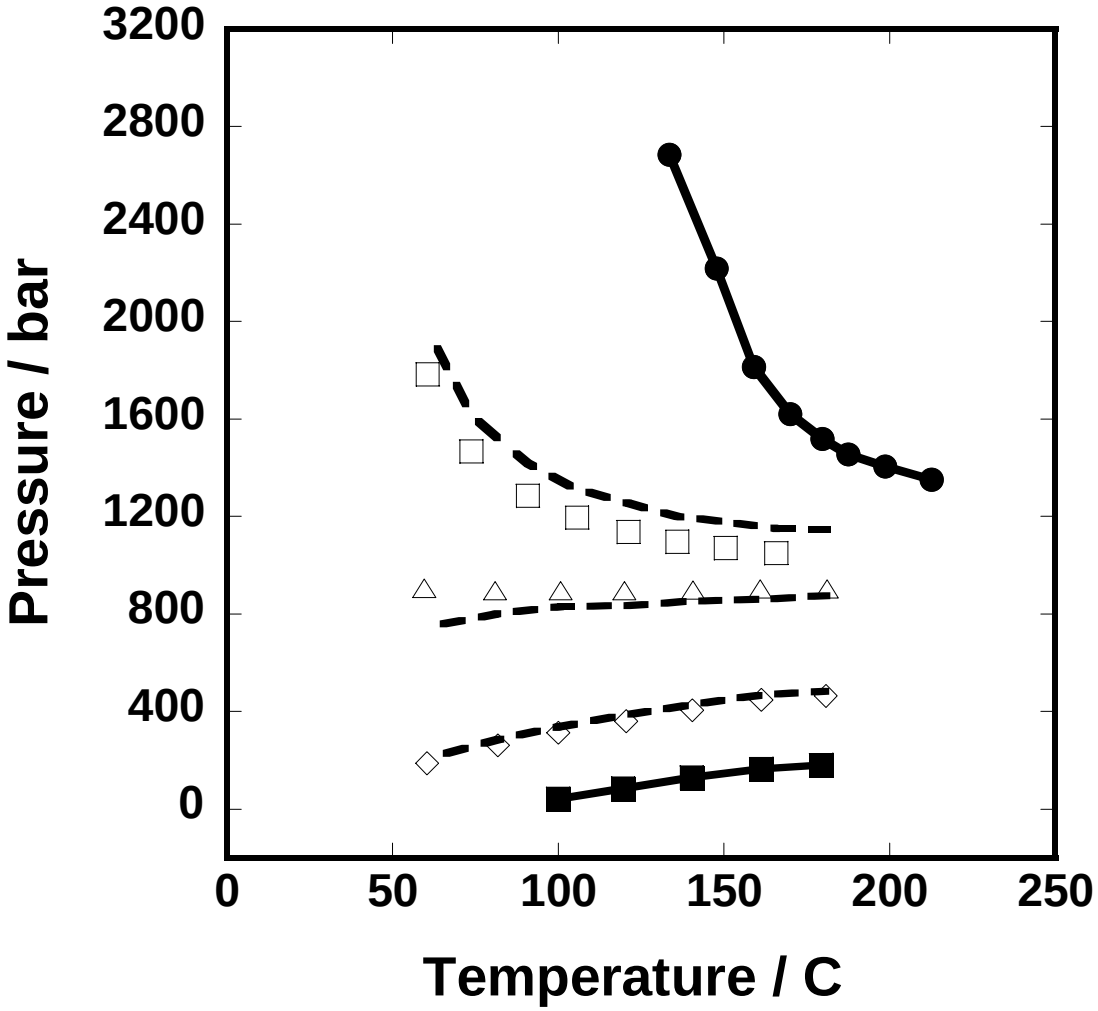

Figure 5.4 Cloud point behavior in CO_2 + DME + PIPA ternary systems. Points represent experimental data for systems containing 0 wt % DME (●); 9.0 wt % DME (O); 14.7 wt % DME (Δ); 47.5 wt % DME (□); 100 wt % DME (■) from Reference [11, 133-134]. Lines represent calculated values for polymer concentrations of ~5.0 wt %.

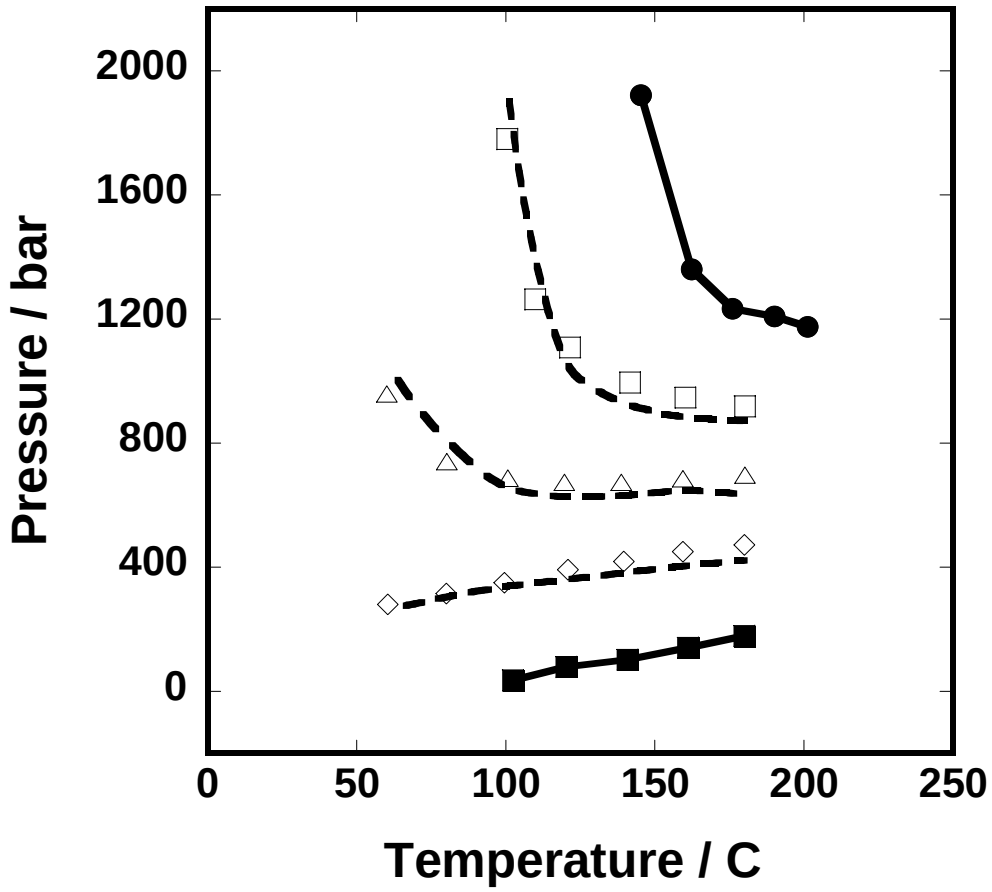

Figure 5.5 Cloud point behavior in CO_2 + DME + PIDA ternary systems. Points represent experimental data for systems containing 0 wt % DME (●); 8.4 wt % DME (O); 21.1 wt % DME (Δ); 41.7 wt % DME (□); 100 wt % DME (■) from [11, 133-134]. Lines represent calculated values for polymer concentrations of ~5.0 wt %.

CHAPTER 6

AN ASSOCIATED LATTICE-FLUID EQUATION OF STATE BASED ON THE COMPRESSILBE LATTICE MODEL

6.1 Introduction

As discussed in Chapter 5, the compressible lattice model is an activity coefficient model and is not therefore directly applicable to the calculation of volumetric property changes, such as swelling, caused by the addition of CO2 to polymers. However, we may follow the approach of Sanchez-Lacombe, Panayiotou-Vera and Flory-Orwoll-Vrij [58] to reformulate the compressible lattice activity coefficient model to an EOS. An advantage of an EOS is that PVT properties as well as phase behavior can be modeled using an EOS.

In this chapter, an Associated Lattice-Fluid Equation of State (ALF EOS) is derived using the combinatorial term from the Compressible Lattice Model in the Sanchez-Lacombe lattice-fluid partition function. Applications of the ALF EOS to the calculation of CO_2 sorption and swelling are also described.

6.2 Model Development

6.2.1 Partition functions

The Sanchez and Lacombe lattice-fluid partition function Q is given by

$$Q = \Omega_c \exp\left(-\frac{E}{RT}\right) \tag{6.1}$$

where Ω_c represents the total number of ways of arranging polymer, solvent and holes into a lattice, and E is the total lattice energy of the system.

For a system of N_0 holes, r_2N_2 polymer segments and r_1N_1 solvent molecules, the number of occupied lattice sites (N) is given by

$$N = \hat{r}\hat{N} = r_1N_1 + r_2N_2 \tag{6.2}$$

where the average segment number in the system $\hat{r} \gg 1$. To calculate Ω_c, we write it in terms of a free volume factor Ω_0 and an association factor $\Omega_{complex}$. Thus

$$\Omega_c = \Omega_0\Omega_{complex} \tag{6.3}$$

According to previous works by Sukhadia and Variankaval [94, 95],

$$\begin{aligned}\Omega_{Complex} = \frac{1}{N_2!}\left[\frac{(z-1)^{N_2(r_2-1)}}{N^{N_2(r_2-1)}}\right]\left(\frac{r_2!}{(r_2-\alpha r_2)!(\alpha r_2)!}\right)^{N_2}\left(r_2(1+\alpha)\right)^{rN_2} \\ \times\left[\frac{\left(\frac{N}{r_2(1+\alpha)}\right)!}{\left(\frac{N}{r_2(1+\alpha)}-N_2\right)!}\right]\left(\frac{N_1!}{(\alpha r_2N_2)!(N_1-\alpha r_2N_2)!}\right)\end{aligned} \tag{6.4}$$

where z is the lattice coordination number(~10), α is the association ratio. Here we have assumed that the polymer and solvent associate to form a chemical complex with a binding ratio of 1:1, which means that one solvent molecule is associated with one polymer segment as follows

$$\mathbf{P} + \mu\mathbf{S} \rightleftharpoons \mathbf{P...S}_{\mu} \tag{6.5}$$

where μ =1. For simplicity, we set r_1=1 so that r_2 will now be the relative segment number.

To estimate the free volume factor, we place $\hat{r}\hat{N}$ quasi-polymer segments and N_0 holes on the lattice and obtain [26],

$$Q_0 = \left(\frac{z-1}{N_0 + \hat{r}\hat{N}} \right)^{\hat{N}(\hat{r}-1)} \frac{\left(N_0 + \hat{r}\hat{N}\right)!}{N_0 ! \hat{N} !} \tag{6.6}$$

Combining Equations (6.1-6.5) and noting that the Gibbs energy is given by

$$G = -RT \ln\left(\Psi\right) \tag{6.7}$$

where

$$\Psi = Q \exp(-\frac{PV}{RT}) \tag{6.8}$$

we obtain

$$\begin{aligned} \frac{G}{NRT} = \frac{E}{NRT} + \frac{PV}{NRT} + \left(\frac{f_0}{1-f_0} \right) \ln f_0 + \frac{1}{\hat{r}} \ln(1-f_0) \\ + \frac{\phi_2}{r_2} \ln \phi_2 + \left(\frac{\phi_1 - \phi_2 \alpha}{1+\alpha} \right) \ln(\phi_1 - \phi_2 \alpha) \\ - \phi_1 \ln \frac{\phi_1}{\phi_1 - \alpha \phi_2} + \alpha \varphi_2 \ln \frac{\alpha \phi_2}{\phi_1 - \alpha \phi_2} \\ + \phi_2 (1-\alpha) \ln(1-\alpha) + \alpha \phi_2 \ln \alpha - (1+\phi_2) \ln \left(\frac{z-1}{e} \right) \end{aligned} \tag{6.9}$$

where f_0 is the fraction of holes (empty sites) defined as

$$f_0 = \frac{N_0}{N_0 + \hat{r}\hat{N}} \tag{6.10}$$

We use the so- called "Flory approximation" [144], to eliminate the last term in Equation 6.9 and express the total lattice energy E as

$$-\frac{E}{NRT} = \frac{\tilde{\rho}\varepsilon^*}{RT} \tag{6.11}$$

where $\tilde{\rho}$ is the reduced density.

$$\tilde{\rho} = \frac{\hat{r}\hat{N}}{N_0 + \hat{r}\hat{N}} = 1 - \frac{N_0}{N_0 + \hat{r}\hat{N}} = 1 - f_0 \tag{6.12}$$

and ε^* is the average interaction energy per segment

$$\varepsilon^* = \phi_1 \varepsilon_1^* + \phi_2 \varepsilon_2^* + \Delta\varepsilon_{ex} \tag{6.13}$$

and

$$-\frac{\Delta\varepsilon_{ex}}{RT} = \frac{\Delta H_{mix}}{NRT} = \alpha\phi_2 \chi_a^* + \phi_2 \left(\phi_1 - \alpha\phi_2\right)\left(z - 2 - a\right)\chi_u^* \tag{6.14}$$

In the above expression, α is the association ratio defined previously (Equation 5.2). If we set α = 0, only dispersion interaction energy is considered in this development, and Equation 6.13 reduces to the lattice energy in SL EOS model.

$$\varepsilon^* = \phi_1 \varepsilon_1^* + \phi_2 \varepsilon_2^* - RT\phi_1\phi_2\chi_u^*\left(z - 2\right) \tag{6.15}$$

The dispersion interaction energy can be expressed in terms of solubility parameters as follows:

$$\chi_u^* = \frac{v^*\left(\delta_1^* - \delta_2^*\right)^2}{\left(z - 2\right)RT} \tag{6.16}$$

Or, in general form as

$$\chi_u^* = \frac{\left(\varepsilon_1^* + \varepsilon_2^* - 2\left(1 - k_{12}\right)\sqrt{\varepsilon_1^*\varepsilon_2^*}\right)}{\left(z - 2\right)RT} = \frac{\left(\sqrt{\varepsilon_1^*} - \sqrt{\varepsilon_2^*}\right)^2 + 2k_{12}\sqrt{\varepsilon_1^*\varepsilon_2^*}}{\left(z - 2\right)RT} \tag{6.17}$$

where k_{12} is accounts for the non-Regular Solution behavior excluding association. To simplify our calculations, we may set k_{12} as zero.

The association interaction energy parameter can expressed in terms of an enthalpy of association as follows:

$$\chi_a^* = \frac{\Delta E_a}{RT} = \frac{\Delta H_a}{RT} \tag{6.18}$$

6.2.2 Equation of state

We can rewrite Equation 6.9 in terms of the following reduced parameters.

$$\begin{aligned} \tilde{\rho} &= \frac{\rho}{\rho^*} = \frac{\rho \hat{r} v^*}{M} & \tilde{P} &= \frac{P}{P^*} = \frac{P v^*}{\varepsilon^*} \\ \tilde{T} &= \frac{T}{T^*} = \frac{TR}{\varepsilon^*} & \tilde{v} &= \frac{1}{\tilde{\rho}} = \frac{1}{1-f_0} = \frac{V}{\hat{r}\hat{N}v^*} \end{aligned} \tag{6.18}$$

and then,

$$\begin{aligned} G = \hat{r}\hat{N}\Bigg\{ & -\tilde{\rho}\varepsilon^* + P\tilde{v}v^* + RT\left[\left(\frac{f_0}{1-f_0}\right)\ln f_0 + \frac{1}{\hat{r}}\ln(1-f_0)\right] \\ & + RT\left[\frac{\phi_2}{r_2}\ln\phi_2 + \left(\frac{\phi_1 - \phi_2\alpha}{1+\alpha}\right)\ln(\phi_1 - \phi_2\alpha) - \phi_1 \ln\frac{\phi_1}{\phi_1 - \alpha\phi_2} + \right. \\ & \left. \alpha\varphi_2 \ln\frac{\alpha\phi_2}{\phi_1 - \alpha\phi_2} + \phi_2(1-\alpha)\ln(1-\alpha) + \alpha\phi_2\ln\alpha\right]\Bigg\} \end{aligned} \tag{6.19}$$

The equation of state can be obtained from the partition function in Equation (6.1) or Gibbs free energy in Equation (6.19) using

$$\frac{P}{RT} = \left(\frac{\partial \ln Q}{\partial V}\right)_{T,N_i} \tag{6.20}$$

or,

$$\left(\frac{\partial G}{\partial f_0}\right)_{T,P,N_i} = 0 \tag{6.21}$$

Here, we use Equations (6.18, 6.19 and 6.21), and obtain

$$\frac{1}{\hat{r}\hat{N}}\left(\frac{\partial G}{\partial f_0}\right)_{T,P,N_i} = \varepsilon^* + \frac{Pv^*}{(1-f_0)^2} + RT\left[\frac{1}{(1-f_0)^2}\ln f_0 + \frac{1}{1-f_0} - \frac{1}{\hat{r}}\left(\frac{1}{1-f_0}\right)\right] = 0 \tag{6.22}$$

After rearrangement of Equation (6.21), we can obtain the equation of state in the following form:

$$\tilde{\rho}^2 + \tilde{P} + \tilde{T}\left[\ln(1-\tilde{\rho}) + \left(1-\frac{1}{\hat{r}}\right)\tilde{\rho}\right] = 0 \tag{6.23}$$

Note that Equation (6.21) is of the same form as the SL EOS, although the average lattice energy per segment is not the same as the SL EOS (Equation (6.13) and (6.14)).

To use the model to calculate thermodynamic properties, we need know $\varepsilon^*, v^*, \hat{r}$ for the mixtures. As discussed above, ε^* can be calculated using Equation (6.13) and (6.14). On the other hand, $v^*, \hat{r}$ are obtained using the mixing rules:

$$\frac{1}{\hat{r}} = \frac{\phi_1}{r_1} + \frac{1-\phi_1}{r_2(1+\alpha)} \tag{6.24}$$

$$v^* = \phi_1 \frac{\varepsilon_1^*}{P_1^*} + \phi_2 \frac{\varepsilon_2^*}{P_2^*} = \phi_1 v_1^* + \phi_2 v_2^* \tag{6.25}$$

6.2.3 Configurational entropy and chemical potential

The configurational entropy of the system can be obtained from Equation (6.3) by using

$$\frac{S}{R} = \ln \Omega_c \tag{6.26}$$

So that

$$\frac{S_C}{R} = -\hat{r}\hat{N}\left\{\left[\left(\frac{f_0}{1-f_0}\right)\ln f_0 + \frac{1}{\hat{r}}\ln(1-f_0)\right]\right.$$
$$+\left[\frac{\phi_2}{r_2}\ln\phi_2 + \left(\frac{\phi_1-\phi_2\alpha}{1+\alpha}\right)\ln(\phi_1-\phi_2\alpha) - \phi_1\ln\frac{\phi_1}{\phi_1-\alpha\phi_2} + \right. \tag{6.27}$$
$$\left.\left.\alpha\varphi_2\ln\frac{\alpha\phi_2}{\phi_1-\alpha\phi_2} + \phi_2(1-\alpha)\ln(1-\alpha) + \alpha\phi_2\ln\alpha\right]\right\}$$

The chemical potential of the system can be obtained from Equation (6.9) by following relation

$$\mu_i = \left(\frac{\partial G}{\partial N_i}\right)_{T,P,N_{j\neq i}} \tag{6.28}$$

$$\frac{\mu_i}{RT} = \frac{1}{RT}\left(\frac{\partial E}{\partial N_i}\right) + \frac{P}{RT}\left(\frac{\partial V}{\partial N_i}\right) - r_i f_0 + \ln(1-f_0) + \frac{r_i}{\hat{r}} f_0 + \ln A_i^{ARTL} \tag{6.29}$$

$$\begin{aligned}
\frac{1}{RT}\left(\frac{\partial E}{\partial N_i}\right) &= -\frac{1}{RT}\frac{\partial\left(N\varepsilon^*\tilde{\rho}\right)}{\partial N_i} = -\frac{1}{RT}\left[\left(\frac{\partial\tilde{\rho}}{\partial N_i}\right)N\varepsilon^* + \left(\frac{\partial\left(N\varepsilon^*\right)}{\partial N_i}\right)\tilde{\rho}\right] \\
&= -\frac{1}{RT}\left[r_i\tilde{\rho}\left(1-\tilde{\rho}\right)\varepsilon^* + \left(\frac{\partial\left(N\varepsilon^*\right)}{\partial N_i}\right)\tilde{\rho}\right] \\
&= -\frac{1}{RT}\left[r_i\tilde{\rho}\left(1-\tilde{\rho}\right)\varepsilon^* + \left(r_i\varepsilon_i^* + \frac{\partial\left(N\Delta\varepsilon_{ex}\right)}{\partial N_i}\right)\tilde{\rho}\right] \\
&= -\frac{1}{RT}\left[r_i\tilde{\rho}\left(1-\tilde{\rho}\right)\varepsilon^* + \left(r_i\varepsilon_i^* - \frac{\partial\left(\Delta H_{mix}^{ARTL}\right)}{\partial N_i}\right)\tilde{\rho}\right]
\end{aligned} \tag{6.30}$$

$$\begin{aligned}
\frac{P}{RT}\left(\frac{\partial V}{\partial N_i}\right) &= \frac{P}{RT}\left(\frac{\partial\left(N_0+\hat{r}\hat{N}\right)v^*}{\partial N_i}\right) = \frac{P}{RT}\left(\frac{\partial\left(N_0+\hat{r}\hat{N}\right)\left(\phi_1 v_1^* + \phi_2 v_2^*\right)}{\partial N_i}\right) \\
&= \frac{r_i P}{RT\tilde{\rho}}\left(-f_0 v^* + v_i\right)
\end{aligned} \tag{6.31}$$

Finally, $\ln A_i^{ARTL}$ is the entropy part in the activity of component *i* in the compressible lattice model (CLM), and can be expressed as

$$\ln A_i^{ARTL} = -\frac{1}{R}\left(\frac{\partial \Delta S_{mix}^{ARTL}}{\partial N_i}\right) \tag{6.32}$$

With Equations (6.29 to 6.32), we can calculate the chemical potentials for both solvent and polymer.

6.2.4 Model parameters

In order to use the ALF EOS, we need know $\varepsilon_i^*, v_i^*, r_i$ for the pure components, as well as K_0 and ΔH_a to determine specific interactions in mixtures. $\varepsilon_i^*, v_i^*, r_i$ as those in SL EOS can be found in the literatures for various polymers and solvents [144], or can be estimated from group contributions [145-146]. The specific interaction energy (ΔH_a) can be obtained from FTIR measurements or molecular modeling calculations; and K_0 is the only adjustable parameter in the model. If we do not know the specific interaction energy, then, two adjustable parameters (K_0 and ΔH_a) can be used to correlate experiment data. Pure component parameters are listed in Table 6.1.

6.3 Sorption Calculations

In the case of CO_2 (1) sorption in a polymer (2) at low pressures, it is appropriate to assume that the polymer does not dissolve in the CO_2 phase. Therefore, only CO_2 partitions between the two phases and the equality of fugacity or chemical potential can be written for CO_2 only. Since the fluid phase may be assumed to be pure CO_2, we may write:

Table 6.1 SL EOS parameters for pure component [149-151]

	ε^* (J/mol)	v*(cm^3/mol lattice)	r	$\delta^{*\,a}$ $(MPa)^{0.5}$
CO_2	2565.7	4.47	6.54	23.96
PMMA	5786.5	11.5	$6.85\times10^{4\,b}$	22.42
PBS	5967.8	11.4	$7.11\times10^{4\,b}$	22.88
EVA40	5096.5	10.3	$9.53\times10^{4\,b}$	22.26
PS	6110.8	8.07	11.2×10^{4}	27.51

Note: (a) $\delta^* = \sqrt{\frac{\varepsilon^*}{v^*}}$

(b) $M_w = 10^6$ g/mol for all polymers.

$$\mu_1^{G,pure} = \mu_1^L \tag{6.33}$$

or

$$\hat{f}_1^G(T,P,y) = P\varphi_1(T,P) = f_1^{0L} x_1 \gamma_1 \tag{6.34}$$

If we use Equation 6.33, with the following Equations (6.35 to 6.37), the chemical potentials will be calculated by Equation 6.29.

$$\begin{aligned} \ln A_1 = &-\frac{\phi_2}{r_2} + \left(\frac{1}{1+\alpha} - \frac{\beta_1}{(1+\alpha)^2}\right)\ln\left(\phi_1 - \alpha\phi_2\right) \\ &+ \left(\frac{\phi_1 - \alpha\phi_2}{1+\alpha}\right)\left(\frac{1-\beta_1\phi_2}{\phi_1 - \alpha\phi_2} - 1\right) - \ln\left(\frac{\phi_1}{\phi_1 - \alpha\phi_2}\right) - 1 + \phi_1\left(\frac{1-\beta_1\phi_2}{\phi_1 - \alpha\phi_2}\right) \\ &+ \beta_1\phi_2 \ln\left(\frac{\alpha\phi_2}{\phi_1 - \alpha\phi_2}\right) + \alpha\phi_2\left(\frac{\beta_1}{\alpha} - \frac{1-\beta_1\phi_2}{\phi_1 - \alpha\phi_2}\right) + \beta_1\phi_2 \ln\left(\frac{\alpha}{1-\alpha}\right) \end{aligned} \tag{6.35}$$

Where,

$$\beta_1 = \left(\frac{\partial\alpha}{\partial N_1}\right) = \frac{\alpha\left(K+1\right) - K}{\left(2\alpha\phi_2 - 1\right)\left(K+1\right)} \tag{6.36}$$

$$\frac{1}{RT}\left(\frac{\partial \Delta H_{mix}^{ARTL}}{\partial N_i}\right) = \beta_1\phi_2\chi_a + \phi_2\left[\left(-\beta_1\phi_2 + \phi_2(1+\alpha)\right)\left(z-3\right) - \beta_1\left(\phi_1 - \alpha\phi_2\right)\right]\chi_u \tag{6.37}$$

We can also use Equation (6.34), the expression for the activity can be calculated from CLM model, by

$$\ln a_1 = \frac{1}{RT}\left(\frac{\partial \Delta H_{mix}^{ATRL}}{\partial N_1}\right) - \frac{1}{R}\left(\frac{\partial \Delta S_{mix}^{ATRL}}{\partial N_1}\right) \tag{6.38}$$

And, the fugacity coefficient of pure gas phase can be calculated by

$$\varphi_1(T,P) = \frac{1}{RT}\int_{v_1}^{\infty}\left(P - \frac{RT}{V}\right)dV - \ln\left(\frac{Pv_1}{RT}\right) \tag{6.39}$$

An equation of state such as the Patel-Teja Equation [141] can now be used to obtain the fugacity coefficient. The fugacity of CO_2 in the polymer phase can be determined using the hypothetical liquid phase fugacity of CO_2, with f_1^{0L} calculated using the Prausnitz and Shair [147] and Barton and Hsu [148] correlations, for $0.6 \le T / T_c \le 2.5$.

$$\ln\left(\frac{f_1^{0L}}{P_c}\right) = 0.4223 + 4.7243\ln\left(\frac{T}{T_c}\right) - 3.5571\left[\ln\left(\frac{T}{T_c}\right)\right]^2 + 1.2465\left[\ln\left(\frac{T}{T_c}\right)\right]^3 \qquad (6.40)$$

6.4 Swelling Calculations

The gas absorbed in a polymer can make the polymer matrix swell , which is important not only in the processing of polymers by CO_2 [21], but also in CO_2 separation by polymer membranes because CO_2 plasticization can dramatically affect the performance of the membrane.

The swelling of a polymer by absorbed gas can be calculated using the new model (ALF EOS) (Equation (6.23)) provided model parameters (K_0) are obtained by fitting sorption data. The swelling ratio can be defined as

$$S_w = \frac{V}{V_0} \times 100\% \qquad (6.41)$$

where V_0 is the volume of the dry polymer (in cm^3/g polymer), and V is the volume after exposure to CO_2 (in cm^3/g polymer). For convenience, we can also use

$$S_w = \frac{\rho_0}{\left(1 - w_{CO_2}\right)\rho_m} \times 100\% \qquad (6.42)$$

where w_{CO_2} is the weight fraction of CO_2, and ρ_0 and ρ_m are the density of the pure polymer and mixture (polymer + CO_2), respectively.

6.5 Results and Discussion

6.5.1 Entropy calculations

Figure 6.1 and 6.2 show the calculated entropy of a mixture in which some of the N_1 solvent molecules are associated with some of the r_2N_2 polymer segments. Equation (6.27) was used to calculate the entropy. When both f_0 and α are set equal to zero, Equation 6.27 reduces to the combinational entropy term in the Flory-Huggins model (FH). When only f_0 is set equal to zero, Equation (6.27) becomes the combinational entropy term in the CLM model. Equation (6.27) therefore represents the combinatorial entropy in the ALF EOS model. Figure 6.1shows that the free volume has a strong effect on entropy, which is expected since the number of configurations in the system will increase with increasing free volume, and therefore entropy will also increase ($S = k \ln \Omega$). By contrast, the effect of association on entropy appears to be small, which is also reasonable for a polymer solution. Because r_2 is large, an increase to (r_2+ar_2) in an associated polymer solution does not have a significant effect on entropy. This can be clearly seen in Figure 6.2, which shows that the entropy per lattice becomes almost independent of the segment number when r_2 is larger than 50.

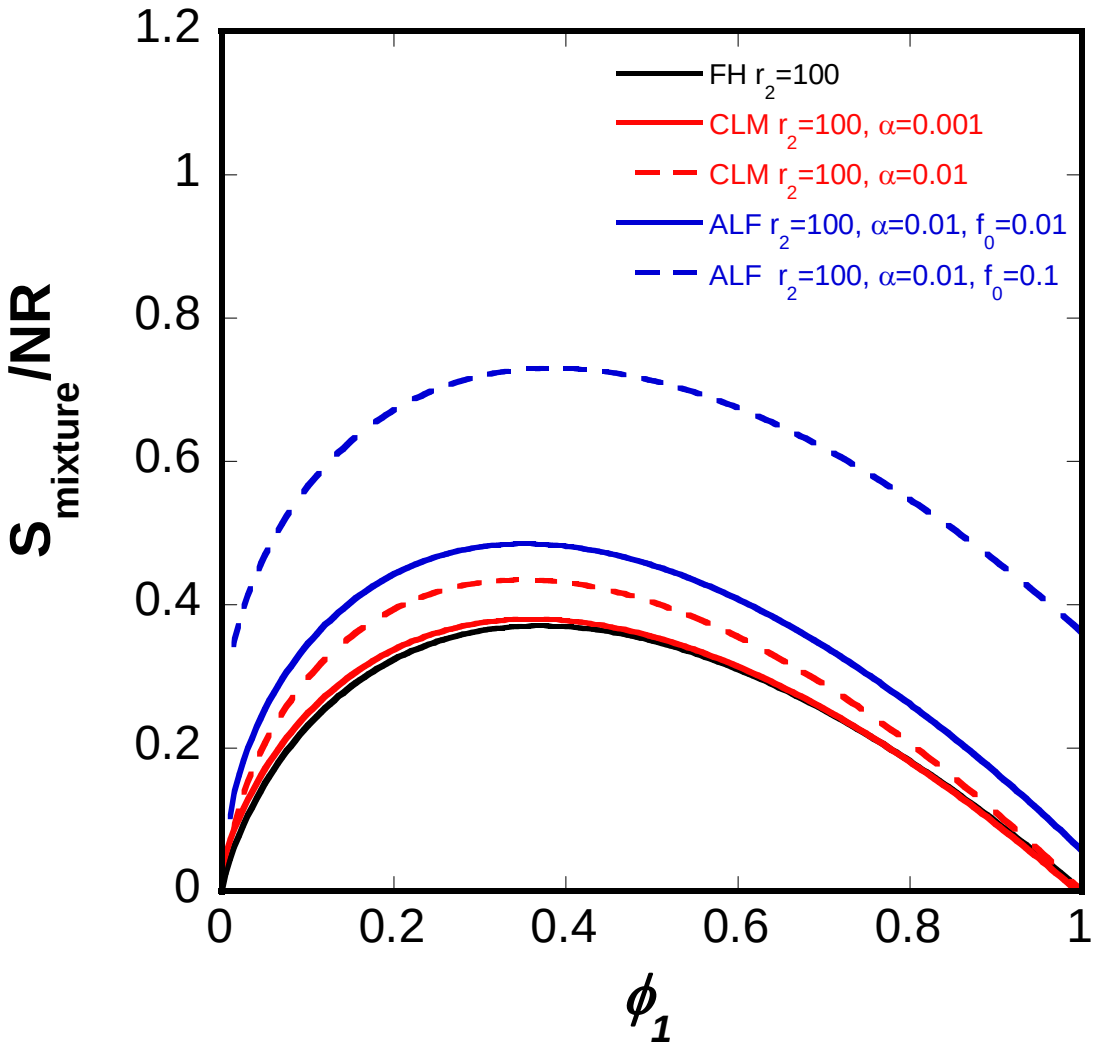

Figure 6.1 The effect of free volume (f_0) and association ratio (α) on the entropy of a mixture ($N_0 + N_1 + r_2N_2$).

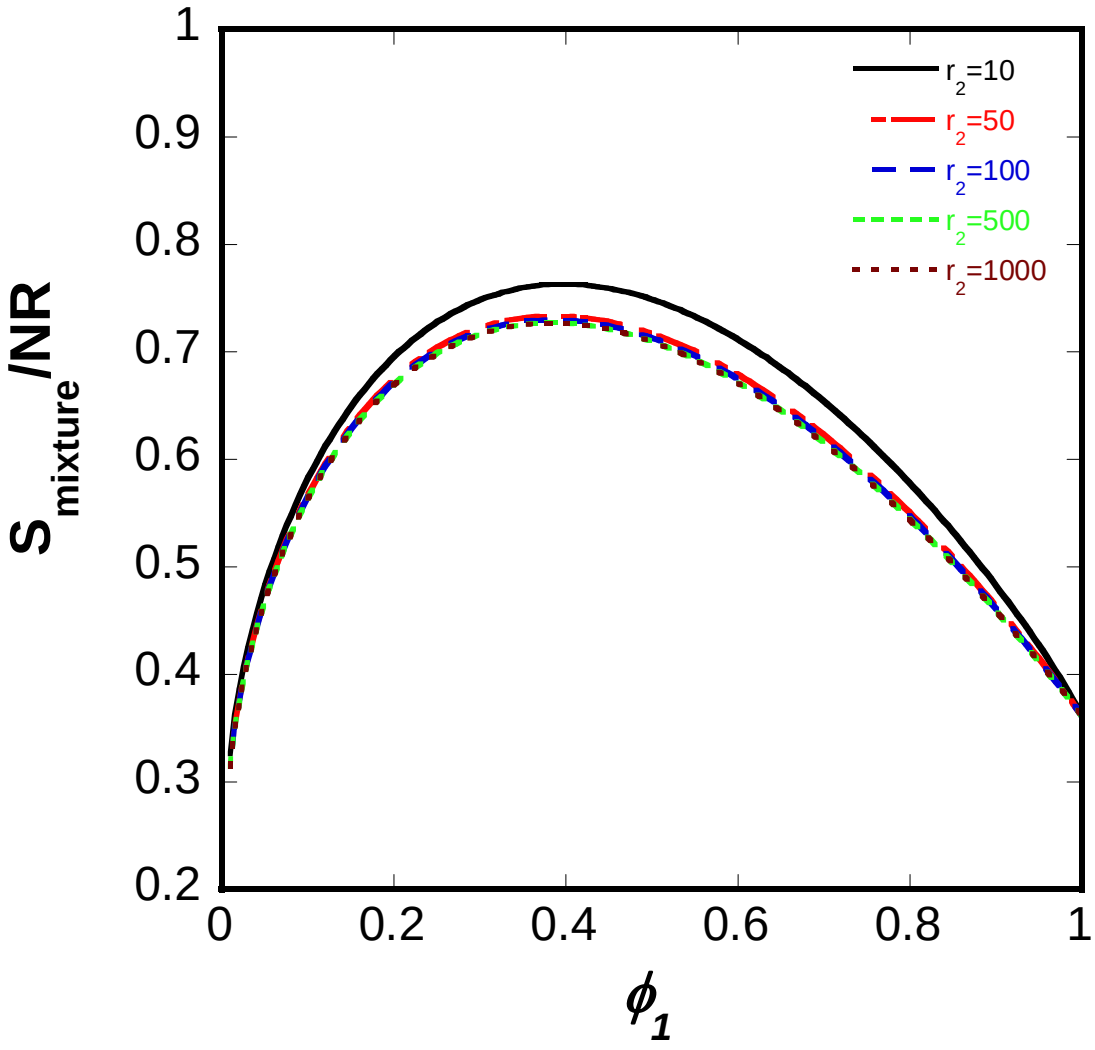

Figure 6.2 The effect of free volume (f_0) and association ratio (α) on th entropy of the system (α =0.01, f_0=0.01).

6.5.2 Model CO_2 sorption and swelling in polymers

Figures 6.3 to 6.6 illustrate the results of our correlation of sorption equilibria in CO_2 +polymer systems using chemical potentials from Equation (6.33). One adjustable parameter (K_0) was used in the calculation of sorption equilibria (Table 6.2) and other model parameters were listed in Table 6.1 [149-151]. Specific interaction energies ($-\Delta H_a$) were obtained from FTIR measurements. The specific interaction energy for PVAc + CO_2 was assumed to be the same as that for EVA40 + CO_2, and that for polyethylene + CO_2 was assumed to be zero. Also, the specific interaction energy for PCL + CO_2 was assumed to be the same as that for PBS + CO_2 system, because PCL and PBS have very similar chemical structures. For CO_2 + PS, no specific interactions were detected from FTIR spectra. Therefore, a specific interaction energy of –4.0 kJ/mol was assumed in the calculations. Good fits of the data were obtained with AAD between calculated and experimental values less than 7 %. In contrast, temperature-dependent binary interaction parameters (k_{ij}) were required for modeling these systems with the SL EOS.

Using the parameters obtained by fitting sorption equlibria, we were able to predict the swelling of polymers. Figures 6.7 to 6.9 show these predictions for PS + CO_2, PMMA + CO_2 and EVA40 + CO_2 systems. No additional parameters were used in these calculations. It is obvious that swelling of polymers can be predicted with less than 10 % average error using our model.

Table 6.2 Adjustable parameters for CO_2 sorption in polymers

System	SL EOS	ALF EOS		$-\Delta H_a$
	k_{ij}	K_0	AAD[c]%	(kJ/mol)
PMMA + CO_2	$-0.9\times10^{-3}T-0.0406$ [152]	0.0145	5.9	8.0
PBS + CO_2	$-1.043\times10^{-3}T+0.310$ [150]	0.024	3.6	8.8[a]
EVA40 + CO_2	–0.00823 [151]	0.035	4.8	9.3
PS + CO_2	$-1.070\times10^{-3}T+0.330$ [153]	(0.083)[b]	(6.7)[b]	(4.0)[b]

Notes:

(a) FTIR measurement from PCL and CO_2;

(b) The values in parentheses are obtained by using ΔH_a = –4.0 (kJ/mol) in PS + CO_2.

(c) $AAD\% = \frac{1}{N}\sum_i \left|\frac{w_{i,cal}-w_{i,\exp}}{w_{i,\exp}}\right| \times 100\%$

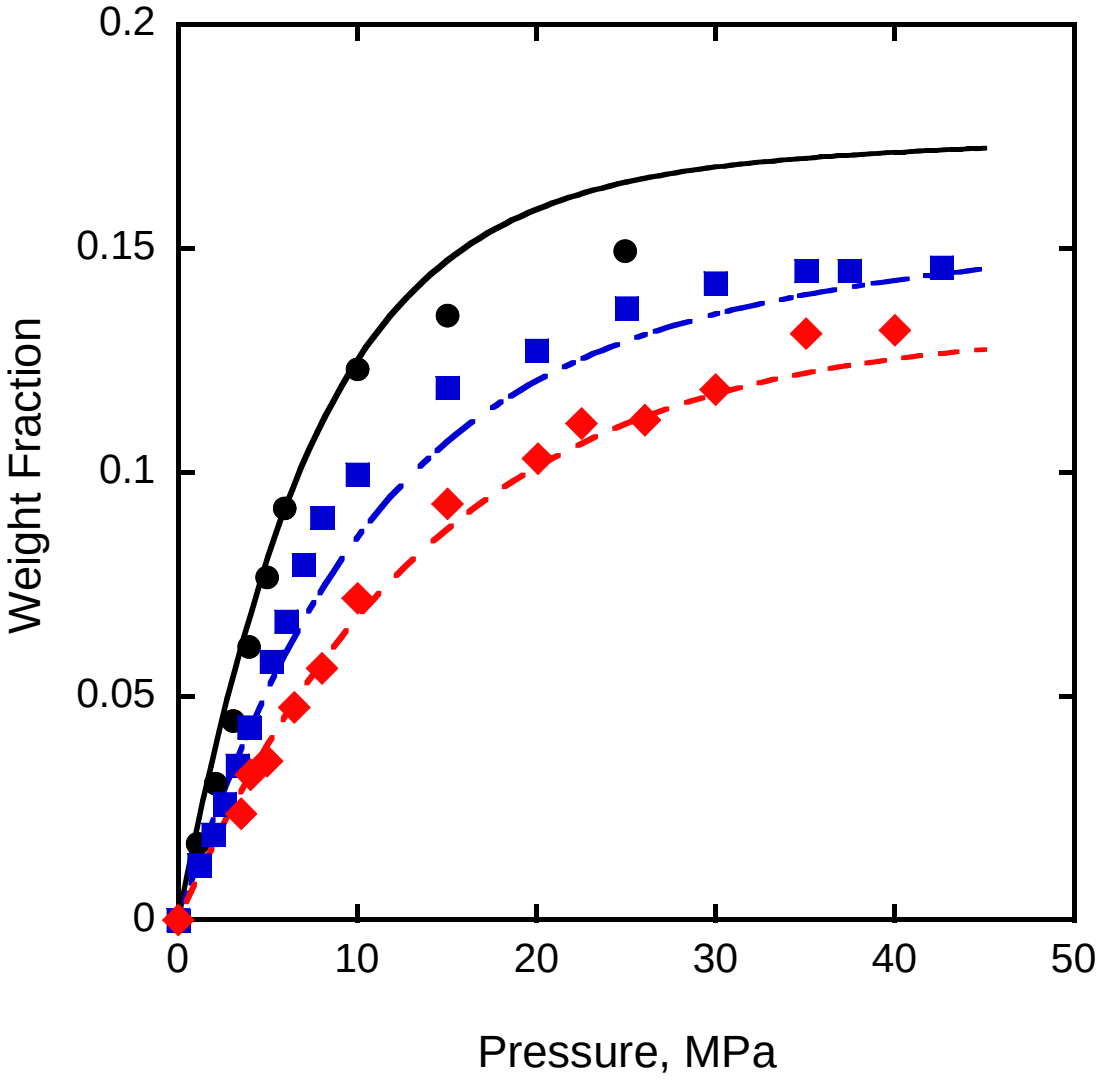

Figure 6.3 Correlations of sorption in CO_2 + PS. The circles, squares, and diamonds, represent experimental data from Ref. [154] at 308.15 K, 324.15 K, and 354.15 K respectively. Lines are calculated values from the model.

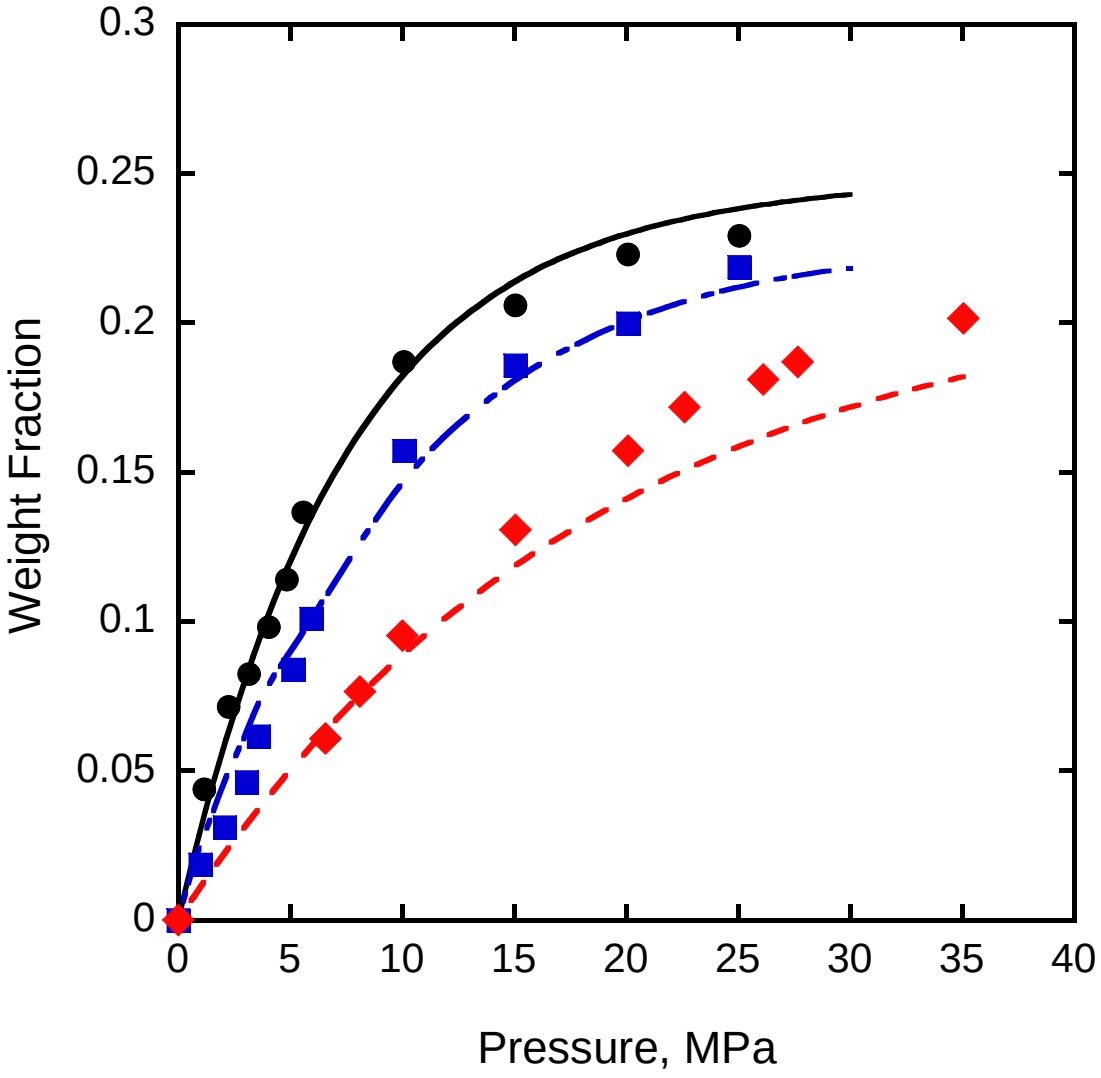

Figure 6.4 Correlation of sorption in CO_2 + PMMA. The circles, squares, and diamonds, represent experimental data from Ref. [154] at 308.15 K, 324.15 K, and 354.15 K respectively. Lines are calculated values from the model.

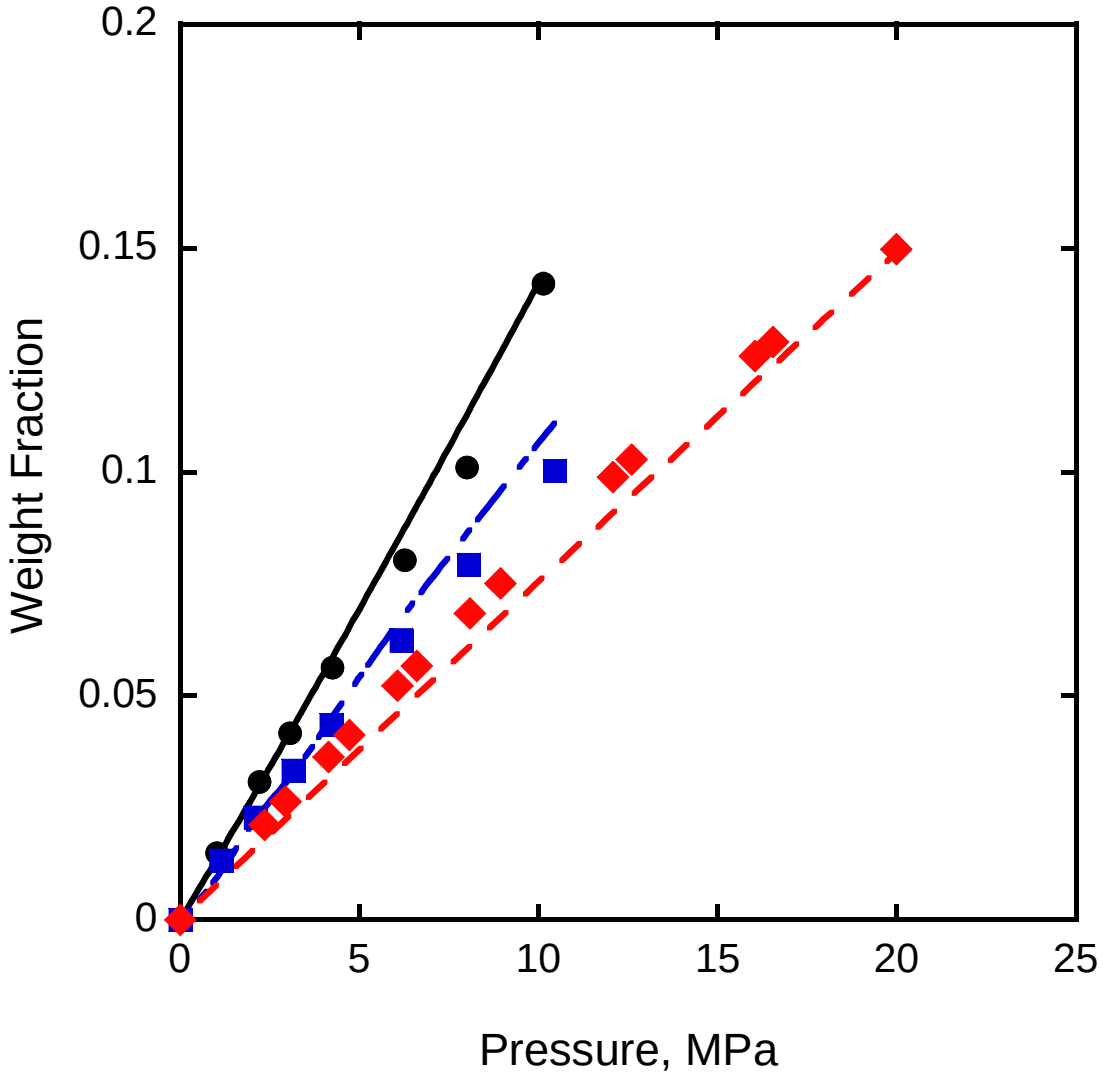

Figure 6.5 Correlation of sorption in CO_2 + PBS. The circles, squares, and diamonds, represent experimental data from Ref. [150] at 323.15 K, 353.15 K, and 393.15 K respectively. Lines are calculated values from the model.

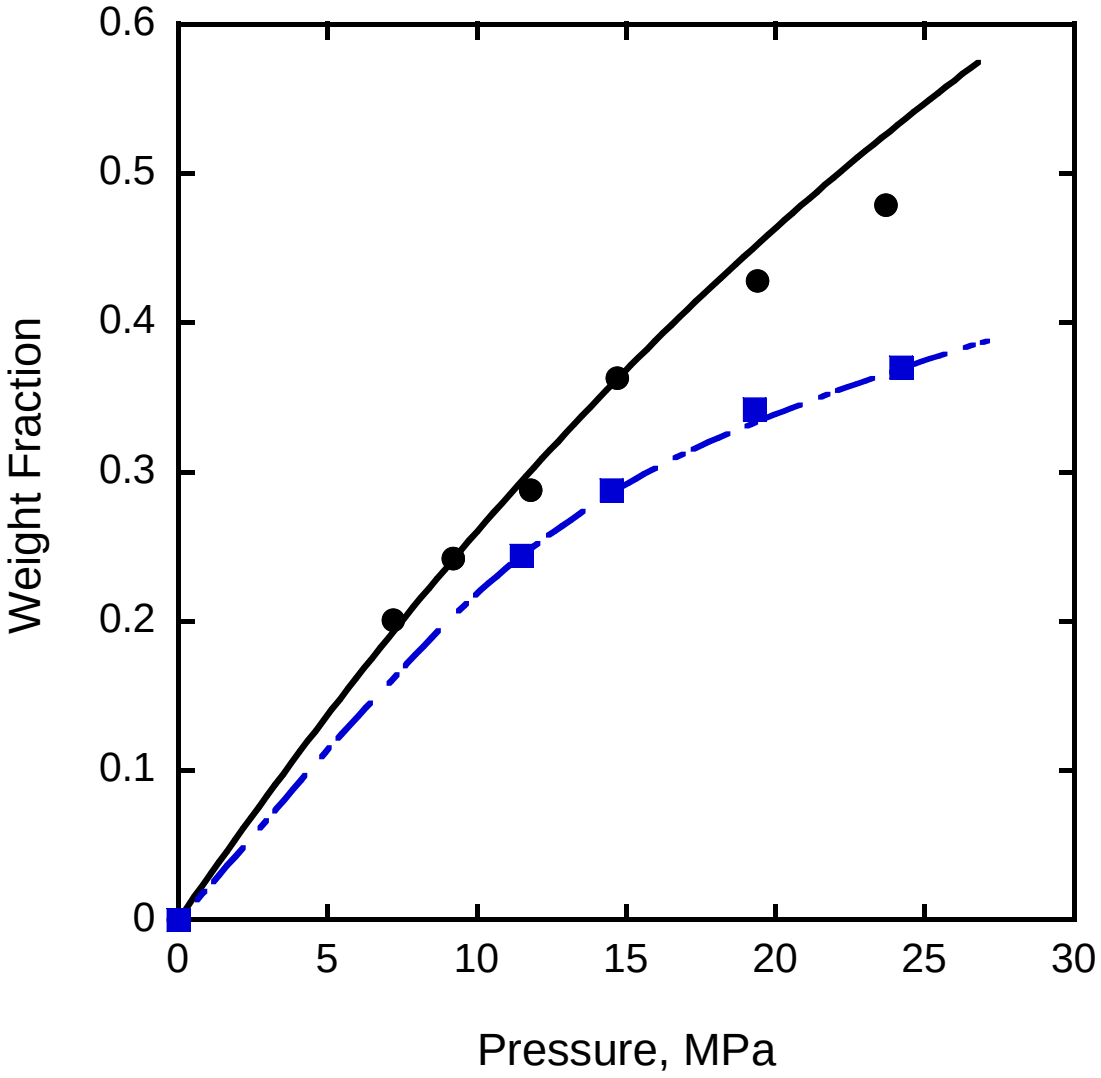

Figure 6.6 Correlation of sorption in CO_2 + EVA40. The circles, squares, and diamonds, represent experimental data from Ref. [151] at 323 K, and 348 K respectively. Lines are calculated from the model.

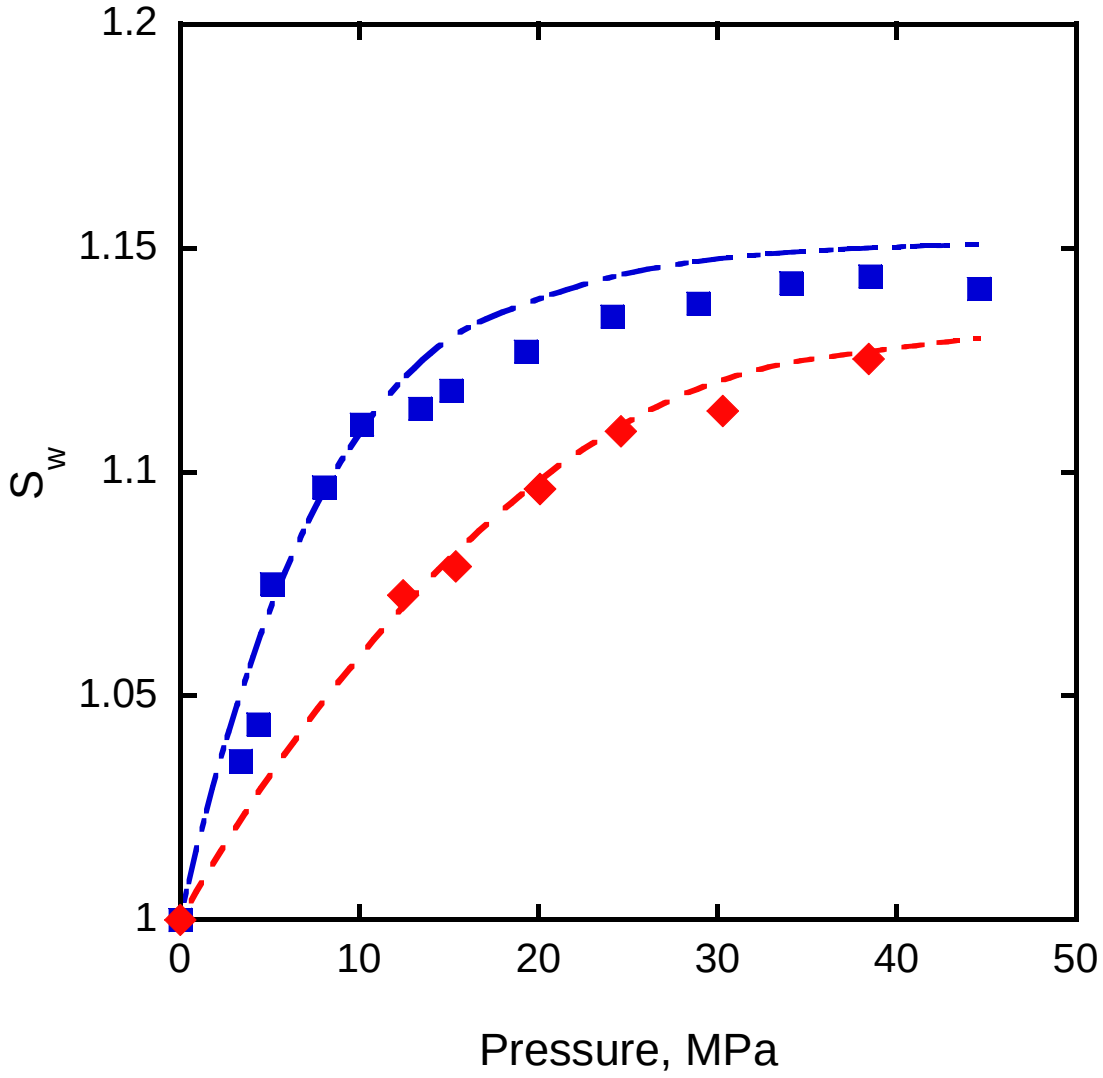

Figure 6.7 Swelling predictions for CO_2 + PS. The squares and diamonds represent experimental sorption data from Ref. [154] at 324.15 K, and 373.15 K respectively. The lines are calculated from the model.

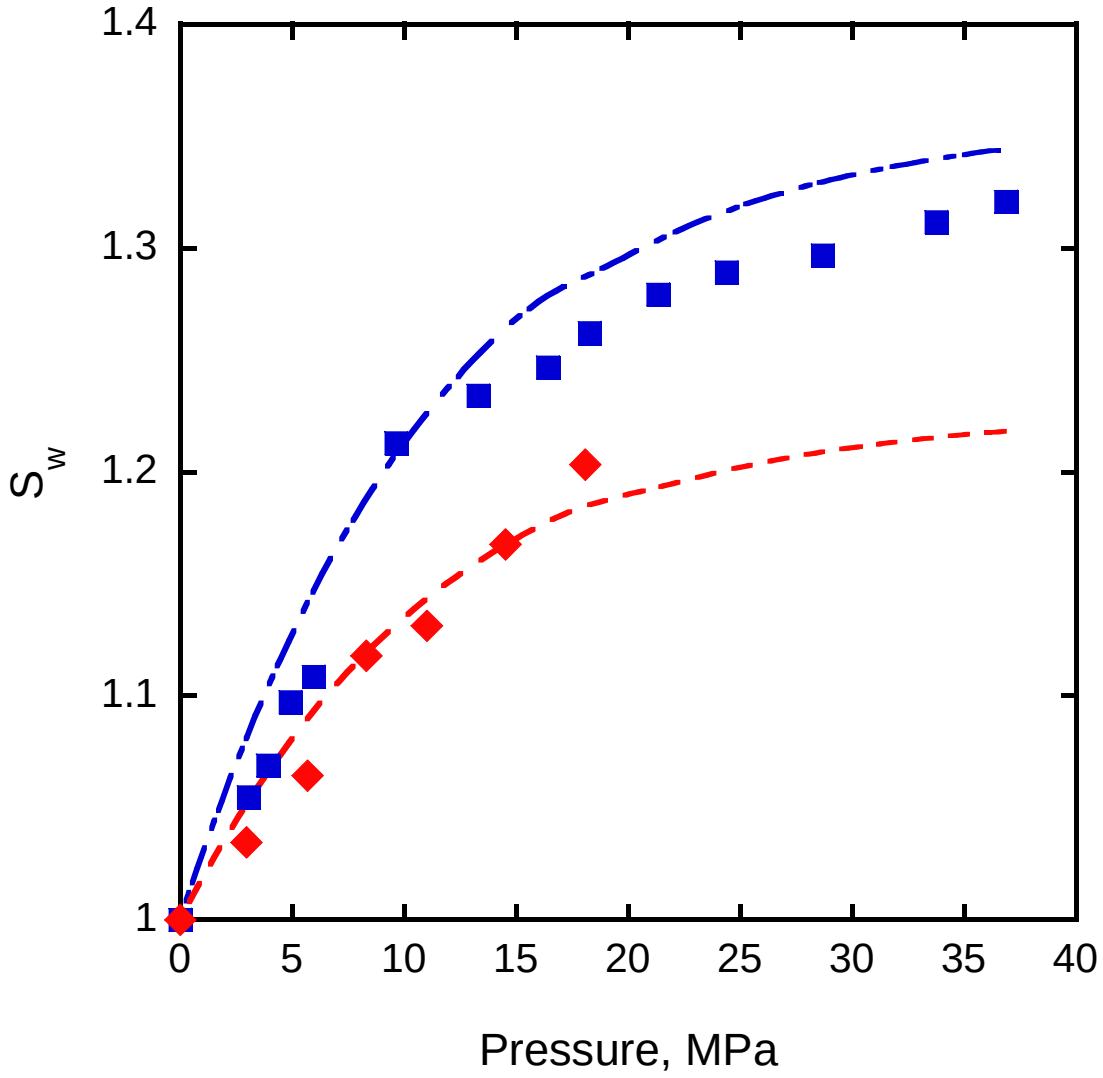

Figure 6.8 Swelling predictions for CO_2 + PMMA. The squares, and diamonds, represent experimental sorption data from Ref. [154] at 324.15 K, and 354.15 K respectively. The lines are calculated from the model.

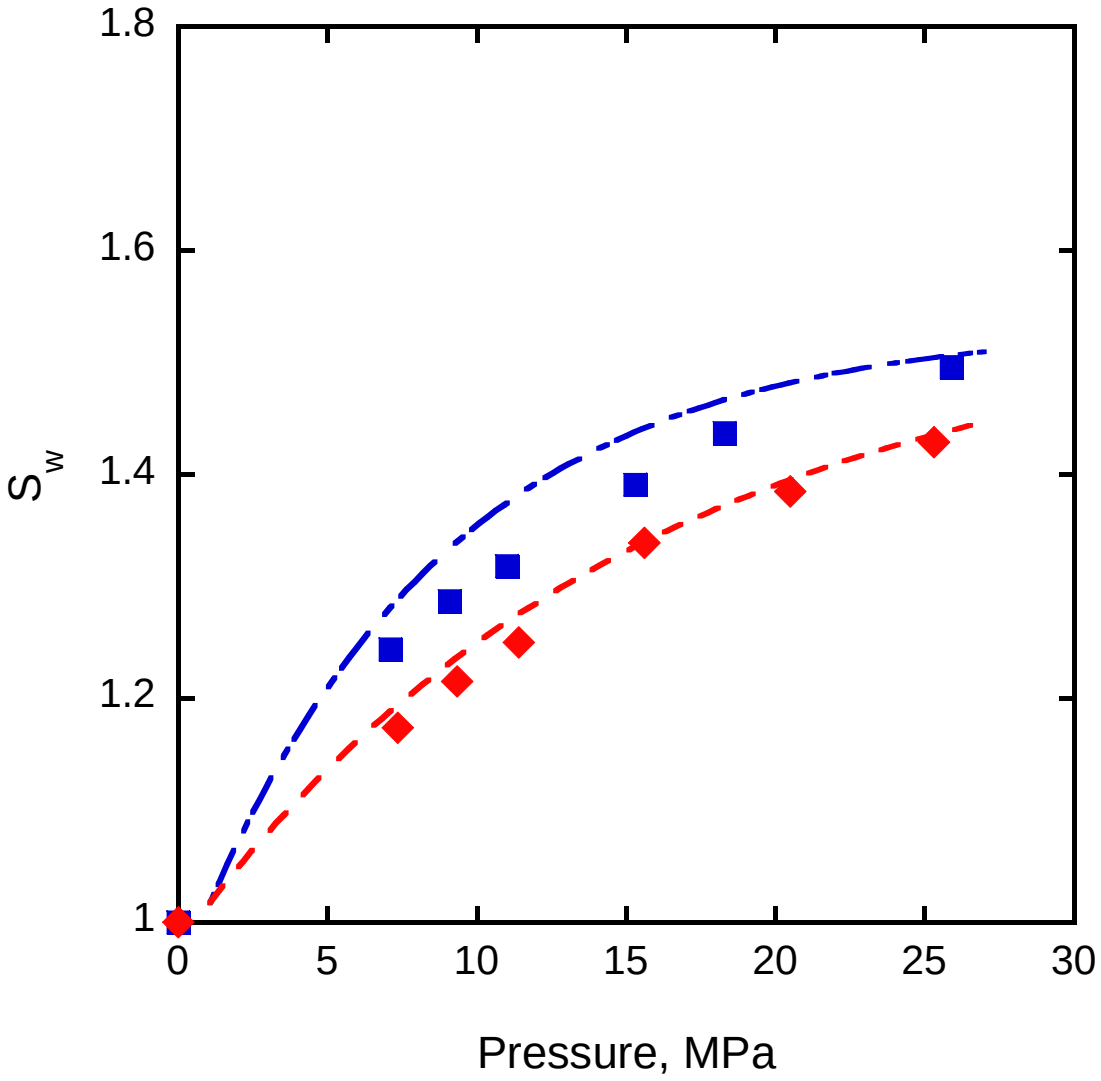

Figure 6.9 Swelling predictions for CO_2 + EVA40. The squares and diamonds, represent experimental sorption data from Ref. [151] at 323 K, and 348 K respectively. The lines are calculated from the model.

6.6 Conclusions

The compressible lattice model was reformulated in terms of an EOS (ALF EOS). The resulting EOS is similar to the SL EOS, but accounts for specific interactions via lattice energies, and chemical potentials. Model parameters obtained by fitting sorption equilibria can be used to predict swelling in polymers with average error less than 10 %.

CHAPTER 7

CONCLUSIONS AND RECOMMENDATIONS

7.1 Conclusions

Specific interactions between CO_2 and polymers with carbonyl, ether, siloxane and sulfone groups were investigated using *in situ* ATR-FTIR spectroscopy. Blue shifts in the carbonyl stretching frequencies were observed in CO_2 + PVAc, + PMMA, + PLA, and+ PLGA85 systems, and these CO_2 induced blue shifts were attributed to dielectric effects. This suggests that CO_2 induced carbonyl stretching frequency shifts cannot be used to quantify complex formation in these systems. Therefore, temperature dependent shifts in the CO_2 bending mode were used to quantify complex formation in CO_2 + carbonyl polymers. Enthalpies of C=O…CO_2 association were found to lie between -7 kJ/mol and -10 kJ/mol in the order: CO_2 + PVAc > CO_2 + PCL ≈ CO_2 + PLA > CO_2 + PLGA85 > CO_2 + PMMA. It was demonstrated that temperature dependent shifts in the CO_2 bending mode can also be used to quantify association in other CO_2-philic polymers, leading to enthalpies of association in the order CO_2 + PEG > CO_2 + PVAc > CO_2 + PSF > CO_2 + PMSSQ >> CO_2 + PVDF & PS.

Specific interactions in polymers + CO_2 systems were also investigated via NVT MD simulations. An analysis of pair distribution functions in these systems identified the association distance to be 3.2 Å. In addition, the accessibility of the CO group to CO_2 was also investigated via the intensity of the first peak in the pair distribution function. Accessibility was found to decrease in the order PVAc > PVMK > PLA > PMA. It was

determined that 96 % of associated CO_2 molecules involved in complex formation with one carbonyl group only and that the enthalpy of association increased in the order : CO_2...C-O-C > CO_2... O-C=O > CO_2...Si-O-Si .

The enthalpies of association obtained via FTIR spectra or MD simulation were incorporated directly into a compressible lattice model for phase behavior in polymer + CO_2 systems. The model was extended to ternary systems and it was shown that model parameters obtained from binary data can be used to predict ternary system behavior with AAD less than 10 %. Both UCST and LCST behavior could be predicted by the model. The results also suggest that DME - polymer complexes may be formed in associated polymer + DME systems, which is one reason why DME is a good solvent for processing acrylate polymers using CO_2.

The compressible lattice model was also reformulated in terms of a lattice-fluid EOS model. The new ALF EOS is similar to the SL EOS, but accounts for specific interaction effects via lattice energies, and chemical potentials. ALF EOS parameters obtained by fitting sorption equilibria can be used to predict swelling of polymers with average error less than 10 %.

7.2 Future Work

In Chapter 3, a general method to quantify specific interactions between CO_2 and polymers was proposed. The method can also be used to study interactions between CO_2 and ions in ionic liquids, poly (ionic liquids), and Metal Organic Framework (MOF) materials. In spite of the fact that some MD simulations have shown that the anion in ionic liquids will affect the CO_2 bending mode [155]. It is necessary to verify these

simulation results using *in situ* ATR-FTIR measurements so that novel ionic liquids for CO_2 capture may be designed that take advantage of specific interactions.

MD simulation should be extended to mixed gases + polymer systems, which are important in the use of polymer membranes for CO_2 separation [156-157]. MD simulations of these systems should provide understanding of CO_2 accessibility and specific interactions. Furthermore, they may help in the rational design of highly selective and permeable polymer membranes.

In Chapter 5, it was found that DME may also interact with the carbonyl group in polymers to form EDA complexes. This should be investigated using ATR-FTIR measurements. The key issue will be to identify the vibration frequency of associated DME molecules. Alternatively, quantum calculations and MD simulations should be used to study complex formation in DME + polymers..

In Chapter 6, the compressible lattice model was reformulated as an EOS model. The resulting EOS was of the same form as the SL EOS. It can be expected that the use of different free volume terms will lead to different types of EOS as suggested by the work of Sandler [158], Prigogine [159], and Nitta et al [160]. The free volume terms for various EOS have been reviewed by Lambert et al [58]. It may also be possible to obtain characteristic parameters from the properties of the pure components (such as density, cohesive energy) at a reference state that is close to the state of interest, so that the properties or phase behavior of mixtures can be extrapolated. This may be valuable for short range predictions.

The use of fugacity coefficients to calculate phase equilibria should be investigated., Recently, Neau [161] suggested that the chemical potentials in SL EOS

cannot be used for thermodynamically consistent phase equilibrium calculations. To overcome this problem, Neau [161] proposed consistent fugacity coefficients φ_i derived from $P(V,T,n)$ of the SL EOS by

$$\ln \varphi_i = -\ln Z + \left(\frac{\partial A^{res}(T,V,n)}{\partial n_i} \right)_{T,V,n_j} = \int_V^{\infty} \left(P - n\frac{RT}{V} \right) \frac{dV}{V} \tag{7.1}$$

where Z is the compressibility factor and A^{res} is the residual Helmholtz energy.

The models developed in this work should also be applied to other systems including ionic liquids and polymer blends in which there is association, or reversible chemical reaction. Even in small molecule systems, Veytsman statistics [162] can be used for the associating contribution in the partition function [163-164].

APPENDIX A

CHEMICAL ABSORPTION OF CO_2 IN [BMIM][ACETATE] FOR CO_2 CAPTURE

A.1 Introduction

There is considerable interest in using ionic liquids and poly (ionic liquids) for selectively removing CO_2 and other acid gases (H_2S and SO_2) from natural gas as well as power plant flue gas streams [165-168]. In particular, imidazolium-based room temperature ionic liquids (ILs) have been shown to be especially promising for CO_2 capture from flue gas streams because of the enhanced solubility of CO_2 in these liquids [168-169].

Imidazolium-based ILs also have the potential to overcome many of the disadvantages associated with current amine-based CO_2 capture technologies which are energy intensive, release volatile organic compounds, and suffer from amine loss and degradation [155, 170]. Enhanced CO_2 solubility and absorption in ILs can be due to physical as well as chemical mechanisms. Physical absorption is the dominant mechanism in ILs such as 1-hexyl-3-methyl-imidazolium bis(trifluoro-methyl-sulfonyl) imide [Hmim][Tf_2N], whereas chemical absorption dominates in ILs containing amine groups [171]. In general, chemical absorption offers higher molar uptake of CO_2 per mole of IL compared with physical absorption [172]. Thus, CO_2 solubility in 1-butyl-3-methylimidazolium ($[Bmim]^+$) based ILs increases in the order $[NO_3]^- < [BF_4]^- < [PF_6]^- < [Tf_2N]^-$ due to physical sorption [166]; however, CO_2 solubility in [Bmim][Ac] at 0.1 atm CO_2 partial pressure is about 30 times greater than in either [Bmim][TFA] or in

[Bmim][Tf_2N] [173]. Yokozeki et al concluded that both physical and chemical sorption of CO_2 must occur in [Bmim] [Ac] (CH_3COO^-) but only physical sorption occurs in [Bmim][TFA] (CF_3COO^-) and [Bmim][Tf_2N] (bis-(trifluoromethyl)sulfonylimide) [173].

CO_2 is thought to form weak complexes with the IL. These complexes have a high carrying capacity, but require very little energy for the reverse reaction. This leads to high capacity for CO_2 while keeping the energy requirements to regenerate the IL low. Chemical complex formation between CO_2 and [Bmim][Ac] has been noted by Maginn [174], Shiflett et al [175], and Barrossee-Antle and Compton [176]. However, the mechanism for their formation remains unknown. This hinders the design of novel acid gas absorbents such as poly ILs [177], zeolitic imidazolate frameworks [178], and supramolecular ionic networks [179] for low partial pressure (less than 10 bar) CO_2 capture.

In the present work, we have used *in-situ* ATR-FTIR (Attenuated Total Reflection- Fourier Transform Infrared Spectroscopy) to study interactions between CO_2 and [Bmim][Ac], as well as the sorption / desorption behavior of CO_2 in this IL. We have used IR and NMR analysis to infer the reversibility of the chemical complex and a mechanism for complex formation.

A.2 Experimental Section

[Bmim][Ac] (HPLC grade $\geq$ 96.0 %, $C_{10}H_{18}N_2O_2$) , [Bmim][TFA] (HPLC grade $\geq$ 96.5 %, $C_{10}H_{15}F_3N_2O_2$), and solvents were purchased from Aldrich (St. Louis, MO). High purity N_2 and CO_2 gas (99.99%) were purchased from Airgas Inc. (Radnor, PA) and used as received. All ILs were dried overnight in a vacuum oven at 323 K before use.

ATR-FTIR measurements were made using a Nicolet 550 Fourier transform spectrometer with a DTGS detector at a resolution of 1 cm^{-1}. Spectra were obtained using 64 scans in the 4000-500 cm^{-1} wavenumber range. The high pressure ATR Cell was made by Axiom Analytical, Inc (Irvine, CA, USA) and consisted of a ZnSe crystal attached to a cylindrical flow cell (volume 2 mL) by a Teflon O-ring. The incident angle of the IR beam was 45 ^{o}, giving 10 specimen-sensing reflections at the top face of the crystal. The cell was heated to a temperature of 353 K by circulating water. A temperature controller (Omega CN9000A) maintained the temperature of the cell within ± 0.2 K. CO_2 from a syringe pump, connected to a pressure gauge (Heise, Model 710A), maintained the pressure in the cell within ± 0.1 bar.

In situ ATR-FTIR measurements of the IL-CO_2 system were performed as follows. Background spectra were recorded under vacuum in the absence of a sample. The IL sample (2.0 mL) was then injected into the cell and the cell was purged by a slow flow of nitrogen. After a film of IL had formed on the ZnSe crystal, the cell was evacuated, heated to a temperature of 353 K, and kept at this temperature for 12 h to eliminate any volatile impurities.

The temperature was then increased to the experimental value and the IR spectrum was collected under vacuum. Thereafter, CO_2 was slowly introduced into the cell until the pressure reached the experimental value. Spectra were collected during this time until no changes could be observed in the absorbance bands of CO_2 or the IL. The spectra are displayed in terms of absorbance, defined as $-\log (I/I_0)$, where I and I_0 represent IR beam l intensities of the sample and reference states, respectively.

^{1}H NMR spectra were measured on a Varian Mercury 400 MHz spectrometer using deuterated chloroform as the lock solvent.

A.3 Results and Discussion

A.3.1 ATR-FTIR analysis

Figure A.1 shows the imidazolium cation and anion of [Bmim][Ac] with the position of the protons labeled. IR spectra of pure [Bmim][Ac] and [Bmim][Ac] exposed to 10 bar CO_2 at 298 K are shown in Figure A.2. New peaks can be clearly seen at (790, 945, 1250, 1321, 1506, 1665, and 2338) cm^{-1} in the CO_2 + [Bmim][Ac] spectrum. The peak at 2338 cm^{-1}can be assigned to the asymmetrical stretching of CO_2, whereas the other peaks must belong to a new compound that is formed when CO_2 is absorbed in [Bmim][Ac]. The peaks at 1665, 1250 and 945 cm^{-1} are characteristic peaks of the carboxylic acid group [180] and suggest that the new compound is a carboxylic acid. Small peaks are also apparent at 1702 cm^{-1} and 3088 cm^{-1}. The peaks at 3088 cm^{-1} and 1665 cm^{-1} can be assigned to the stretching of OH and C=O bonds in the carboxylic acid group (-COOH) of the chemical complex CO_2…[Bmim][Ac]. By comparison, similar spectra for [Bmim][TFA] do not have any new peaks except for CO_2 peaks at 2338 cm^{-1} and 670 cm^{-1}. Therefore, we may conclude that there is no complex formation in the CO_2 + [Bmim][TFA] system. It should be added that there is a broad peak at 660 cm^{-1} in both [Bmim][Ac] and [Bmim][TFA] systems that overlaps with the CO_2 bending mode. However, it is not clear if splitting of the CO_2 bending mode occurs in these systems.

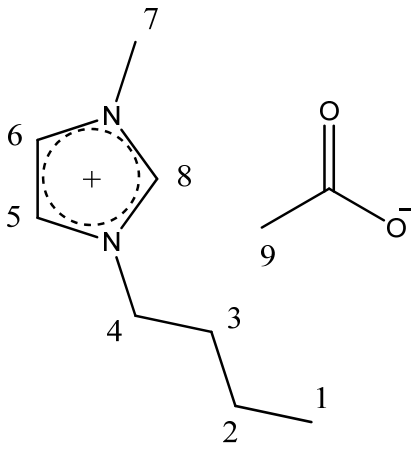

Figure A.1 Chemical structure and proton numbering on the imidazolium cation and anion of [Bmim][Ac].

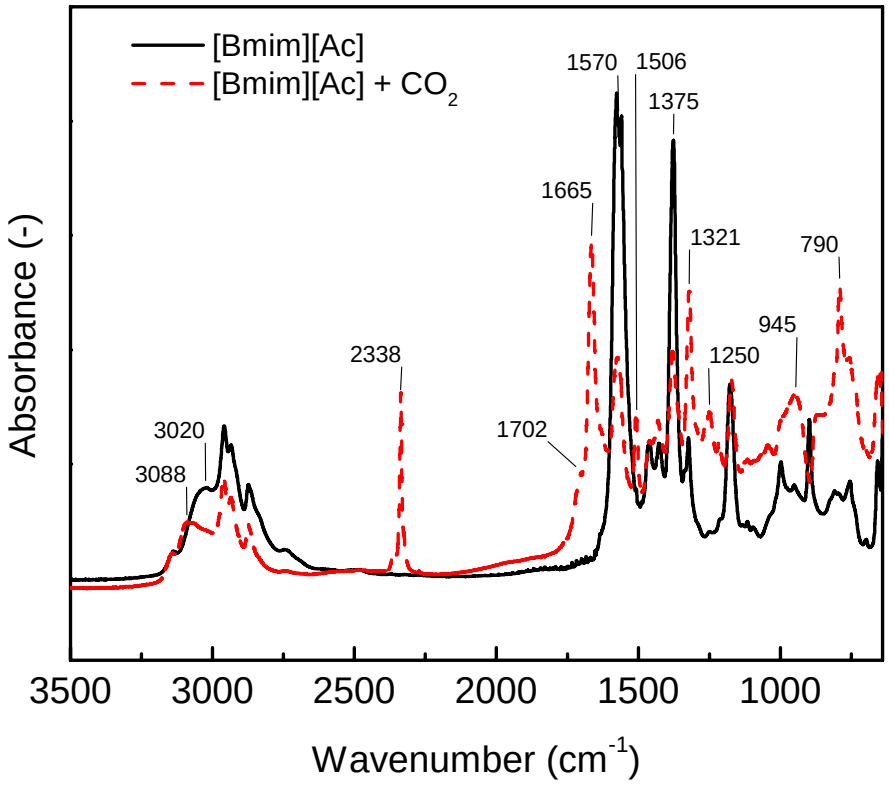

Figure A.2 ATR-FTIR spectra of [Bmim][Ac] and CO_2 + [Bmim][Ac] at 298 K.

Figure A.3 shows the carbonyl stretching bands in the spectra of CO_2 + ethyl acetate, CO_2 + acetic acid, CO_2 + [Bmim][Ac], and CO_2 + [Bmim][TFA] with the positions of the peaks listed in Table 1. Figure 3 and Table 1 confirm that new peaks are present in the spectra of [Bmim][Ac] exposed to CO_2, and also that there are no significant changes in the IR spectra when [Bmim][TFA], ethyl acetate, or acetic acid are exposed to CO_2. This also suggests that any Lewis acid-base interactions between CO_2 and C=O groups in [Bmim][TFA], ethyl acetate, or acetic acid, are weak and do not lead to significant frequency shifts in the IR spectra. By contrast, a new carbonyl stretching peak can be found at 1665 cm^{-1} in CO_2 + [Bmim][Ac] compared with the carbonyl stretching peak at 1570 cm^{-1}in [Bmim][Ac]. Both Maginn [174] and Shiflett et al [175] suggested that acetic acid could be a product of the reaction between CO_2 and [Bmim][Ac]. Clearly, the new peak at 1665 cm^{-1} is not from acetic acid, because the C=O stretching peaks of acetic acid occur at 1755 and 1710 cm^{-1}.

A.3.2 Dynamic absorption and desorption behavior

The ATR-FTIR analysis presented in the previous section confirms that a chemical complex is formed between CO_2 and [Bmim][Ac], which is promising for the use of [Bmim][Ac] for CO_2 capture. We have therefore investigated the dynamics of CO_2 sorption and desorption in [Bmim][Ac]. Figure A.4 shows the evolution of ATR-FTIR spectra for CO_2 absorption in [Bmim][Ac] at 298 k and 10 bar CO_2 pressure. The most interesting bands in these spectra are the carbonyl stretching bands at 1500 to 1700 cm^{-1}. At t = 0, only pure [Bmim][Ac] is in the system and the carbonyl stretching band can be found at 1570 cm^{-1}. The intensity of this peak gradually decreases with time and the

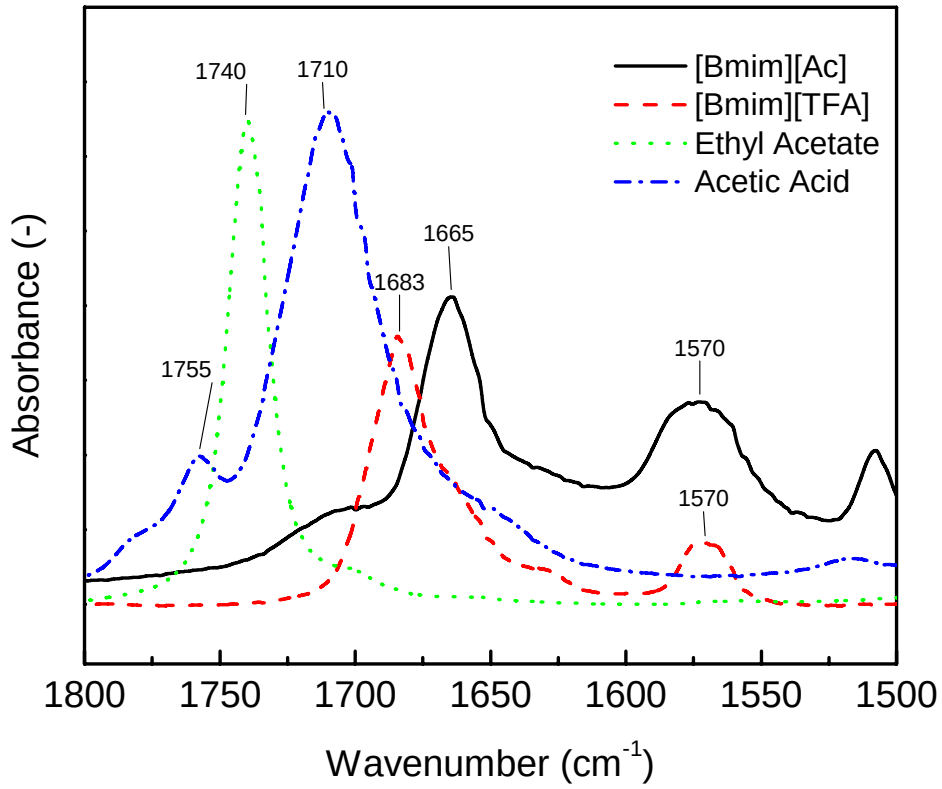

Figure A.3 ATR-FTIR spectra of CO_2 + ethyl acetate, CO_2 + acetic acid, CO_2 + [Bmim][Ac], and CO_2 + [Bmim][TFA], at 298 K and 10 bar CO_2 pressure.

Table A.1 Carbonyl stretching bands (cm^{-1}) in FTIR spectra of compounds groups.

Chemical compound	Without CO_2	With 10 Bar CO_2
[Bmim][Ac]	1570	1665, 1570
[Bmim][TFA]	1683, 1570	*
Ethyl Acetate	1740	*
Acetic Acid	1755, 1710	*

* No significant change without/with CO_2

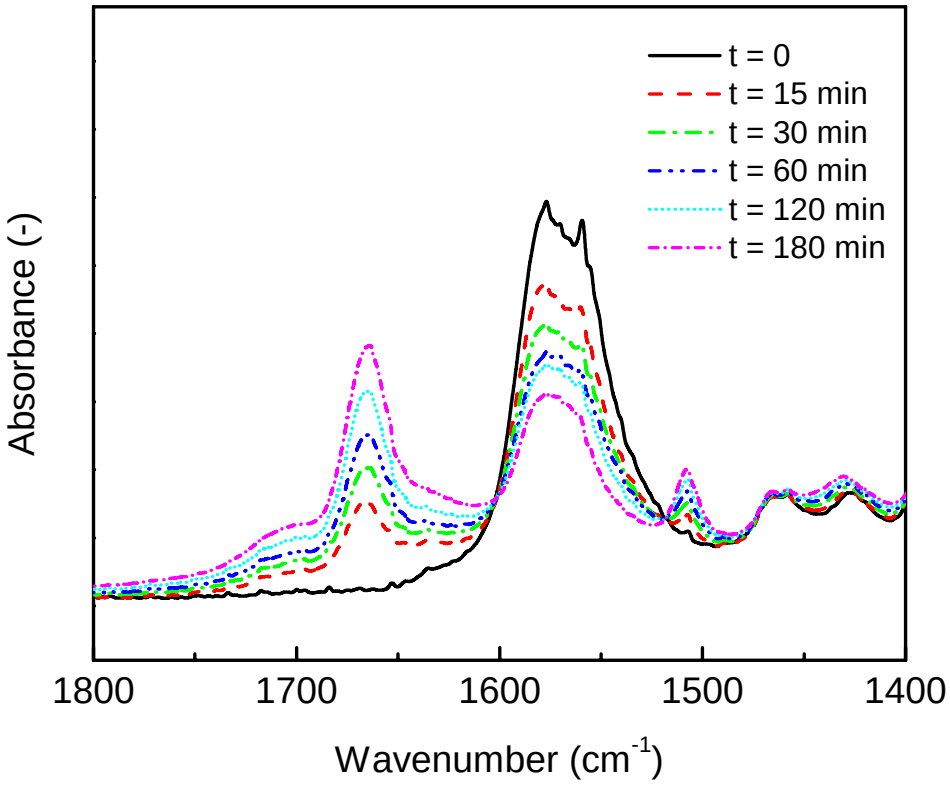

Figure A.4 ATR-FTIR spectra for CO_2 absorption in [Bmim][Ac] at 298 K and 10 bar CO_2 pressure.

intensity of the new peak at 1665 cm^{-1} increases. After 3 h, when the system has attained equilibrium, the intensity of the new peak surpasses that of the old peak. By integrating the area under the 1570 cm^{-1} peak and assuming that the molar absorbtivity does not depend on composition, we estimate that about 60 % of [Bmim][Ac] had reacted with CO_2 in 3 h. The apparent absorption reaction rate is therefore quite small. However, absorption could be mass transfer limited because the diffusion coefficients of CO_2 in ILs are about 10-100 times smaller than those of common liquids [181].

Figure A.5 shows the dynamics of CO_2 desorption in [Bmim][Ac] when the system is quickly depressurized to 0.01 bar from an initial equilibrium CO_2 pressure of 12.5 bar at 353 K. We can clearly see that the C=O band at 1570 cm^{-1} was recovered within 5 min. The intensity of the C=O band at 1665 cm^{-1} also decreased quickly for 5 min, but decreased very slowly after that. It should be noted that Shiflett et al [11] did not observe any new bands in the case of CO_2 desorption at 323 K. However, the new C=O peak could still be found at 353 K in our experiments, implying that [Bmim][Ac] was not fully recovered at this temperature. This could have important implications for the regeneration of [Bmim][Ac] during CO_2 capture.

A.3.3 NMR Analysis

^1H NMR spectra before and after CO_2 absorption are shown in Figure A.6. In the absence of CO_2, the ratio of the areas under the H [8] and H [1] peaks was about 1/3. After 24 h under 12.5 bar CO_2 pressure at 298 K, the H[8] peak at 7.29 ppm disappeared whereas a new peak could be found at 11.4 ppm. The latter peak is characteristic of a proton shift in the carboxylic acid group (COOH). However, the peak for the COOH

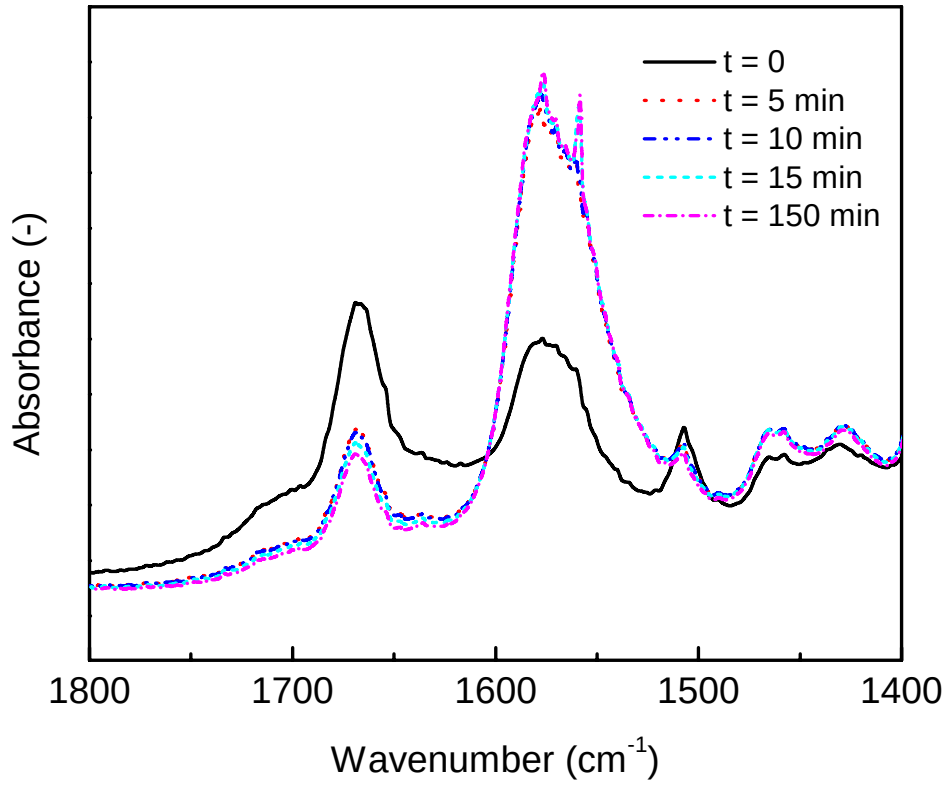

Figure A.5 ATR-FTIR spectra for CO_2 desorption in [Bmim][Ac] at 353 K starting from an initial CO_2 pressure of 12.5 bar and depressurizing to 0.01 bar.

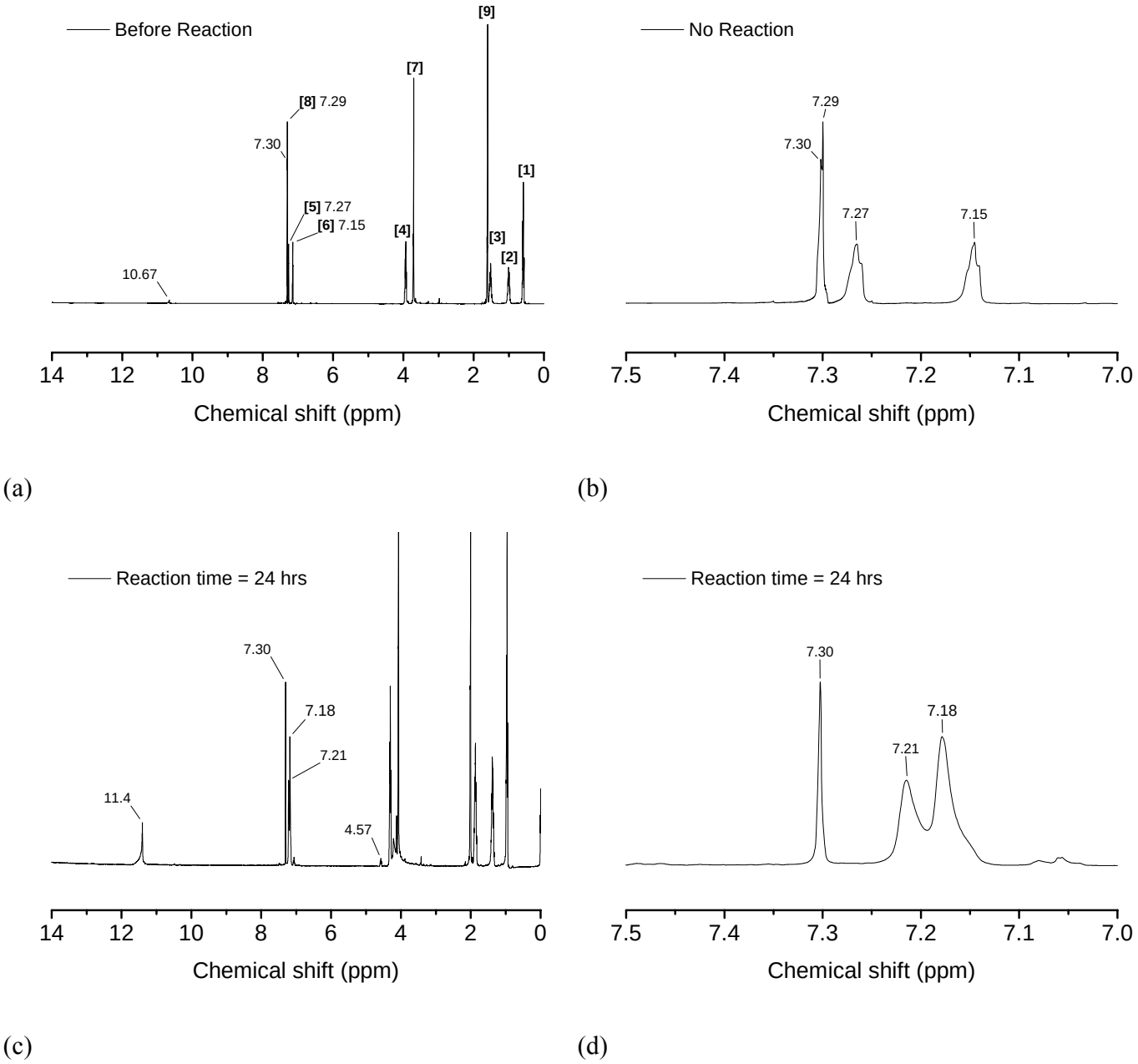

Figure A.6 ^{1}H NMR spectra for [Bmim][Ac] before (a-b) and after (c-d) exposure to 12.5 bar CO_2 pressure for 24 h at 298 K.

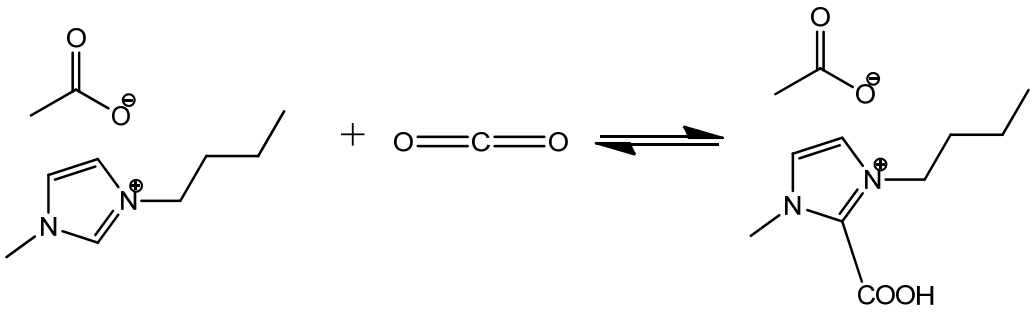

Figure A.7 Proposed chemical reaction between CO_2 and [Bmim][Ac].

proton shift in acetic acid occurs at 12.4 ppm, and not at 11.4 ppm. Therefore, the COOH peak found in the spectra for CO_2 + [Bmim][Ac] is not from acetic acid. The ratio of areas under the H [11.4ppm] and H[1] peaks was found to be about 0.92/3. These data imply ~ 90 % conversion for the chemical reaction between CO_2 and [Bmim][Ac].

A.3.4 Reaction between CO_2 and [Bmim][Ac]

Based on the above results, we propose that chemisorption of CO_2 in [Bmim][Ac] occurs as shown in Figure A.7, and that the molar uptake of CO_2/[Bmim][Ac] equals 1. The amount of chemisorbed CO_2 can now be estimated and found to be 47 mol % for ~ 90 % conversion of [Bmim][Ac]. This value is close to the value of 40.6 mol % at 13 bar and 298 K estimated from gravimetric sorption measurements [175]. Therefore, the abnormal high solubility of CO_2 in [Bmim][Ac] at low pressures must be the result of the chemical reaction between CO_2 and [Bmim][Ac]. This may also be true for other imidazolium acetate based ILs such as [Bmim][ISB] (isobutyrate), [Bmim][IAAc] (iminoacetic acid acetate), and [Bmim][TMA] (trimethylacetate), as suggested by Yokozeki et al [173].

A.4 Conclusions

The absorption of CO_2 in [Bmim][Ac] was studied via in-situ ATR-FTIR and NMR experiments and found to be enhanced by a reversible chemical reaction between CO_2 and [Bmim][Ac]. NMR analysis was used to identify a new carboxylic acid (rather than acetic acid) as the chemical reaction product of CO_2 and [Bmin][Ac]. In dynamic studies, ATR-FTIR spectra could not be fully recovered after CO_2 desorption at 353 K, suggesting that the reaction is not completely reversible at this temperature. This has

important implications for CO_2 capture at low temperatures using [Bmim][Ac] and perhaps other imidazolium acetate based ILs.

Yuan, Yanhui; Zhu, Xun-Jin and Teja, Amyn S., *Chemisorption of CO_2 in [Bmim] [Acetate] for CO_2 capture*, Green Chemistry, submitted.

APPENDIX B

DERIVATION OF THE ACTIVITY OF COMPONENT *i* FOR THE TERNARY COMPRESSILLBE LATTICE MODEL

Let us consider a system contain polymer (P), solvent (S), and cosolvent (C). We will use binary system model to describe P + S, P + C, and S + C, respectively, and then, a ternary system model was proposed based on piece-wise addition of excess free energy.

Binary systems:

For Polymer + CO_2 system

$$\frac{\Delta G_{PS}^{mix}}{NRT} = \alpha_{PS}\phi_P\chi_{PS}^{a} + \phi_P\left(\phi_S - \alpha_{PS}\phi_P\right)\left[z-2-\alpha_{PS}\right]\chi_{PS}^{u} + \frac{\phi_P}{\xi_P}\ln\phi_P + \left(\frac{\phi_S - \alpha_{PS}\phi_P}{1+\alpha_{PS}}\right)\ln\left(\phi_S - \alpha_{PS}\phi_P\right) - \phi_S\ln\frac{\phi_S}{\phi_S - \alpha_{PS}\phi_P} + \alpha_{PS}\phi_P\ln\frac{\alpha_{PS}\phi_P}{\phi_S - \alpha_{PS}\phi_P} + \phi_P\left(1-\alpha_{PS}\right)\ln\left(1-\alpha_{PS}\right) + \alpha_{PS}\phi_{PS}\ln\alpha \tag{B.1}$$

To simplify Equation (B.1)

$$\frac{\Delta G_{PS}^{mix}}{NRT} = \alpha_{PS}\phi_P\chi_{PS}^{a} + \phi_P\left(\phi_S - \alpha_{PS}\phi_P\right)\left[z-2-\alpha_{PS}\right]\chi_{PS}^{u} + \frac{\phi_P}{\xi_{PS}}\ln\phi_P + \left(\frac{2+\alpha_{PS}}{1+\alpha_{PS}}\right)\left(\phi_S - \alpha_{PS}\phi_P\right)\ln\left(\phi_S - \alpha_{PS}\phi_P\right) - \phi_S\ln\phi_S + \left(\alpha_{PS}\phi_P\right)\ln\left(\alpha_{PS}\phi_P\right) + \phi_P\left(1-\alpha_{PS}\right)\ln\left(1-\alpha_{PS}\right) + \alpha_{PS}\phi_P\ln\alpha_{PS} \tag{B.2}$$

Based on Equation (B.2), for Polymer + Cosolvent system

$$\frac{\Delta G_{PC}^{mix}}{NRT} = \alpha_{PC}\phi_P\chi_{PC}^{a} + \phi_P(\phi_C - \alpha_{PC}\phi_P)[z-2-\alpha_{PC}]\chi_{PC}^{u} + \frac{\phi_P}{\xi_{PC}}\ln\phi_P + \left(\frac{2+\alpha_{PC}}{1+\alpha_{PC}}\right)(\phi_C - \alpha_{PC}\phi_P)\ln(\phi_C - \alpha_{PC}\phi_P) - \phi_C\ln\phi_C + (\alpha_{PC}\phi_P)\ln(\alpha_{PC}\phi_P) + \phi_P(1-\alpha_{PC})\ln(1-\alpha_{PC}) + \alpha_{PC}\phi_P\ln\alpha_{PC} \quad \text{(B.3)}$$

For CO_2 + Cosolvent system

Assumption 1.: No association interaction between CO_2 + Cosolvent,

Assumption 2.: Segment number is same for CO_2 and Cosolvent (Reason: both are small molecules; Easy to count association sites with polymer)

Based on Flory-Huggins Equation,

$$\frac{\Delta G_{SC}^{mix}}{NRT} = \phi_S\phi_C[z-2]\chi_{SC}^{u} + \phi_S\ln(\phi_S) + \phi_C\ln(\phi_C) \quad \text{(B.4)}$$

Ternary system:

Based on Equation (B.2 to B.4)

$$\begin{aligned}\frac{\Delta G_{PSC}^{mix}}{NRT} &= \alpha_{PS}\phi_P\chi_{PS}^{a} + \phi_P(\phi_S - \alpha_{PS}\phi_P)[z-2-\alpha_{PS}]\chi_{PS}^{u} \\ &+ \alpha_{PC}\phi_P\chi_{PC}^{a} + \phi_P(\phi_C - \alpha_{PC}\phi_P)[z-2-\alpha_{PC}]\chi_{PC}^{u} \\ &+ (\phi_S - \alpha_{PS}\phi_P)(\varphi_C - \alpha_{PC}\phi_P)[z-2]\chi_{SC}^{u} \\ &+ \frac{\phi_P}{\xi_{PSC}}\ln\phi_P + \left(\frac{2+\alpha_{PS}}{1+\alpha_{PS}}\right)(\phi_S - \alpha_{PS}\phi_P)\ln(\phi_S - \alpha_{PS}\phi_P) - \phi_S\ln\phi_S \\ &+ \left(\frac{2+\alpha_{PC}}{1+\alpha_{PC}}\right)(\phi_C - \alpha_{PC}\phi_P)\ln(\phi_C - \alpha_{PC}\phi_P) - \phi_C\ln\phi_C \\ &+ (\alpha_{PS}\phi_P)\ln(\alpha_{PS}\phi_P) + \phi_P(1-\alpha_{PS})\ln(1-\alpha_{PS}) + \alpha_{PS}\phi_P\ln\alpha_{PS} \\ &+ (\alpha_{PC}\phi_P)\ln(\alpha_{PC}\phi_P) + \phi_P(1-\alpha_{PC})\ln(1-\alpha_{PC}) + \alpha_{PC}\phi_P\ln\alpha_{PC}\end{aligned} \quad \text{(B.5)}$$

To use the model, we need following parameters:

$\chi_{PS}^{a}; \chi_{PS}^{u}$

$\chi_{PC}^{a}; \chi_{PC}^{u}$

χ_{SC}^{u}

$\xi_P; \alpha_{PS}; \alpha_{PC}$

Where,

$$\chi_{ij}^{u} = \frac{V_{ij}\left(\delta_i - \delta_j\right)^2}{\left(z-2-\alpha_{ij}\right)RT} \tag{B.6}$$

$$\chi_{ij}^{a} = \frac{\Delta H_{ij}^{a}}{RT} \tag{B.7}$$

$$K_{ij} = \frac{\alpha_{ij}}{1-\alpha_{ij}}\left(\frac{1-\alpha_{ij}\phi_j}{\phi_i - \alpha_{ij}\phi_j}\right) \tag{B.8}$$

$$\ln\frac{K_{ij}}{K_{ij0}} = -\frac{\Delta H_{ij}^{a}}{R}\left(\frac{1}{T}-\frac{1}{T_0}\right) \tag{B.9}$$

$$\xi_P = \frac{V_P\left[T,P\right] - 1.2V_P^{vdW}}{V_S\left[T,P\right] - V_S^{vdW}} \tag{B.10}$$

<u>Activity of component *i*</u>

$$\ln a_i = \frac{1}{RT}\left(\frac{\partial \Delta G_{mix}}{\partial N_i}\right)_{T,P,N_{j\neq i}} = \frac{r_i}{RT}\left[\Delta G_{mix}^{V} + \left(1-\phi_i\right)\left(\frac{\partial \Delta G_{mix}^{V}}{\partial \phi_i}\right)_{T,P,N_{j\neq i}}\right] \tag{B.11}$$

Where,

$$\Delta G_{mix} = \left(\sum_i r_i N_i\right)\Delta G_{mix}^{V} = N\Delta G_{mix}^{V} \tag{B.12}$$

$$\left(\frac{\partial \phi_j}{\partial \phi_i}\right)_{j\neq i} = -\frac{\phi_j}{1-\phi_i} \tag{B.13}$$

In a binary system with polymer (P) + solvent (S)

$$\begin{aligned}\ln a_S = {} & \beta_s\phi_P\chi^a_{PS} + \phi_P\left[\left(-\beta_S\phi_P + \phi_P(1+\alpha)\right)(z-3) - \beta_S\left(\phi_S - \alpha\phi_P\right)\right]\chi^u_{PS} \\ & -\frac{\phi_P}{r_P} + \left(\frac{1}{1+\alpha} - \frac{\beta_S}{(1+\alpha)^2}\right)\ln\left(\phi_S - \alpha\phi_P\right) \\ & + \left(\frac{\phi_S - \alpha\phi_P}{1+\alpha}\right)\left(\frac{1-\beta_S\phi_P}{\phi_S - \alpha\phi_P} - 1\right) - \ln\left(\frac{\phi_S}{\phi_S - \alpha\phi_P}\right) - 1 + \phi_S\left(\frac{1-\beta_S\phi_P}{\phi_S - \alpha\phi_P}\right) \\ & + \beta_S\phi_P\ln\left(\frac{\alpha\phi_P}{\phi_S - \alpha\phi_P}\right) + \alpha\phi_P\left(\frac{\beta_S}{\alpha} - \frac{1-\beta_S\phi_P}{\phi_S - \alpha\phi_P}\right) + \beta_S\phi_P\ln\left(\frac{\alpha}{1-\alpha}\right)\end{aligned} \tag{B.14}$$

$$\beta_S = \left(\frac{\partial\alpha}{\partial N_S}\right) = \frac{\alpha(K+1) - K}{(2\alpha\phi_P - 1)(K+1)} \tag{B.15}$$

In a ternary system, the activity of component *i* can be obtained as following:

$$\mathrm{S}_1 = \alpha_{PS}\phi_P\chi^a_{PS}$$

$$\left(\frac{\partial(N\mathrm{S}_1)}{\partial N_i}\right) = \left(\frac{\partial\alpha_{PS}}{\partial N_i}\right)r_P N_P\chi^a_{PS} + \alpha_{PS}r_P\left(\frac{\partial N_P}{\partial N_i}\right)\chi^a_{PS} = \left(\beta^{(i)}_{PS}r_p N_p + \alpha_{PS}r_P N^{(i)}_P\right)\chi^a_{PS} \tag{B.16}$$

Where,

$$\Gamma^{(i)} = \left(\frac{\partial\Gamma}{\partial N_i}\right), \text{ and } \beta^{(i)} = \alpha^{(i)} = \left(\frac{\partial\alpha}{\partial N_i}\right)$$

$$\mathrm{S}_2 = \phi_P\left(\phi_S - \alpha_{PS}\phi_P\right)\left[z - 2 - \alpha_{PS}\right]\chi^u_{PS}$$

$$\left(\frac{\partial(N\mathrm{S}_2)}{\partial N_i}\right) = \begin{pmatrix} r_P N^{(i)}_P\left(\phi_S - \alpha_{PS}\phi_P\right)\left[z - 2 - \alpha_{PS}\right] \\ + r_P N_P\left(\phi^{(i)}_s - \beta^{(i)}_{PS}\phi_P - \alpha_{PS}\phi^{(i)}_P\right)\left[z - 2 - \alpha_{PS}\right] \\ - r_P N_P\left(\phi_s - \alpha_{PS}\phi_P\right)\beta^{(i)}_{PS} \end{pmatrix}\chi^u_{PS} \tag{B.17}$$

$$\mathrm{S}_3 = \alpha_{PC}\phi_P\chi^a_{PC}$$

$$\left(\frac{\partial(N\mathrm{S}_3)}{\partial N_i}\right) = \left(\beta^{(i)}_{PC}r_p N_p + \alpha_{PC}r_P N^{(i)}_P\right)\chi^a_{PC} \tag{B.18}$$

$$\mathrm{S}_4 = \phi_P\left(\phi_C - \alpha_{PC}\phi_P\right)\left[z - 2 - \alpha_{PC}\right]\chi^u_{PC}$$

$$\left(\frac{\partial(N\mathrm{S}_4)}{\partial N_i}\right)=\begin{pmatrix} r_P N_P^{(i)}\left(\phi_C-\alpha_{PC}\phi_P\right)\left[z-2-\alpha_{PC}\right] \\ +r_P N_P\left(\phi_C^{(i)}-\beta_{PC}^{(i)}\phi_P-\alpha_{PC}\phi_P^{(i)}\right)\left[z-2-\alpha_{PC}\right] \\ -r_P N_P\left(\phi_C-\alpha_{PC}\phi_P\right)\beta_{PC}^{(i)} \end{pmatrix}\chi_{PC}^{u} \tag{B.19}$$

$$\mathrm{S}_5=\left(\phi_S-\alpha_{PS}\phi_P\right)\left(\phi_C-\alpha_{PC}\phi_P\right)\left[z-2\right]\chi_{SC}^{u}$$

$$\left(\frac{\partial(N\mathrm{S}_5)}{\partial N_i}\right)=\begin{pmatrix} \left(r_S N_S^{(i)}-\beta_{PS}^{(i)}r_P N_P-\alpha_{PS}r_P N_P^{(i)}\right)\left(\phi_C-\alpha_{PC}\phi_P\right) \\ +\left(r_S N_S-\alpha_{PS}r_P N_P\right)\left(\phi_C^{(i)}-\beta_{PC}^{(i)}\phi_P-\alpha_{PC}\phi_P^{(i)}\right) \end{pmatrix}\chi_{SC}^{u}\left[z-2\right] \tag{B.20}$$

$$\mathrm{S}_6=\frac{\phi_P}{r_P}\ln\phi_P$$

$$\left(\frac{\partial(N\mathrm{S}_6)}{\partial N_i}\right)=N_P^{(i)}\ln\phi_P+\frac{N_P}{\phi_P}\phi_P^{(i)} \tag{B.21}$$

$$\mathrm{S}_7=\left(\frac{2+\alpha_{PS}}{1+\alpha_{PS}}\right)\left(\phi_S-\alpha_{PS}\phi_P\right)\ln\left(\phi_S-\alpha_{PS}\phi_P\right)$$

$$\left(\frac{\partial(N\mathrm{S}_7)}{\partial N_i}\right)=\begin{bmatrix} \left(\frac{-\beta_{PS}^{(i)}}{\left(1+\alpha_{PS}\right)^2}\right)\left(r_S N_S-\alpha_{PS}r_P N_P\right)\ln\left(\phi_S-\alpha_{PS}\phi_P\right) \\ +\left(\frac{2+\alpha_{PS}}{1+\alpha_{PS}}\right)\left(r_S N_S^{(i)}-\beta_{PS}^{(i)}r_P N_P-\alpha_{PS}r_P N_P^{(i)}\right)\ln\left(\phi_S-\alpha_{PS}\phi_P\right) \\ +\left(\frac{2+\alpha_{PS}}{1+\alpha_{PS}}\right)\frac{\left(r_S N_S-\alpha_{PS}r_P N_P\right)}{\left(\phi_S-\alpha_{PS}\phi_P\right)}\left(\phi_S^{(i)}-\beta_{PS}^{(i)}\phi_P-\alpha_{PS}\phi_P^{(i)}\right) \end{bmatrix} \tag{B.22}$$

$$\mathrm{S}_8=-\phi_S\ln\phi_S$$

$$\left(\frac{\partial(N\mathrm{S}_8)}{\partial N_i}\right)=-\left(r_S N_S^{(i)}\ln\phi_S+\frac{r_S N_S}{\phi_S}\phi_S^{(i)}\right) \tag{B.23}$$

$$\mathrm{S}_9=\left(\frac{2+\alpha_{PC}}{1+\alpha_{PC}}\right)\left(\phi_C-\alpha_{PC}\phi_P\right)\ln\left(\phi_C-\alpha_{PC}\phi_P\right)$$

$$\left(\frac{\partial(N\mathrm{S}_9)}{\partial N_i}\right)=\left[\begin{array}{l}\left(\frac{-\beta_{PC}^{(i)}}{\left(1+\alpha_{PC}\right)^2}\right)\left(r_C N_C-\alpha_{PC} r_P N_P\right)\ln\left(\phi_C-\alpha_{PC}\phi_P\right)\\+\left(\frac{2+\alpha_{PC}}{1+\alpha_{PC}}\right)\left(r_C N_C^{(i)}-\beta_{PC}^{(i)} r_P N_P-\alpha_{PC} r_P N_P^{(i)}\right)\ln\left(\phi_C-\alpha_{PC}\phi_P\right)\\+\left(\frac{2+\alpha_{PC}}{1+\alpha_{PC}}\right)\frac{\left(r_C N_C-\alpha_{PC} r_P N_P\right)}{\left(\phi_C-\alpha_{PC}\phi_P\right)}\left(\phi_C^{(i)}-\beta_{PC}^{(i)}\phi_P-\alpha_{PC}\phi_P^{(i)}\right)\end{array}\right] \tag{B.24}$$

$$\mathrm{S}_{10}=-\phi_C\ln\phi_C$$

$$\left(\frac{\partial(N\mathrm{S}_{10})}{\partial N_i}\right)=-\left(r_C N_C^{(i)}\ln\phi_C+\frac{r_C N_C}{\phi_C}\phi_C^{(i)}\right) \tag{B.25}$$

$$\mathrm{S}_{11}=\alpha_{PS}\phi_P\ln\left(\alpha_{PS}\phi_P\right)$$

$$\left(\frac{\partial(N\mathrm{S}_{11})}{\partial N_i}\right)=\left(\beta_{PS}^{(i)} r_P N_P\ln\left(\alpha_{PS}\phi_P\right)+\alpha_{PS} r_P N_P^{(i)}\ln\left(\alpha_{PS}\phi_P\right)+\frac{r_P N_P}{\phi_P}\left(\beta_{PS}^{(i)}\phi_P+\alpha_{PS}\phi_P^{(i)}\right)\right) \tag{B.26}$$

$$\mathrm{S}_{12}=\phi_P\left(1-\alpha_{PS}\right)\ln\left(1-\alpha_{PS}\right)$$

$$\left(\frac{\partial(N\mathrm{S}_{12})}{\partial N_i}\right)=\left(r_P N_P^{(i)}\left(1-\alpha_{PS}\right)\ln\left(1-\alpha_{PS}\right)+r_P N_P\left(-\beta_{PS}^{(i)}\right)\ln\left(1-\alpha_{PS}\right)+r_P N_P\left(-\beta_{PS}^{(i)}\right)\right) \tag{B.27}$$

$$\mathrm{S}_{13}=\alpha_{PS}\phi_P\ln\left(\alpha_{PS}\right)$$

$$\left(\frac{\partial(N\mathrm{S}_{13})}{\partial N_i}\right)=\left(r_P N_P^{(i)}\alpha_{PS}\ln\left(\alpha_{PS}\right)+r_P N_P\left(\beta_{PS}^{(i)}\right)\ln\left(\alpha_{PS}\right)+r_P N_P\left(\beta_{PS}^{(i)}\right)\right) \tag{B.28}$$

$$\mathrm{S}_{14}=\alpha_{PC}\phi_P\ln\left(\alpha_{PC}\phi_P\right)$$

$$\left(\frac{\partial(N\mathrm{S}_{14})}{\partial N_i}\right)=\left(\beta_{PC}^{(i)} r_P N_P\ln\left(\alpha_{PC}\phi_P\right)+\alpha_{PC} r_P N_P^{(i)}\ln\left(\alpha_{PC}\phi_P\right)+\frac{r_P N_P}{\phi_P}\left(\beta_{PC}^{(i)}\phi_P+\alpha_{PC}\phi_P^{(i)}\right)\right) \tag{B.29}$$

$$\mathrm{S}_{15}=\phi_P\left(1-\alpha_{PC}\right)\ln\left(1-\alpha_{PC}\right)$$

$$\left(\frac{\partial(N\mathrm{S}_{15})}{\partial N_i}\right)=\left(r_P N_P^{(i)}\left(1-\alpha_{PC}\right)\ln\left(1-\alpha_{PC}\right)+r_P N_P\left(-\beta_{PC}^{(i)}\right)\ln\left(1-\alpha_{PC}\right)+r_P N_P\left(-\beta_{PC}^{(i)}\right)\right) \quad \text{(B.30)}$$

$$\mathrm{S}_{16}=\alpha_{PC}\phi_P\ln\left(\alpha_{PC}\right)$$

$$\left(\frac{\partial(N\mathrm{S}_{16})}{\partial N_i}\right)=\left(r_P N_P^{(i)}\alpha_{PC}\ln\left(\alpha_{PC}\right)+r_P N_P\left(\beta_{PC}^{(i)}\right)\ln\left(\alpha_{PC}\right)+r_P N_P\left(\beta_{PC}^{(i)}\right)\right) \quad \text{(B.31)}$$

Therefore,

$$\boxed{\ln a_i=\sum_{j=1}^{16}\mathrm{S}_j} \quad \text{(B.32)}$$

Where,

$$N_K^{(i)}=\begin{cases} i=K & 1 \\ i\neq K & 0 \end{cases} \quad \text{(B.33)}$$

$$\phi_K^{(i)}=\left(\frac{r_K N_K}{\sum_j r_j N_j}\right)^{(i)}=\begin{cases} i=K & \dfrac{r_i\left(1-\phi_i\right)}{N} \\ i\neq K & -\dfrac{r_i\phi_K}{N} \end{cases} \quad \text{(B.34)}$$

$$\alpha_{PX}=\frac{(1+K_{PX})-\sqrt{(1+K_{PX})^2-4\phi_P\phi_X K_{PX}(1+K_{PX})}}{2\phi_P(1+K_{PX})}\text{, where X = S, or C} \quad \text{(B.35)}$$

$$\beta_{PX}^{(i)}=\alpha_{PX}^{(i)}=\frac{1}{2}\begin{pmatrix} \dfrac{-\phi_P^{(i)}}{\left(\phi_P\right)^2}\left[1-\sqrt{1-4\phi_P\phi_X\left(\dfrac{K_{PX}}{1+K_{PX}}\right)}\right] \\ +\dfrac{1}{2\phi_P}\left[\sqrt{1-4\phi_P\phi_X\left(\dfrac{K_{PX}}{1+K_{PX}}\right)}\right]^{-\frac{1}{2}}\left(\dfrac{K_{PX}}{1+K_{PX}}\right)\left(\phi_P^{(i)}\phi_X+\phi_P\phi_X^{(i)}\right) \end{pmatrix} \quad \text{(B.36)}$$

APPENDIX C

PAIR DISTRIBUTION FUNCTION CODE

```
#svl

global function pdf[file,t1,t2]
/* The function vacf takes an MDB style database file as an input (MOE output result file) and calculates the radial pair distribution function averaged over time from t1 to t2 for r=0 to r=15= edge/2 in increments of 0.1 angstroms. */

//open the database file
local fkey = db_Open tok_cat[file,'.mdb'];

//define entrykeys, database fields and number of entries
local EntryKeys = db_Entries fkey;
local [fieldnames,fieldtypes]=db_Fields fkey;
local nentries=length EntryKeys;

//Setup and initialize the g(r) and r vectors
local r,g,i,Nr;
Nr = 15/0.1 + 1;

for i=1,Nr loop

  r(i)= (i-1)*0.1;
  g(i)=0;

endloop


//Read in the time values from the database
local tvalues=db_ReadColumn [fkey,'t'];
local row1=indexof [t1,tvalues];


if row1 == 0 then
  pr "WARNING start time t1 does not exist";
endif
local row2=indexof [t2,tvalues];
if row2 == 0 then
  pr "WARNING end time t2 does not exist";
```

```
endif


//Calculate the cube edge for use in determining the minimum
//image position of the atoms
//Note the MOE databases store the edge length vector in
//the database field "box" not in the molecule field
local size,edge;
size = cat db_ReadFields [fkey,EntryKeys(1),'box'];
pr size;
if not ((size(1)==size(2)) and (size(1)==size(3))) then
  pr "WARNING periodic cell is not a cube";
endif
edge=size(1);
//pr edge;


//Initilize the database
local dbentry=row1;
local entrycount=0;
local myavgcount=0;
local filenum = fopenw '1.txt';

//Loop over all the database entry rows (time values) in the averaging
while dbentry <= row2 loop

    local dbmol = cat db_ReadFields[fkey,EntryKeys(dbentry),'mol'];
    local dbvalue = cat mol_aPos dbmol;
//    local dbname = cat mol_aName dbmol;
    local   dbname=dbmol(4)(MOL_ATOM_NAME);
//    local chain_keys = mol_Create dbmol;
// pr dbmol(4)(MOL_ATOM_NAME);
// fwrite [filenum, '{c:}\n',[dbname]];

//pr length dbname;
//  local dbvalue = cat db_ReadFields[fkey,EntryKeys(dbentry),'pos'];


//break atoms coordinates into x,y and z components
  local natoms=length dbvalue/3;
  local xpos= keep[dbvalue,natoms];
  local ypos= keep [keep[dbvalue,2*natoms],-natoms];
  local zpos= keep[dbvalue,-natoms];

//Declare variables used in nested loops below
```

```
  local rdiff,rindex,j,aux;
  local ncount=0;
  local nullcount=0;
  local mycount=0;
  local myatoms=0;

//pr natoms;
//Count atom pairs and place resulting histogram in g(r)
  for i=1,natoms loop

     for j=i+1,natoms loop
 if dbname(i)=='C9' and dbname(j)=='O2' then
//Calculate a vector containing the interatomic distance components
       rdiff= [xpos(i)-xpos(j),ypos(i)-ypos(j),zpos(i)-zpos(j)];

//Convert the interatomic distance components to their minimum
//image versions by shifting the coordinates by the edge length
//of the periodic cell if the interatomic distance is more than
//half the cell length
       rdiff=rdiff-(edge*round(rdiff/edge));
//pr rdiff;

//Calculate the the interatomic distance based on the edge
//length above
       rdiff=sqrt(add sqr rdiff);
       myatoms=myatoms+1;
//pr rdiff;

//pr rdiff;
if rdiff < 4.5 then
mycount=mycount+1;
fwrite [filenum, '{n:12.6f\n}',[rdiff,i,j,dbname(i),dbname(j),mycount,entrycount]];

endif

//Calculate the index in the g and r vectors for the rdiff
       aux=rdiff*10;
       aux=ceil aux;
       rindex=aux+1;
//       pr rindex;
//       rindex= indexof[((ceil(rdiff*10))/10),r];
//       pr rindex;

//If the index is not zero then the rdiff is withing the 0-10 range
//If so increment the g(r) and count variable ncount
```

```
        if (rindex >= 0) and (rindex <= Nr) then
            g(rindex)=g(rindex)+1;
            ncount=ncount+1;
        else
            nullcount=nullcount+1;
//          pr rdiff;
//          pr rindex;
        endif
 else
rdiff =0;
 endif
     endloop

   endloop
   myavgcount= myavgcount+ mycount;
   entrycount=entrycount+1;
   dbentry=dbentry+1;

endloop

myavgcount = myavgcount/entrycount;

//Normalize g(r)
local cnorm=2*cube(edge)/(entrycount*natoms*(natoms-1));
local gn = g;
local gm =g;
for i=2,Nr loop
g(i)=g(i)/((4*PI/3)*(cube(r(i))-cube(r(i-1))));
g(i)=g(i)*cnorm;
gm(i)= g(i) /cnorm *(2*cube(edge)/(entrycount*2*myatoms));
fwrite [filenum, '{n:12.6f}
\n',[r(i),g(i),gn(i),gm(i),myatoms,natoms, myavgcount,entrycount,cube(edge)]];
//pr cnorm;
endloop

//pr ncount;
//pr nullcount;

fclose filenum;
pr 'success';

local outputvect=[r,g];
return outputvect;

endfunction
```

APPENDIX D

CO_2 BENDING MODE IN ATR-FTIR SPECTRA OF CO_2 + SMALL MOLECULE SOLVENTS

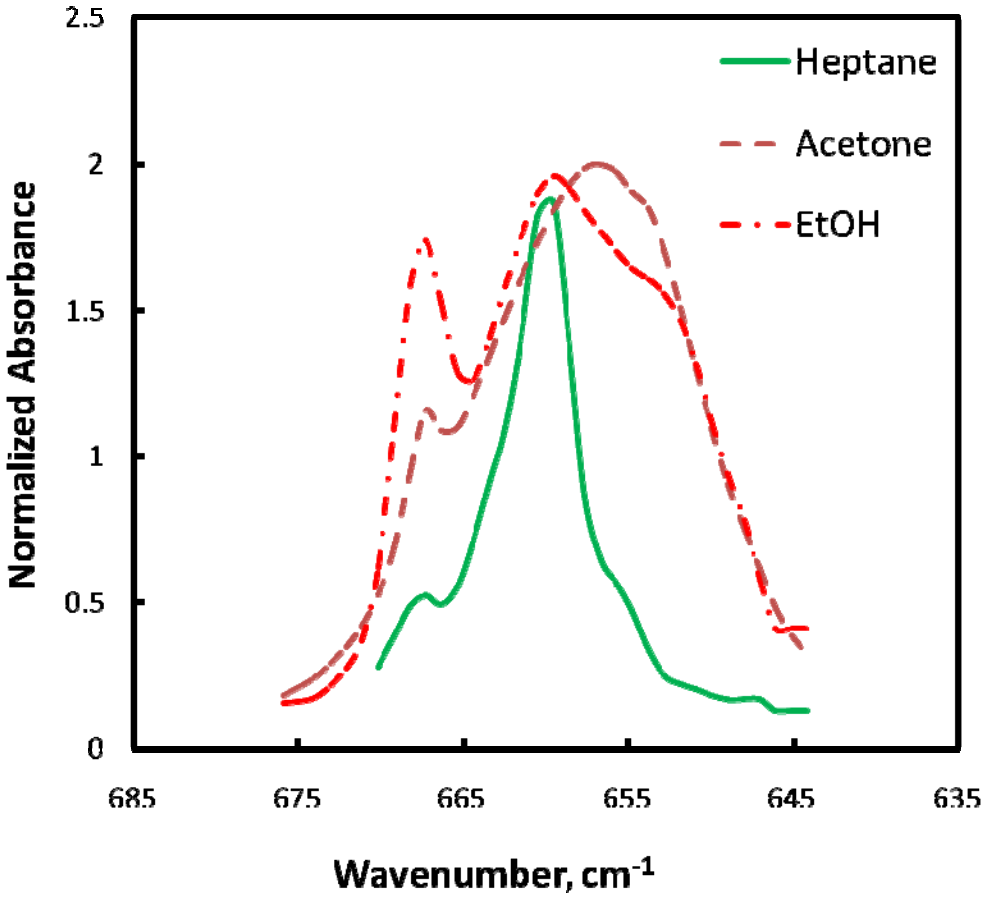

Figure D.1 Bending mode of CO_2 in the IR spectrum of CO_2 + heptane, CO_2 + acetone and CO_2 + ethanol, at 10 bar CO_2 and 298 K.

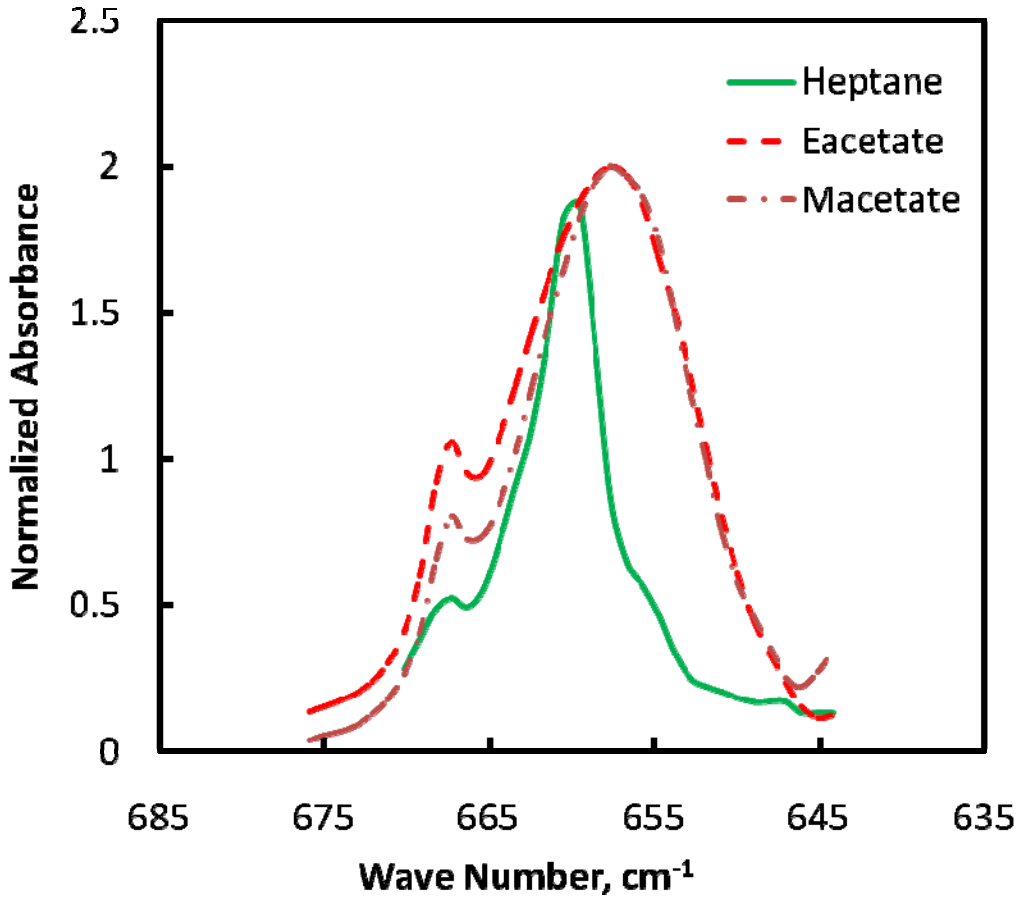

Figure D.2 Bending mode of CO_2 in the IR spectrum of CO_2 + heptane, CO_2 + ethyl acetate and CO_2 + methyl acetate, at 10 bar CO_2 and 298 K.

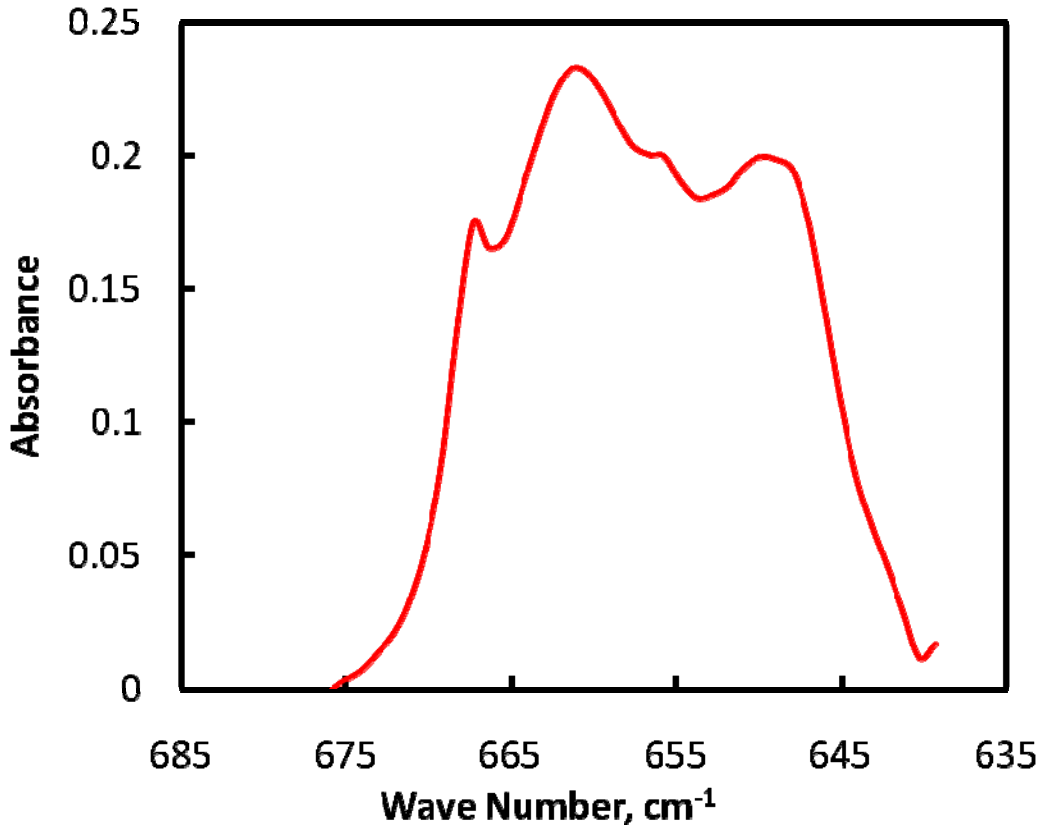

Figure D.3 Bending mode of CO_2 in the IR spectrum of CO_2 + tributyl phosphate, at 10 bar CO_2 and 298 K.

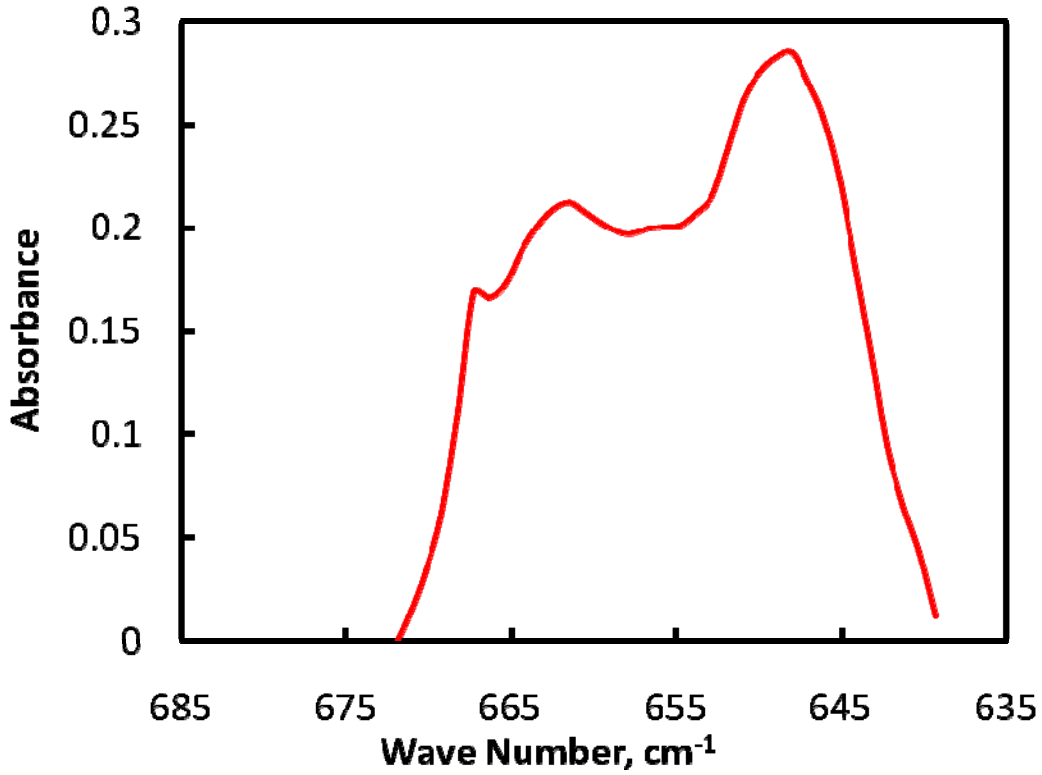

Figure D.4 Bending mode of CO_2 in the IR spectrum of CO_2 + tetramethyl Urea, at 10 bar CO_2 and 298 K.

REFERENCES

1. Cooper, A.I., *Polymer synthesis and processing using supercritical carbon dioxide.* Journal of Materials Chemistry, 2000. **10**(2): p. 207-234.
2. Tomasko, D.L., et al., *A review of CO_2 applications in the processing of polymers.* Industrial & Engineering Chemistry Research, 2003. **42**(25): p. 6431-6456.
3. Kendall, J.L., et al., *Polymerizations in supercritical carbon dioxide.* Chemical Reviews, 1999. **99**(2): p. 543-564.
4. Hile, D.D., et al., *Active growth factor delivery from poly(D,L-lactide-co-glycolide) foams prepared in supercritical CO_2.* Journal of Controlled Release, 2000. **66**(2-3): p. 177-185.
5. Woods, H.M., et al., *Materials processing in supercritical carbon dioxide: surfactants, polymers and biomaterials.* Journal of Materials Chemistry, 2004. **14**(11): p. 1663-1678.
6. Baker, R.W., *Future directions of membrane gas separation technology.* Industrial & Engineering Chemistry Research, 2002. **41**(6): p. 1393-1411.
7. Taylor, D.K., R. Carbonell, and J.M. DeSimone, *Opportunities for pollution prevention and energy efficiency enabled by carbon dioxide technology platform.* Annual Review of Energy and the Environment, 2000. **25**: p. 115-146.
8. Yeo, S.-D. and E. Kiran, *Formation of polymer particles with supercritical fluids: A review.* The Journal of Supercritical Fluids, 2005. **34**(3): p. 287-308.
9. Baker, R.W. and K. Lokhandwala, *Natural gas processing with membranes: An overview.* Ind. Eng. Chem. Res., 2008. **47**(7): p. 2109-2121.
10. Palakodaty, S. and P. York, *Phase behavioral effects on particle formation processes using supercritical fluids.* Pharmaceutical Research, 1999. **16**(7): p. 976-985.
11. Byun, H.S., et al., *Phase behavior of the binary and ternary mixtures of biodegradable poly(epsilon-caprolactone) in supercritical fluids.* Industrial & Engineering Chemistry Research, 2006. **45**(10): p. 3366-3372.

12. Kirby, C.F. and M.A. McHugh, *Phase behavior of polymers in supercritical fluid solvents.* Chemical Reviews, 1999. **99**(2): p. 565-602.
13. OzKan, I., *A Thermodynamic Model for Associating Polymer Solutions*. 2004, PhD thesis, Georgia Institute of Technology.
14. Kasturirangan, A., *Specific Interactions in CO_2 + Polymer Systems*. 2007, PhD thesis, Georgia Institute of Technology.
15. Dixon, D.J. and K.P. Johnston ed., *Supercritical Fluids*, Vol. 23. 1997, NewYork: John Wiley and Sons Inc.
16. Kazarian, S.G., *Review: polymer processing with supercritical fluids.* Polymer Science, Ser.C, 2000. **42**: p. 78-101.
17. Cansell, F., S. Rey, and P. Beslin, *Thermodynamic aspects of supercritical fluids processing: Applications to polymers and wastes treatment.* Revue De L Institut Francais Du Petrole, 1998. **53**(1): p. 71-98.
18. Lora, M. and I. Kikic, *Polymer processing with supercritical fluids: An overview.* Separation and Purification Methods, 1999. **28**(2): p. 179-220.
19. Nalawade, S.P., F. Picchioni, and L. Janssen, *Supercritical carbon dioxide as a green solvent for processing polymer melts: Processing aspects and applications.* Progress in Polymer Science, 2006. **31**(1): p. 19-43.
20. McHugh, M.A. and V.J. Krukonis, *Supercritical Fluid Extraction: Principles and Practice*. 2nd ed. 1994, Boston: Butterworths-Heinemann.
21. Kemmere, M.F. and T. Meyer ed., *Supercritical Carbon Dioxide in Polymer Reaction Enginering*. 2005, Weinheim: Wiley-VCH.
22. Byun, H.S. and C. Park, *Monomer concentration effect on the phase behavior of poly(propyl acrylate) and poly(propyl methacrylate) with supercritical CO_2 and C_2H_4.* Korean Journal of Chemical Engineering, 2002. **19** (1): p. 126-131
23. Byun, H.S. and K.P. Yoo, *Phase behavior on the poly[octyl (meth)acrylate] plus supercritical fluid solvents plus monomer and CO_2 plus monomer mixtures at high pressure.* The Journal of Supercritical Fluids, 2007. **41**(3): p. 472-481.

24. Dinoia, T.P., et al., *Solubility of vinylidene fluoride polymers in supercritical CO_2 and halogenated solvents.* Journal of Polymer Science Part B-Polymer Physics, 2000. **38**(21): p. 2832-2840.
25. Wohlfarth, C., *High-pressure fluid phase equilibrium (HPPE) data of polymer solutions*, in *CRC Handbook of Thermodynamic Data of Polymer Solutions at Elevated Pressures*. 2005, Boca Raton: CRC Press.
26. Prausnitz, J.M., R.N. Lichtenthaler, and E.G.d. Azevedo, *Molecular Thermodynamics of Fluid-Phase Equilibria* 3rd ed. 1998, Upper Saddle River: Prentice Hall.
27. Rindfleisch, F., T.P. DiNoia, and M.A. McHugh, *Solubility of polymers and copolymers in supercritical CO_2.* Journal of Physical Chemistry, 1996. **100**(38): p. 15581-15587.
28. Kazarian, S.G., et al., *Specific intermolecular interaction of carbon dioxide with polymers.* Journal of the American Chemical Society, 1996. **118**(7): p. 1729-1736.
29. Shen, Z., et al., *CO_2-solubility of oligomers and polymers that contain the carbonyl group*. Polymer, 2003. **44**(5): p. 1491-1498.
30. Hildebrand, J.H., J.M. Prausnitz, and R.L. Scott, *Regular and Related Solutions*. 1970, New York: Van Nostrand Reinhold Co.
31. Hildebrand, J.H. and R.L. Scott, *The Solubility of Nonelectrolytes*, ed. 3. 1950, New York: Reinhold.
32. Hansen, C.W., *The three dimensional solubility parameter-key to paint component affinities.* Journal of Paint Technology, 1967. **39**: p. 511-514.
33. Giddings, C.J., et al., *High pressure gas chromatography of nonvolatile species.* Science, 1968. **162**: p. 67-73.
34. Williams, L.L., J.B. Rubin, and H.W. Edwards, *Calculation of Hansen solubility parameter values for a range of pressure and temperature conditions, including the supercritical fluid region.* Industrial & Engineering Chemistry Research, 2004. **43**(16): p. 4967-4972.
35. Hyatt, J.A., *Liquid and supercritical carbon dioxide as organic solvents.* The Journal of Organic Chemistry, 1984. **49**: p. 5097-5101.

36. Kilic, S., et al., *Effect of grafted Lewis base groups on the phase behavior of model poly(dimethyl siloxanes) in CO_2.* Industrial & Engineering Chemistry Research, 2003. **42**(25): p. 6415-6424.
37. Nelson, M.R. and R.F. Borkman, *Ab initio calculations on CO_2 binding to carbonyl groups.* Journal of Physical Chemistry A, 1998. **102**(40): p. 7860-7863.
38. Raveendran, P. and S.L. Wallen, *Cooperative C-H···O hydrogen bonding in CO_2-Lewis base complexes: Implications for solvation in supercritical CO_2.* Journal of the American Chemical Society, 2002. **124**(42): p. 12590-12599.
39. Kilic, S., et al., *Phase behavior of oxygen-containing polymers in CO_2.* Macromolecules, 2007. **40**(4): p. 1332-1341.
40. Drago, R.S., N. O'Bryan, and G.C. Vogel, *A frequency shift-enthalpy correlation for a given donor with various hydrogen-bonding acids.* Journal of the American Chemical Society, 1970. **92**(13): p. 3924-3929.
41. Purcell, K.F. and R.S. Drago, *Theoretical aspects of the linear enthalpy wavenumber shift relation for hydrogen-bonded phenols.* Journal of the American Chemical Society, 1967. **89**(12): p. 2874-2879.
42. Purcell, K.F., J.A. Stikeleather, and S.D. Brunk, *Spectroscopic studies of hydrogen bonding: Hexafluoroisopropanol.* Journal of Molecular Spectroscopy, 1969. **32**: p. 202-213.
43. Fowkes, F.M., et al., *Acid-base complexes of polymers.* Journal of Polymer Science: Polymer Chemistry Edition, 1984. **22**(3): p. 547-566.
44. Cangelosi, F. and M.T. Shaw, *Hydrogen bonding in polymer systems.* Polymer Engineering & Science, 1983. **23**(12): p. 669-675.
45. Kwei, T.K., et al., *Hydrogen bonding in polymer mixtures.* Journal of Polymer Science Part B: Polymer Physics, 1986. **24**(7): p. 1597-1609.
46. Meredith, J.C., et al., *Quantitative equilibrium constants between CO_2 and Lewis bases from FTIR spectroscopy.* Journal of Physical Chemistry, 1996. **100**(26): p. 10837-10848.

47. Dharmalingam, K. and K. Ramachandran, *Solvent effects on hydrogen bonding between 1-pentanol and butyl methacrylate.* Physics and Chemistry of Liquids, 2006. **44**(1): p. 77-81.
48. Dharmalingam, K., et al., *Molecular interactions in alcohol-ethyl methacrylate mixtures.* Spectrochimica Acta Part A: Molecular and Biomolecular Spectroscopy, 2008. **69**(2): p. 467-470.
49. Nash, C.P., *The Calculation of equilibrium constants from spectro-photometric data.* Journal of Physical Chemistry, 1960. **64**(7): p. 950-953.
50. Diep, P., et al., *CO_2−fluorocarbon and CO_2−hydrocarbon interactions from first-principles calculations.* The Journal of Physical Chemistry A, 1998. **102**(12): p. 2231-2236.
51. Kim, K.H. and Y. Kim, *Theoretical studies for Lewis acid-base interactions and C-H···O weak hydrogen bonding in various CO_2 complexes.* Journal of Physical Chemistry A, 2008. **112**(7): p. 1596-1603.
52. Smith, B.C., *Fundamentals of Fourier Transform Infrared Spectroscopy*. 1996, Boca Raton: CRC Press.
53. Hind, A.R., S.K. Bhargava, and A. McKinnon, *At the solid/liquid interface: FTIR/ATR - the tool of choice.* Advances in Colloid and Interface Science, 2001. **93**(1-3): p. 91-114.
54. Kazarian, S.G., *Polymers and supercritical fluids: Opportunities for vibrational spectroscopy.* Macromolecular Symposia, 2002. **184**: p. 215-228.
55. Kazarian, S.G., et al., *Potential of ATR-IR spectroscopy in applications to supercritical fluids and liquefied gases.* American Laboratory, 2001. **33**(16): p. 44.
56. Wei, Y.S. and R.J. Sadus, *Equations of state for the calculation of fluid-phase equilibria.* AIChE Journal, 2000. **46**(1): p. 169-196.
57. Sengers, J.V., et al., eds. *Equations of State for Fluids and Fluid Mixtures*. Experimental Thermodynamics. 2000, New York: Elsevier.
58. Economou, I.G. and M.D. Donohue, *Equations of state for hydrogen bonding systems.* Fluid Phase Equilibria, 1996. **116**(1-2): p. 518-529.

59. Gupta, R.B. and K.P. Johnston, *Lattice fluid hydrogen bonding model with a local segment density.* Fluid Phase Equilibria, 1994. **99**: p. 135-151.
60. Grenner, A., et al., *Evaluation of the nonrandom hydrogen bonding (NRHB) theory and the simplified perturbed-chain-statistical associating fluid theory (sPC-SAFT). 1. Vapor−liquid equilibria.* Industrial & Engineering Chemistry Research, 2008. **47**(15): p. 5636-5650.
61. Panayiotou, C., et al., *Nonrandom hydrogen-bonding model of fluids and their mixtures. 1. Pure fluids.* Industrial & Engineering Chemistry Research, 2004. **43**(20): p. 6592-6606.
62. Kontogeorgis, G.M., et al., *An equation of state for associating fluids.* Industrial & Engineering Chemistry Research, 1996. **35**(11): p. 4310-4318.
63. Voutsas, E.C., et al., *Correlation of liquid-liquid equilibria for alcohol/ hydrocarbon mixtures using the CPA equation of state.* Fluid Phase Equilibria, 1997. **132**(1-2): p. 61-75.
64. Adidharma, H. and M. Radosz, *SAFT1 for associating fluids: Alkanols.* Journal of Physical Chemistry B, 2001. **105**(40): p. 9822-9827.
65. Sanchez, I.C. and R.H. Lacombe, *Statistical thermodynamics of polymer solutions.* Macromolecules, 1978. **11**(6): p. 1145-1156.
66. Koak, N. and R.A. Heidemann, *Polymer-solvent phase behavior near the solvent vapor pressure.* Industrial & Engineering Chemistry Research, 1996. **35**(11): p. 4301-4309.
67. Liu, D. and D.L. Tomasko, *Carbon dioxide sorption and dilation of poly(lactide-co-glycolide).* The Journal of Supercritical Fluids, 2007. **39**(3): p. 416-425.
68. Sanchez, I.C., *Sanchez-Lacombe model for polymer solutions.* Journal of Physical Chemistry, 1976. **80**(19): p. 2352-2568.
69. Kiran, E., W.H. Zhuang, and Y.L. Sen, *Solubility and demixing of polyethylene in binary fluid mixtures: carbon dioxide-cyclohexane, carbon dioxide-tolutene, carbon dioxide-petane.* Journal of Applied Polymer Science, 1993. **47**(5): p. 895-909.

70. Kiran, E., Y. Xiong, and W.H. Zhuang, *Modeling polyethylene solutions in near and supercritical fluids using the Sanchez-Lacombe model.* The Journal of Supercritical Fluids, 1993. **6**(4): p. 193-203.
71. Chapman, W.G., et al., *Mixtures of polar and associating molecules.* Pure And Applied Chemistry, 1987. **59**(1): p. 53-60.
72. Huang, S.H. and M. Radosz, *Equation of state for small, large, polydisperse and associating molecules.* Industrial & Engineering Chemistry Research, 1990. **29**(11): p. 2284-2294.
73. Huang, S.H. and M. Radosz, *Phase-behavior of reservoir fluids. 5. SAFT model of CO_2 and bitumen systems.* Fluid Phase Equilibria, 1991. **70**(1): p. 33-54.
74. Huang, S.H. and M. Radosz, *Equation of state for small, large, polydisperse and associating molecules - Extension to fluid mixtues.* Industrial & Engineering Chemistry Research, 1991. **30**(8): p. 1994-2005.
75. Wertheim, M.S., *Fluids with highly directional attractive forces. 2. Thermodynamic perturbation theorgy and integration equations.* Journal of Statistical Physics, 1984. **35**(1-2): p. 35-47.
76. Wertheim, M.S., *Fluids with highly directional attractive forces. 1. Statistical thermodynamics.* Journal of Statistical Physics, 1984. **35**(1-2): p. 19-34.
77. Chapman, W.G., et al., *Statistical associating fluid theory.* Industrial & Engineering Chemistry Research, 1990. **29**: p. 1709.
78. Hasch, B.M. and M.A. McHugh, *Calculating poly(ethylene-co-acrylic acid)-solvent phase behavior with the SAFT equation of state.* Journal of Polymer Science Part B-Polymer Physics, 1995. **33**(4): p. 715-723.
79. Hasch, B.M., S.H. Lee, and M.A. McHugh, *Strengths and limitations of SAFT for calculating polar copolymer-solvent phase behavior.* Journal of Applied Polymer Science, 1996. **59**(7): p. 1107-1116.
80. Gross, J. and G. Sadowski, *Perturbed-chain SAFT: An equation of state based on a perturbation theory for chain molecules.* Industrial & Engineering Chemistry Research, 2001. **40**(4): p. 1244-1260.

81. von Solms, N., M.L. Michelsen, and G.M. Kontogeorgis, *Computational and physical performance of a modified PC-SAFT equation of state for highly asymmetric and associating mixtures.* Industrial & Engineering Chemistry Research, 2003. **42**(5): p. 1098-1105.
82. von Solms, N., M.L. Michelsen, and G.M. Kontogeorgis, *Prediction and correlation of high-pressure gas solubility in polymers with simplified PC-SAFT.* Industrial & Engineering Chemistry Research, 2005. **44**: p. 3330.
83. Kontogeorgis, G.M. and G.K. Folas, *Thermodynamic Models for Industrial Applications: From Classical and Advanced Mixing Rules to Association Theories*. 2010, West Sussex: John Wiley & Sons.
84. Huggins, M.L., *Solutions of long-chain compounds.* Journal of Chemical Physics, 1941. **9**: p. 440.
85. Flory, P.J., *Thermodynamics of high polymer solutions.* Journal of Chemical Physics, 1942. **10**(1): p. 51-61.
86. Tompa, H., Polymer Solutions. 1956, New York: Academic Press Inc.
87. Flory, P.J., *Statistical thermodynamics of liquid mixtures*. Journal of the American Chemical Society, 1965. 87(9): p. 1833-1838.
88. Coleman, M., J. Graf, and P. Painter, *Specific Interactions and the Miscibility of Polymer Blends*. 1991, Lancaster: Technomic.
89. Coleman, M.M., et al., *Functional group accessibility in hydrogen bonded polymer blends.* Macromolecules, 1996. **29**: p. 6820-6831.
90. Coleman, M.M. and P.C. Painter, *Hydrogen bonded polymer blends.* Progress in Polymer Science, 1995. **20**(1): p. 1-59.
91. Kasturirangan, A. and A.S. Teja, *Phase behavior of CO_2 + biopolymer and CO_2 + fluoropolymer systems*. Fluid Phase Equilibria, 2007. 261(1-2): p. 64-68
92. Oishi, T. and J.M. Prausnitz, *Estimation of solvent activities in polymer solutions using a group-contribution method.* Industrial & Engineering Chemistry Process Design and Development, 1978. **17**: p. 333-339.

93. Fredenslud, A., R.L. Jones, and J.M. Prausnitz, *Group-contribution estimation of activity coefficients in nonideal liquid mixtures.* AIChE Journal, 1975. **21**: p. 1086-1099.

94. Sukhadia, T., *Prediction of Phase Equilibria in Solutions: An Associative Reformulation of Thermodynamic Theories of Solutions*. 1998, PhD thesis, Georgia Institute of Technology.

95. Variankaval, N., *Structure and Thermodynamics of Associationg Solutions: Prediction of Phase Equilibria*. 2001, PhD thesis, Georgia Institute of Technology.

96. Ozkan, I.A. and A.S. Teja, *Phase equilibria in systems with specific CO_2-polymer interactions.* Fluid Phase Equilibria, 2005. **228-229**: p. 487-491.

97. Gibbs, J.H. and E.A. Dimarzio, *Nature of the glass transition and the glassy state.* Journal of Chemical Physics, 1958. **28**(3): p. 373-383.

98. Arce, P. and M. Aznar, *Modeling the thermodynamic behavior of poly(lactide-co-glycolide) + supercritical fluid mixtures with equations of state.* Fluid Phase Equilibria, 2006. **244**(1): p. 16-25.

99. Rindfleisch, F., T.P. DiNoia, and M.A. McHugh, *Solubility of polymers and copolymers in supercritical CO_2.* Journal of Physical Chemistry, 1996. **100**(38): p. 15581-15587.

100. Kazarian, S.G., *Applications of FTIR spectroscopy to supercritical fluid drying, extraction and impregnation.* Applied Spectroscopy Reviews, 1997. **32**(4): p. 301-348.

101. Dardin, A., J.M. DeSimone, and E.T. Samulski, *Fluorocarbons dissolved in supercritical carbon dioxide. NMR evidence for specific solute-solvent interactions.* Journal of Physical Chemistry B, 1998. **102**(10): p. 1775-1780.

102. Kilic, S., et al., *Influence of tert-amine groups on the solubility of polymers in CO_2.* Polymer, 2009. **50**(11): p. 2436-2444.

103. Raveendran, P. and S.L. Wallen, *Exploring CO_2-philicity: Effects of stepwise fluorination.* Journal of Physical Chemistry B, 2003. **107**(6): p. 1473-1477.

104. Yonker, C.R. and B.J. Palmer, *Investigation of CO_2/fluorine interactions through the intermolecular effects on the ^{1}H and ^{19}F Shielding of CH_3F and CHF_3 at various temperatures and pressures.* Journal of Physical Chemistry A, 2001. **105**(2): p. 308-314.
105. Fink, R., et al., *Toward the development of "CO_2-philic" hydrocarbons. 1. Use of side-chain functionalization to lower the miscibility pressure of polydimethylsiloxanes in CO_2.* Journal of Physical Chemistry B, 1999. **103**(31): p. 6441-6444.
106. DeSimone, J.M., Z. Guan, and C.S. Elsbernd, *Synthesis of fluoropolymers in supercritical carbon dioxide.* Science, 1992. **257**(5072): p. 945-947.
107. Wang, Y., et al., *Design and evaluation of nonfluorous CO_2-soluble oligomers and Polymers.* Journal of Physical Chemistry B, 2009. **113**(45): p. 14971-14980.
108. Huang, J.H. and T. Ruther, *Why are ionic liquids attractive for CO_2 absorption? An overview.* Australian Journal of Chemistry, 2009. **62**(4): p. 298-308.
109. Drago, R.S., G.C. Vogel, and T.E. Needham, *4-Parameter equation for predicting enthalpies of adduct formation.* Journal of the American Chemical Society, 1971. **93**(23): p. 6014.
110. Nalawade, S.P., et al., *Investigation of the interaction of CO_2 with poly (L-lactide), poly(DL-lactide) and poly(ε-caprolactone) using FTIR spectroscopy.* Journal of Applied Polymer Science, 2008. **109**(5): p. 3376-3381.
111. Tekin, N. and M. Cebe, *Solvents effect on infrared spectra of trimethyl phosphate in organic solvents.* Vibrational Spectroscopy, 2004. **36**(1): p. 129-133.
112. Kolling, O.W., *FTIR study of the solvent influence on the carbonyl absorption peak of ethyl-acetate.* Journal of Physical Chemistry, 1992. **96**(15): p. 6217-6220.
113. Reichardt, C., *Solvent Effects in Organic Chemistry*. Monographs in Modern Chemistry. 1978, New York: Weinheim.
114. May, E.F., M.R. Moldover, and J.W. Schmidt, *The dielectric permittivity of saturated liquid carbon dioxide and propane measured using cross capacitors.* International Journal of Thermophysics, 2005. **26**(3): p. 563-576.

115. Nakagawa, T., et al., *Electrical properties of biodegradable polylactic acid film.* IEEE Transactions on Industry Applications, 2004. **40**(4): p. 1020-1024.
116. Dobrowolski, J.C. and M.H. Jamroz, *Infrared evidence for CO_2 electron donor--acceptor complexes.* Journal of Molecular Structure, 1992. **275**: p. 211-219.
117. Temtem, M., et al., *Molecular interactions and CO_2-philicity in supercritical CO_2. A high-pressure NMR and molecular modeling study of a perfluorinated polymer in $scCO_2$.* Journal of Physical Chemistry B, 2007. **111**(6): p. 1318-1326.
118. Rivelino, R., *Lewis acid-base interactions in weakly bound formaldehyde complexes with CO_2, HCN, and FCN: Considerations on the cooperative H-bonding effects.* Journal of Physical Chemistry A, 2008. **112**(2): p. 161-165.
119. Bhargava, B.L., A.C. Krishna, and S. Balasubramanian, *Molecular dynamics simulation studies of CO_2 - bmim PF_6 solutions: Effect of CO_2 concentration.* AIChE Journal, 2008. **54**(11): p. 2971-2978.
120. Saharay, M. and S. Balasubramanian, *Ab initio molecular-dynamics study of supercritical carbon dioxide.* Journal of Chemical Physics, 2004. **120**(20): p. 9694-9702.
121. Saharay, M. and S. Balasubramanian, *Electron donor-acceptor interactions in ethanol-CO_2 mixtures: An ab initio molecular dynamics study of supercritical carbon dioxide.* Journal of Physical Chemistry B, 2006. **110**(8): p. 3782-3790.
122. Saharay, M. and S. Balasubramanian, *Evolution of intermolecular structure and dynamics in supercritical carbon dioxide with pressure: An ab initio molecular dynamics study.* Journal of Physical Chemistry B, 2007. **111**(2): p. 387-392.
123. Lim, S.Y., et al., *Molecular dynamics simulation of diffusion of gases in a carbon-nanotube-polymer composite.* Physical Review E, 2007. **76**(1): p. 011810.
124. Spyriouni, T., G.C. Boulougouris, and D.N. Theodorou, *Prediction of sorption of CO_2 in glassy atactic polystyrene at elevated pressures through a new computational scheme.* Macromolecules, 2009. **42**(5): p. 1759-1769.
125. Keskin, S. and D.S. Sholl, *Selecting metal organic frameworks as enabling materials in mixed matrix membranes for high efficiency natural gas purification.* Energy & Environmental Science, 2010. **3**(3): p. 343-351.

126. MOE. *http://www.chemcomp.com/*.
127. Swann, A.T., *Characterization of Polymer-Supported Homogeneous Catalysts By Molecular Modeling*. 2008, PhD thesis, Georgia Institute of Technology.
128. Taylor, D.K., R. Carbonell, and J.M. DeSimone, *Opportunities for pollution prevention and energy efficiency enabled by the carbon dioxide technology platform.* Annual Review of Energy and the Environment, 2000. **25**: p. 115-146.
129. Yeo, S.D. and E. Kiran, *Formation of polymer particles with supercritical fluids: A review.* The Journal of Supercritical Fluids, 2005. **34**(3): p. 287-308.
130. Kiran, E., *Polymer miscibility, phase separation, morphological modifications and polymorphic transformations in dense fluids.* The Journal of Supercritical Fluids, 2009. **47**(3): p. 466-483.
131. Wissinger, R.G. and M.E. Paulaitis, *Swelling and sorption in polymer-CO2 mixtues at elevated pressures.* Journal of Polymer Science Part B-Polymer Physics, 1987. **25**(12): p. 2497-2510.
132. Kasturirangan, A., C. Grant, and A.S. Teja, *Compressible lattice model for phase equilibria in CO_2 + polymer systems.* Industrial & Engineering Chemistry Research, 2008. **47**(3): p. 645-649.
133. Byun, H.-S. and M.A. McHugh, *High pressure phase behavior of poly[isopropyl acrylate] and poly[isopropyl methacrylate] in supercritical fluid (SCF) solvent and SCF solvent + cosolvent mixtures.* The Journal of Supercritical Fluids, 2007. **41**(3): p. 482-491.
134. Byun, H.-S., C.-H. Bang, and J.-S. Lim, *Effect of cosolvent concentration on phase behavior for the poly(isodecyl acrylate) in supercritical carbon dioxide, propane, propylene, butane, 1-butene and dimethyl ether.* Journal of Macromolecular Science, Part B: Physics, 2008. **47**(1): p. 150 - 165.
135. Beinhoff, M., J. Frommer, and K.R. Carter, *Photochemical attachment of reactive cross-linked polymer films to Si/SiO_2 surfaces and subsequent polymer brush growth.* Chemistry of Materials, 2006. **18**(15): p. 3425-3431.

136. Sakdapipanich, J., N. Thananusont, and N. Pukkate, *Synthesis of acrylate polymers by a novel emulsion polymerization for adhesive applications.* Journal of Applied Polymer Science, 2006. **100**(1): p. 413-421.
137. Huggins, M.L., *Some properties of solutions of long-chain compounds.* Journal of Physical Chemistry, 1942. **46**(1): p. 151-158.
138. Soria, V., et al., *Ternary polymer solutions with hydrogen bonds, 1 - Theory.* Macromolecular Theory and Simulations, 2007. **16**(1): p. 53-61.
139. Patrick, A.R., *Pressure-volume-temperature relationships for polymeric liquids: A review of equations of state and their characteristic parameters for 56 polymers.* Journal of Applied Polymer Science, 1993. **48**(6): p. 1061-1080.
140. Sato, Y., et al., *Prediction of PVT properties of polymer melts with a new group-contribution equation of state.* Fluid Phase Equilibria, 1998. **144**(1-2): p. 427-440.
141. Patel, N.C. and A.S. Teja, *A new cubic equation of state for fluids and fluid mixtures.* Chemical Engineering Science, 1982. **37**(3): p. 463-473.
142. Van Krevelen, D.W., ed. *Properties of Polymers, Their Estimation and Correlation with Chemical Structure*. 1976, New York: Elsevier.
143. Fedors, R.F., *Method for estimating both solubility parameters and molar volumes of liquids*. Polymer Engineering and Science, 1974. **14**(2): p. 147-154.
144. Sandler, S.I., *Models for Thermodynamic and Phase Equilibria Calculations*. 1994, New York: Dekker.
145. Parekh, V.S. and R.P. Danner, *Prediction of polymer PVT behavior using the group contribution lattice-fluid EOS.* Journal of Polymer Science Part B: Polymer Physics, 1995. **33**(3): p. 395-402.
146. Danner, R.P., M. Hamedi, and B.C. Lee, *Applications of the group-contribution, lattice-fluid equation of state.* Fluid Phase Equilibria, 2002. **194**: p. 619-639.
147. Prausnitz, J.M. and F.H. Shair, *A thermodynamic correlation of gas solubilities.* AIChE Journal, 1961. **7**(4): p. 682-687.
148. Barton, J.R. and C.C. HSU, *A correlation for the solubility of non-polar gases in carboxylic acids.* Chmical Engineering Science, 1972. **27**: p. 1315-1323.

149. Condo, P.D., et al., *Glass-transition behavior including retrorade vitrification of polymers with compressed fluid diluents.* Macromolecules, 1992. **25**(23): p. 6119-6127.

150. Sato, Y., et al., *Solubility and diffusion coefficient of carbon dioxide in biodegradable polymers.* Industrial & Engineering Chemistry Research, 2000. **39**(12): p. 4813-4819.

151. Jacobs, M.A., M.F. Kemmere, and J.T.F. Keurentjes, *Foam processing of poly (ethylene-co-vinyl acetate) rubber using supercritical carbon dioxide.* Polymer, 2004. **45**(22): p. 7539-7547.

152. Liu, D., et al., *CO_2-induced PMMA swelling and multiple thermodynamic property analysis using Sanchez-Lacombe EOS.* Macromolecules, 2005. **38**(10): p. 4416-4424.

153. Sato, Y., et al., *Solubilities and diffusion coefficients of carbon dioxide in poly(vinyl acetate) and polystyrene.* The Journal of Supercritical Fluids, 2001. **19**(2): p. 187-198.

154. Pantoula, M. and C. Panayiotou, *Sorption and swelling in glassy polymer/carbon dioxide systems: Part I. Sorption.* The Journal of Supercritical Fluids, 2006. **37**(2): p. 254-262.

155. Sudha, S.Y. and A. Khanna, *Evaluating the interactions of CO_2-ionic liquid systems through molecular modeling.* World Academy of Science, Engineering and Technology, 2009. **57**: p. 539-542.

156. Makrodimitri, Z.A. and L.G. Economou, *Atomistic simulation of poly(dimethylsiloxane) permeability properties to gases and n-alkanes.* Macromolecules, 2008. **41**(15): p. 5899-5907.

157. Sadrzadeh, M., K. Shahidi, and T. Mohammadi, *Effect of operating parameters on pure and mixed gas permeation properties of a synthesized composite PDMS/PA membrane.* Journal of Membrane Science, 2009. **342**(1-2): p. 327-340.

158. Sandler, S.I., *The generalized van der waals partition function. I. Basic theory.* Fluid Phase Equilibria, 1985. **19**(3): p. 238-257.

159. Prigogine, I., A. Bellemans, and C. Mathot, *The Molecular Theory of Solutions*. 1957, Amsterdam: North-Holland.
160. Nitta, T., et al., *Group contribution molecular model of liquids and solutions.* AIChE Journal, 1977. **23**(2): p. 144-160.
161. Neau, E., *A consistent method for phase equilibrium calculation using the Sanchez-Lacombe lattice-fluid equation-of-state.* Fluid Phase Equilibria, 2002. **203**(1-2): p. 133-140.
162. Veytsman, B.A., *Are lattice models valid for fluids with hydrogen bonds?* Journal of Physical Chemistry, 1990. **94**(23): p. 8499-8500.
163. Shin, M.S. and H. Kim, *A quasi-chemical nonrandom lattice fluid model: General derivation and application to pure fluids and mixtures.* Fluid Phase Equilibria, 2006. **246**(1-2): p. 79-88.
164. Shin, M.S. and H. Kim, *A multi-fluid nonrandom associating lattice fluid model.* Fluid Phase Equilibria, 2007. **253**(1): p. 29-35.
165. Werner, S., M. Haumann, and P. Wasserscheid, *Ionic liquids in chemical engineering,.* Annual Review of Chemical and Biomolecular Engineering, 2010. **1**: p. 203-230.
166. Muldoon, M.J., et al., *Improving carbon dioxide solubility in ionic liquids.* The Journal of Physical Chemistry B, 2007. **111**(30): p. 9001-9009.
167. Kohler, F., et al., *Continuous gas-phase desulfurisation using supported ionic liquid phase (SILP) materials.* Green Chemistry, 2010. **12**(6): p. 979-984.
168. Bara, J.E., et al., *Room-temperature ionic liquids and composite materials: platform technologies for CO_2 capture.* Accounts of Chemical Research, 2010. **43**(1): p. 152-159.
169. Bara, J.E., et al., *Guide to CO_2 Separations in imidazolium-based room-temperature ionic liquids.* Industrial & Engineering Chemistry Research, 2009. **48**(6): p. 2739-2751.
170. Cadena, C., et al., *Why is CO_2 so soluble in imidazolium-based ionic liquids?* Journal of the American Chemical Society, 2004. **126**(16): p. 5300-5308.

171. Gurkan, B.E., et al., *Equimolar CO_2 absorption by anion-functionalized ionic liquids.* Journal of the American Chemical Society, 2010. **132**(7): p. 2116-2117.
172. Bates, E.D., et al., *CO_2 capture by a task-specific ionic liquid.* Journal of the American Chemical Society, 2002. **124**(6): p. 926-927.
173. Yokozeki, A., et al., *Physical and chemical absorptions of carbon dioxide in room-temperature ionic liquids.* Journal of Physical Chemistry B, 2008. **112**(51): p. 16654-16663.
174. Maginn, E.J., Quarterly Technical Report to DOE, May 31, 2005.
175. Shiflett, M.B., et al., *Phase behavior of {carbon dioxide + [bmim][Ac] } mixtures.* Journal of Chemical Thermodynamics, 2008. **40**(1): p. 25-31.
176. Barrosse-Antle, L.E. and R.G. Compton, *Reduction of carbon dioxide in 1-butyl-3-methylimidazolium acetate.* Chemical Communications, 2009(25): p. 3744-3746.
177. Green, O., et al., *The design of polymeric ionic liquids for the preparation of functional materials.* Polymer Reviews, 2009. **49**(4): p. 339 - 360.
178. Banerjee, R., et al., *High-throughput synthesis of zeolitic imidazolate frameworks and application to CO_2 capture.* Science, 2008. **319**(5865): p. 939-943.
179. Wathier, M. and M.W. Grinstaff, *Synthesis and properties of supramolecular ionic networks.* Journal of the American Chemical Society, 2008. **130**(30): p. 9648-9649.
180. Lide, D.R., ed. *CRC Handbook of Chemistry and Physics.* 84th edn. 2004, Boca Raton: CRC Press.
181. Shiflett, M. and A. Yokozeki, *Solubilities and diffusivities of carbon dioxide in ionic liquids: [bmim][PF_6] and [bmim][BF_4].* Industrial & Engineering Chemistry Research, 2005. **44**(12): p. 4453-4464.

VITA

YANHUI YUAN

Yanhui Yuan was born in Kuerle, Xinjiang, P. R. China, on September 30, 1979 to Chunhua Zhang and Jianping Yuan. He received his Bachelor of Science degree in Chemical Engineering from the East China University of Science and Technology in Shanghai in 2001. Then, he received his Master of Science degree in Chemical Engineering from Tsinghua University in Beijng in 2004. From 2004 until 2006, he worked for Shanghai Research Institute of Petrochemical Technology, SINOPEC, before coming to Georgia Tech in 2006 to pursue a doctorate in chemical engineering. On May 8, 2007, he married Yi Ding in Beijing. Following his graduation from Georgia Tech, he will work on CO_2 capture at Algenol Biofuels in Fort Myers, FL, as a senior engineer.